

Master's thesis

NTNU
Norwegian University of
Science and Technology
Faculty of Engineering Science and Technology
Department of Geology and
Mineral Resources Engineering

Kristian Loftesnes

Svaddenipun, Rjukan – Stability analysis of potentially unstable mountainside

Trondheim, June 4th 2010





MASTEROPPGAVEN

- Kandidatens navn:** Kristian Loftesnes
- Oppgavens tittel:** SVADDENIPUN, RJUKAN – STABILITETSANALYSE AV MULIG USTABILT FJELLPARTI
- English title:** Svaddenipun, Rjukan – Stability analysis of potentially unstable mountainside
- Utfyllende tekst:**
1. Masteroppgaven representerer en oppfølging av prosjektoppgave gjennomført av kandidaten i høstsemesteret 2009, hvor det på grunnlag av gjennomgang av tilgjengelig grunnlagsmateriale, feltkartlegging og kinematiske analyser ble foretatt en første vurdering av mulighet for utrasning og av mulige konsekvenser av eventuelt ras. I denne masteroppgaven skal det foretas videre bearbeiding av felt- og LIDAR-data innsamlet høsten 2009, og på dette grunnlag skal det foretas analyse av stabilitet og, hvis tiden tillater det, også av utløpsdistanse ved eventuell utrasning. Som hjelpemidler for databearbeiding og analyser skal benyttes følgende:
 - Programmet Polyworks for analyse av LIDAR-data, som gjennomføres i samarbeid med NGI.
 - Numerisk modellering ved hjelp av SLIDE eller Phase² ("Shear Strength Reduction Method") som del av vurderingsgrunnlaget for stabilitetsanalyse.Analyse av mulig utløpsdistanse kan baseres på empirisk analyse eller program som for eksempel Rockfall.
 2. Oppgaven gjennomføres i samarbeid med NGI/ICG (International Centre for Geohazards) med Dr. Vidar Kveldevik som ekstern veileder og kontaktperson. Ansvarlig faglærer for oppgaven er prof. Bjørn Nilsen, Institutt for geologi og bergteknikk. Oppgaven skal leveres i 4 trykte eksemplarer samt pdf-versjon.
- Studieretning:** Teknisk geologi
- Hovedprofil:** Ingeniørgeologi/bergteknikk
- Tidsrom:** 11.01.-07.06.2010



Faglærer

SKJEMAET TAS INN SOM SIDE 1 I MASTEROPPGAVEN
NTNU, 11 januar 2010

Extended abstract

The steep topography of Norway has caused numerous of large-scale rock slope failures with fatal consequences and the Norwegian Geological Survey landslide database covers over 3000 landslide events. Large-scale slope failures, such as the devastating tsunami triggering events in Loen (1905, 1936) and Tafjord (1934) highlight the importance in detecting instabilities in order to protect human lives and property (Kveldsvik and Einstein et al 2008).

A potential slope instability has been detected at Svaddenipun, Rjukan (Dahlgren and Sletten et al 2004, NGI 2009). The municipality of Tinn have assigned the Norwegian Geotechnical Institute (NGI) to carry out a slope stability investigation. This master thesis is a contribution to this work, and the thesis main goal is to investigate the potential for large-scale failure through use of numerical modelling and processing of LiDAR-scans (Light Detection And Ranging laser) of the slope.

By using new remote sensing technologies, such as LiDAR laser scanning, inaccessible sections within slopes may be evaluated; ensuring that the most important features, representative for the overall slope conditions, are detected. A LiDAR scanning of the Svaddenipun slope was completed in 2009 and processing of these data are one main objective in this thesis. Two scans from the upper section of the slope are processed with the goal of extracting structural geological information on discontinuities controlling stability.

Numerical analysis of rock slope stability has gained popularity in pace with the technological development, allowing huge amounts of data to be processed and evaluated. By applying the “*shear strength reduction technique*” (SSR-analysis) in a Phase² finite element model of the Svaddenipun slope, both factor of safety (FOS) and the location of the most probable failure surface may be obtained. The latter is vital in stability analysis when the failure mode is complex, as is expected to be the case at Svaddenipun. A present shear zone at Svaddenipun is assumed to have major influence on slope stability. A parameter study is thus conducted to detect critical shear zone strengths parameters causing slope failure.

Results from processing of LiDAR data confirm the discontinuity pattern found in the field investigations, indicating that all fracture planes influencing slope stability have been detected. The two major fracture sets are recognized, and in addition, a third fracture set (K3) shows high appearance in LiDAR scans. An additional fracture set that could serve as a daylighting failure surface, extending from the present shear zone to the terrain surface, is not detected. For total slope failure to occur, failure must thus propagate through intact metarhyolite. The high strength of the metarhyolite increases the total shear strength along the most likely failure surface, and the probability of failure is reduced.

Numerical modelling results indicate that the Svaddenipun slope is at a non-critical stability state. A critical stability state is indicated by a factor of safety value of 1, however unrealistic shear zone strength values have to be applied to the different slope models in order to obtain such low factor of safety values. The actual factor of safety within the Svaddenipun slope is thus higher than 1. According to Hoek and Bray 1981, a factor of safety larger than 1,5 indicates a long-term slope stability state. Simulations with shear zone parameters similar to the assumed sliding surface in the Åknes rock slope, western Norway, show factor of safety values close to this criterion. Based on this result, in addition to the fact that the actual factor

of safety for the Svaddenipun slope is unknown, the potential for long-term instability within the Svaddenipun slope cannot be excluded.

Modelling results detect the most probable failure surface to occur mainly along the shear zone, with propagation through intact metarhyolite creating a daylighting surface around 725 m.a.s.l. The minimum, and most likely large-scale failure volume includes approximately 2,2 million m^3 . According to Loftesnes 2009, this volume is larger than the minimum release volume that is needed for a rock avalanche to cross the entire Vestfjord valley. Maximum failure volume involves 5,15 million m^3 .

Uncertainties both regarding model setup and input parameters may reduce representativeness of the completed calculations. Most critical parameters governing slope stability are the strength properties of the shear zone. A different slope model with outcropping of the shear zone in the lower talus slope would dramatically change stability assessment. Shear zone strength parameters would then become even more vital in controlling slope failure. Model sensitivity to water is high, indicated by significant reduction in stability; however the numerical model is more sensitive to changes in shear zone strength parameters.

The present uncertainties in model setup and input parameters combined with the severe consequences of a slope failure at Svaddenipun highlight the importance of further slope stability investigations. Deformation measurements across open fractures may detect whether processes at Svaddenipun are active or remnant. Further LiDAR survey may detect whether active displacement along shear zone are occurring or not. If such investigations detect substantial ongoing shear zone displacement, the focus of obtaining good estimates on shear zone strength parameters should be increased. Core drillings should then be considered despite the high costs of such methods.

Utvida samandrag

Den bratte topografien i Noreg har ført til mange storskala fjellskred med alvorlege konsekvensar. Norges Geologiske Undersøkelse sin skreddatabase inneheld over 3000 hendingar, og storskala fjellskred, slik som dei fatale skreda i Loen (1905, 1936) og Tafjord (1934) viser viktigheita av å oppdage slike ustabile fjellparti (Kveldsvik and Einstein et al 2008).

Eit potensielt ustabil fjellparti er oppdaga ved Svaddenipun, Rjukan (Dahlgren og Sletten m fl 2004, NGI 2009). På bakgrunn av dette har Tinn kommune engasjert Norges Geotekniske Institutt (NGI) til å foreta undersøkingar av stabiliteten til dette fjellpartiet. Denne masteroppgåva er ein del av undersøkingsopplegget, og hovudmålet med oppgåva er å vurdere potensialet for storskala utrasning gjennom bruk av numerisk analyse og bearbeiding av LiDAR (Light Detection And Ranging laser) data.

Ved å ta i bruk nye metodar for fjernanalyse, som til dømes LiDAR skanning, kan utilgjengelege delar av skråningar kartleggast. Dette bidreg til å sikre at dei mest kritiske eigenskapane, representative for ei skråning som heilheit, vert avdekka. Ei LiDAR – undersøking ved Svaddenipun vart utført i 2009, og prosessering av desse data er ei av hovudoppgåvene i denne masteroppgåva. To scannar frå den øvre delen av skråninga er analysert med hensyn på å hente ut informasjon om sprekkorientering i skråninga.

Numerisk analyse av skråningsstabilitet har vorte meir og meir vanleg i takt med den teknologiske utviklinga som tillet prosessering og evaluering av store mengder data. Ved å bruke ein såkalla “skjærstyrkereduksjonsteknikk” (SSR-analyse) i det numeriske modelleringsprogrammet Phase² kan ein få viktig informasjon om stabiliteten til ei fjellskråning. Informasjon om sikkerhetsfaktor (FOS) og plasseringa av den mest sannsynlege bruddflata kan beregnast. I skråningar der bruddmekanismen er kompleks, bestående av fleire ulike bruddflater, er simuleringar for bestemmelse av lokasjonen til bruddflata særskilt viktig. Ved Svaddenipun ventast ei slik kompleks bruddflate, difor er bruk av SSR-teknikken godt egna for denne analysen. Eit parameterstudie er også gjennomført for å avdekke dei kritiske skjærstyrkeparametranne som fører til utglidning for den markante skjærsona ved Svaddenipun. Det er antekje at denne sona har stor innflytelse på stabilitetssituasjonen.

Resultat frå LiDAR scanninga samsvarar med resultatata frå sprekkemålingar utført i felt. Dei to mest markante sprekkessett er også avdekka av scanneren, i tillegg er eit tredje sprekkesett tydeleg på LiDAR – skanningane. Eit fjerde sprekkesett med utgåande i fjellsida som vil kunne danne eit bruddplan saman med skjærsona, er ikkje oppdaga av LiDAR – undersøkinga. For å få storskala utglidning må dermed bruddflata gå gjennom intakt metaryolitt. Den høge styrken til metaryolitt aukar dermed den totale skjærstyrken langs bruddflata, og sannsynet for utglidning vert redusert.

Modelleringsresultata indikerer at Svaddenipun – fjellsida er i ein stabil tilstand. Kritisk stabilitet indikerast ved ein sikkerhetsfaktor lik 1. For å oppnå dette for dei ulike modellane i den numeriske analysen, må urealistiske skjærsonparametrar brukast som input. Den faktiske sikkerhetsfaktoren for skråninga må difor være større enn 1. Ifølgje Hoek og Bray 1981, indikerer ein sikkerhetsfaktor større enn 1,5 at ei skråning er stabil over lang tid. Simuleringar med skjærsonparametrar lik dei for eit antatt bruddplan ved ustabiliteten Åknes

i Møre og Romsdal, resulterer i ein sikkerheitsfaktor i nærleiken av dette kriteriet. På bakgrunn av dette, samt at den faktiske sikkerheitsfaktoren for Svaddenipun – skråninga ikkje er kjent, kan ein ikkje utelukke ustabilitet over eit lengre tidsperspektiv.

Det mest sannsynlege bruddplanet vil i følge den numeriske modelleringa hovudsakeleg følge skjærsona, med utgåande i fjellsida gjennom intakt metaryolitt om lag 725 m.o.h. Det minste og mest sannsynlege storskala utrasningsvolumet er på om lag 2,2 millionar m^3 . Ifølge Loftesnes 2009, er dette volumet stort nok til at ei utrasning vil krysse heile Vestfjorddalen. Maksimalt utrekna utfallsvolum er på 5,15 millionar m^3 .

Usikkerheiter både for oppsettet av den numeriske modellen og i inputparameterane kan redusere representativiteten til dei utførte beregningane. Den mest kritiske parameteren for stabiliteten til fjellsida er styrkeparameterane til skjærsona. Ein annan skråningsmodell, med til dømes utgåande skjærssone i nedre del av ura i fjellsida, vil endre stabilitetsvurderinga dramatisk, og styrkeparameterane til skjærsona vil då verte endå viktigare for stabiliteten. Den numeriske modellen viser også ein betydeleg reduksjon av stabiliteten når skråninga er delvis metta av vatn, likevel er modellen meir sensitiv for variasjon i styrkeparametraner til skjærsona.

Usikkerheitene i skråningsmodellen og i input parametrar, kombinert med dei alvorlege konsekvensane av ei utglidning ved Svaddenipun, gjer at vidare undersøkingar av fjellsida er viktig. Defomasjonsmålingar over åpne sprekker vil kunne avdekke om prosessane ved Svaddenipun er aktive, og vidare LiDAR-undersøkingar vil kunne avdekke pågåande deformasjonar langs skjærsona. Dersom slike undersøkingar viser aktive prosessar bør ein auke fokus på å avdekke betre styrkeparametrar for skjærsona. Kjerneboringar er då eit alternativ som bør vurderast, på tross av høge kostnader ved denne metoden.

Preface and acknowledgements

This master thesis is written over a total of 21 weeks in the 2010 spring semester at NTNU Trondheim. It is equivalent to 30 credits (ECTS), and accomplishes the author's master's degree at the Department of Geology and Mineral Resources Engineering at the Norwegian University of Science and Technology (NTNU). The thesis is a continuation of a Specialization project written by the author in 2009. Vidar Kveldevisk at the Norwegian Geotechnical Institute (NGI) suggested the topic in summer 2009. The thesis forms a contribution to a commission from the municipality of Tinn regarding a rock slope stability analysis of the Svaddenipun slope located above the town centre of Rjukan. The thesis is written in collaboration with the NGI and the International Centre for Geohazards (ICG) with Vidar Kveldevisk as the external supervisor. The Norwegian Geological Survey (NGU) has also played an important role in parts of the data collection and interpretations. The internal supervisor from NTNU is professor Bjørn Nilsen.

My two main supervisors Bjørn Nilsen and Vidar Kveldevisk deserve large gratitude for valuable input and help throughout the entire thesis period. Their dedicated works have inspired a lot and I have had great benefit from interesting discussions throughout the work-period. I would like to once again thank the NGI and the ICG for giving me the opportunity to work with a really interesting project, and providing personnel, funding and helpful tools. The NGU deserves gratitude for letting me apply their PolyWorks licence and give me the opportunity to work at their main office in Trondheim. Here Martina Böhme and Thierry Oppikhofer from NGU have given me careful training in the software PolyWorks, for processing of LiDAR data. In addition, Elin Morgan from the NGI has also given valuable help in PolyWorks training and discussion of the results. Ming Lu from NTNU/SINTEF has given valuable input regarding numerical modelling in Phase². The municipality of Tinn have provided necessary funding and maps over the slope.

I would also like to thank my student colleagues at the “lesesal” for a nice working atmosphere and interesting discussions.

Trondheim, June 4th 2010

Kristian Loftesnes

Table of content

Extended abstract	iii
Utvida samandrag	v
Preface and acknowledgements	vii
Table of content	ix
List of figures	xiii
List of tables	xvii
Abbreviations	xix
Nomenclatures	xix
Chapter 1: Introduction	1
1.1 Background	1
1.2 Structure of the thesis	1
1.3 Aims and scope	1
1.4 Available software and site specific literature	2
1.5 Description of the Svaddenipun site	2
1.5.1 Location and topography	2
1.5.2 Geology	3
1.5.3 Historical events.....	3
1.6 Completed investigations and preliminary findings	4
1.6.1 Background.....	4
1.6.2 Confinement of the potential instability	4
1.6.3 Discontinuities and controlling structures	6
1.6.4 Mechanical properties	7
1.6.5 Kinematic analysis and preliminary stability assessment.....	7
Chapter 2: LiDAR scanning	9
2.1 Introduction	9
2.2 Description of Light Detect And Ranging (LiDAR) technique and the application in rock slope investigations	9
2.2.1 Description of the LiDAR method.....	9
2.2.2 Applications	9
2.2.3 Limitations and uncertainties	10
2.3 Scanning purpose and procedure at Svaddenipun	12
2.4 Processing of data	13
2.4.1 Methodology.....	13
2.4.2 First inspection of the scanned files.....	13
2.4.3 Creating input files for PolyWorks.....	13
2.4.4 Georeferencing data in PolyWorks.....	15
2.4.5 Extracting structural data in PolyWorks.....	17
Chapter 3: Methodology for rock slope stability analysis	19
3.1 Introduction	19
3.2 Limit equilibrium analysis	20
3.3 Numerical analysis	22
3.3.1 Numerical analysis in general.....	22
3.3.2 Continuous models vs. discontinuous models.....	22
Chapter 4: Stability analysis of the Svaddenipun slope	25
4.1 Introduction	25

4.2 Finite Element Method	25
4.2.1 FEM in general.....	25
4.2.2 Shear Strength Reduction Analysis (SSR).....	25
4.3 Analysis method chosen for the Svaddenipun slope	26
4.4 Finite element numerical modelling with Phase²	27
4.4.1 About Phase ²	27
4.4.2 Choosing the optimal numerical method.....	27
4.4.3 Methodology for Phase ² numerical analysis, and subdivision of model setups	28
Chapter 5: Svaddenipun model setup and input parameters	29
5.1 Introduction	29
5.2 Slope model	29
5.2.1 General settings	29
5.2.2 Geometry.....	29
5.2.3 Boundary conditions.....	29
5.2.4 Shear Strength Reduction setup.....	30
5.2.5 Mesh setup	30
5.3 Slope materials and failure criterion	30
5.3.1 Introduction.....	30
5.3.2 Metarhyolite	31
5.3.3 Shear zone	34
5.4 Rock mass parameters for metarhyolite and shear zone	35
5.4.1 Young's modulus and Poisson's ratio	35
5.4.2 Tensile strength.....	36
5.4.3 Dilation angle.....	36
5.4.4 Specific weight.....	37
5.4.5 Peak vs. residual shear strength	37
5.4.6 Summary of input parameters for metarhyolite and shear zone	38
5.5 Discontinuities	38
5.5.1 Implementing discontinuities in Phase ² model	38
5.5.2 Barton-Bandis criterion for shear strength of discontinuities	38
5.5.3 Statistical appearance of fracture set K1	40
5.6 Stresses	40
5.7 Water	41
5.8 Parametric study	42
5.9 Evaluation of input parameters and Phase² model limitations	43
5.10 Summary of input parameters for Svaddenipun slope model	44
5.10.1 Input parameters for the initial model (Svaddenipun 1 – model)	44
5.10.2 Input parameters for the parametric study	44
5.10.3 Phase ² Svaddenipun model	46
Chapter 6: Results from LiDAR survey	47
6.1 Introduction	47
6.2 Fracture orientations detected in LiDAR survey	47
Chapter 7: Results from Phase² modelling	49
7.1 Introduction	49
7.2 Calculations with initial strength parameters for metarhyolite and K1 discontinuities (Svaddenipun 1 – model)	49
7.2.1 Introduction.....	49
7.2.2 Calculations with shear zone parameters corresponding to Åknes sliding plane.....	49
7.2.3 Result of critical shear zone strength calculations.....	51
7.3 Calculations with 30% reduced strength parameters for metarhyolite and K1 discontinuities (Svaddenipun 2 – model)	54
7.3.1 Introduction.....	54

7.3.2 Calculations with shear zone parameters corresponding to Åknes sliding plane.....	55
7.3.3 Result of critical shear zone strength calculations.....	55
7.4 Calculations with 30% increased strength parameters for metarhyolite and K1 discontinuities (Svaddenipun 3 – model)	58
7.4.1 Introduction.....	58
7.4.2 Calculations with shear zone parameters corresponding to Åknes sliding plane.....	58
7.4.3 Result of critical shear zone strength calculations.....	58
Chapter 8: Discussion of results from LiDAR survey and Phase² modelling.....	61
8.1 LiDAR scanning.....	61
8.1.1 Achievement of scanning goals	61
8.1.2 Structural geological information	61
8.1.3 Error sources	62
8.2 Numerical modelling in Phase²	63
8.2.1 Location of the failure surface	63
8.2.2 Factor of safety and assessment of calculated critical shear zone strengths.....	63
8.2.3 General trends and patterns of different model setups.....	65
8.2.4 Representativeness of initial Åknes strength parameters.....	66
8.2.5 Reliability of results and model uncertainties.....	66
Chapter 9: Assessment of slope stability based on results and recommended further investigations.....	69
9.1 Introduction	69
9.2 Assessment of slope stability based on existing knowledge.....	69
9.3 Uncertainties.....	70
9.4 Recommended further investigations	70
Chapter 10: Conclusion	71
Chapter 11: References	73
Appendices.....	A
Appendix 1: LiDAR scanning locations	A
Appendix 2: LiDAR processing setup parameters.....	B
Appendix 3: List of all relevant Phase ² files	C
Appendix 4: Screenshots of RocData input parameters for metarhyolite.....	E
Appendix 5: Estimation of shear modulus for metarhyolite.....	G
Appendix 6: Contourplots of LiDAR Scan 6 and Scan 7	H
Appendix 7: Relevant Phase ² input parameters for shear zone strength and resulting FOS.....	I
Appendix 8: Memory stick with relevant Phase ² - and PolyWorks-files.....	J

List of figures

Figure 1.1: Left: Location of Svaddenipun. Right: Topographical map over Svaddenipun. (Figure from Loftesnes 2009)

Figure 1.2: Rock slope at Svaddenipun on the southern side of the Vestfjord-valley. City centre of Rjukan is seen at valley floor. Photo towards east. (Figure from Loftesnes 2009)

Figure 1.3: Top plateau at Svaddenipun. Southern shear zone is seen in the left of the photo along the shadow margin. Subdivision of the plateau is made along black dotted lines where depressions strike SW-NE into the valley slope. Photo taken towards west.

Figure 1.4: Structural geological map over Svaddenipun with confinements and subdivision of area into sections. Black line show the profile line used for the numerical modelling in this thesis. (Figure from Loftesnes 2009)

Figure 1.5: Stereoplot of all field measurements at Svaddenipun. Distinction between open and closed fractures is given. Fracture set K1 and K2 is clear, set K3 have only a few observations. (Figure from Loftesnes 2009)

Figure 1.6: Left: Open fracture at edge of top plateau. Right: K1 fractures parallel to valley slope in upper section of the potential instability. (Figures from Loftesnes 2009)

Figure 2.1: Illustrates the influence of occlusion on laser scanning measurements. a) Point cloud of a rock slope as seen from the laser scanner position. b) Point cloud of the same slope rotated using processing software showing occluded or hidden zones. (Figure from Sturzenegger and Yan et al 2007)

Figure 2.2: Illustration of the three forms of orientation bias. a) Rock slope orientation relative to discontinuity sets A, B and C (Terzaghi bias), b) horizontal line of sight of laser scanner with respect to rock slope (azimuth bias), c) shows discontinuity traces when line of sight is sub parallel of discontinuity set. (Figure from Sturzenegger and Yan et al 2007)

Figure 2.3: LiDAR positions (Left) and ILRIS-3D scanner at location 5 (Right). Locations 1-4 are in the valley floor and location 5 and 6 are at the top plateau. (Figure from Loftesnes 2009)

Figure 2.4: Screenshot of Scan 6 in the software Matchview during calibration of the IXF-point cloud file to a digital photo. Red marks represents identical points on scan and photo

Figure 2.5: Screenshots from software pif-edit showing Scan6 (Left) and Scan7 (Right). Point cloud calibrated to digital photo makes detection of snow free surfaces easier. Effect of occlusion is shown in right scan.

Figure 2.6: Workflow for surveying purposes and the different modules that are applied to each task in PolyWorks. The module IMView is not used. (Figure from InnovMetric 2005)

Figure 2.7: Error map of Scan 6. Show deviations between DEM and point cloud in meters, Green values indicate zero deviation. Positive value indicates that point cloud is situated on top (outside) of DEM, negative values indicate that point cloud is situated under (inside).

Figure 2.8: Error map of Scan 7. Show deviations between DEM and point cloud in meters, Green values indicate zero deviation. Positive value indicates that point cloud is situated on top (outside) of DEM, negative values indicate that point cloud is situated under (inside).

Figure 2.9: Screenshot IMInspect from a section of Scan 6. Marked planes are shown

Figure 2.10: Screenshot IMInspect from a section of Scan 7. Marked planes are shown.

Figure 3.1: Flowchart shows different analytical methods for slope stability analysis. Different commercial codes are given in red. (Figure modified from Nilsen and Palmstrøm 2000)

Figure 3.2: Flowchart for different levels of slope stability analysis showing what failure mechanisms they may be applied to. (Figure from Stead and Eberhardt et al 2006)

Figure 3.3: Subdivision of a slope into a number of slices. Right figure show sum of forces acting on one slice. (Figure from Coduto 2007)

Figure 5.1: Recommendations for size of numerical model to avoid boundary effects. (Figure from Wyllie and Mah 2004)

Figure 5.2: Guidelines for using Hoek-Brown material model for different rock masses. Equation 1 referred to in the figure is the same as Equation 5.1 in the text above. Equation 5 referred to in the figure 5 is the same as to Equation 5.1 in the text above with $a=0,5$. (Figure from Hoek 2000)

Figure 5.3: Linear fitting of the Mohr-Coulomb failure criterion to the curved Hoek-Brown line. Definition of the instantaneous cohesion c_i and friction angle ϕ_i for a specific value of σ_n . (Figure from Hoek 2000)

Figure 5.4: Upper and lower left: Laboratory test of shear strength along a discontinuity surface and the related stress/deformation curve. Lower right: Mohr plot of peak and residual shear strength. Figure from Hoek 2000.

Figure 5.5: Definition of discontinuity persistence as L1/L2 in Phase2. Figure from Rocscience 2010 c.

Figure 5.6: Screenshot of completed model built in Phase² used for the numerical analysis.

Figure 6.1: Stereoplot for 143 discontinuities found on LiDAR Scan 6 (red) and Scan 7 (blue). The scanning direction for both scans is shown in red and blue lines. Green line shows average slope dip.

Figure 6.2: Contourplot for 143 discontinuities from LiDAR scans with fisher concentrations.

Figure 7.1: Maximum shear strain in the Svaddenipun – 1 model with Åknes sliding plane properties for the shear zone. Critical FOS is 1,70, figure show situation at FOS=1,71.

Figure 7.2: Maximum shear strain in the partially saturated Svaddenipun – 1 model with Åknes sliding plane properties for the shear zone.

Figure 7.3: Shear strain plot for reduced shear zone properties corresponding to critical SRF (1,01) for Svaddenipun 1 – model. The plot is presented for a SRF of 1,02 to illustrate where the failure plane is likely to be located. Cross sectional area of the upper slope lying above the shear zone and the 30°-line trough metarhyolite is around 14 700 m².

Figure 7.4: Major stress distribution for Svaddenipun 1 – slope model with critical shear zone properties. Black dotted line shows location of stress plot values given in Figure 7.5. Maximum normal stress along a K1 joint surface is given in red, and the location of this fracture is in the area with largest major stress.

Figure 7.5: σ_1 (left) and σ_3 (right) graphs along marked line in Figure 7.4. Horizontal axis value increases towards slope surface. σ_1 values decrease towards shear zone, before a large increase in region close to slope surface. σ_3 show highest values in the shear zone.

Figure 7.6: Deviatoric stress plots for isotropic stresses (left) and initial stress conditions (right) for critical shear zone strength in the Svaddenipun 1 – model. Numbers indicate the magnitude of deviatoric stresses at critical FOS close to 1,0.

Figure 7.7: Plot of friction angle and corresponding FOS for dry (blue) and partially saturated (red) analysis for Svaddenipun 1 – model setup. FOS values are listed next to each point in plot. A linear relationship between friction angle and FOS is clear, although sensitivity to changing friction angle is different for the two cases.

Figure 7.8: Shear strain plot for dry Svaddenipun 2 – model with Åknes sliding plane parameters applied in the shear zone. Strains occur only in upper part of shear zone and in the underlying metarhyolite along SSR search area boundary.

Figure 7.9: Maximum shear strain figure for critical shear zone strengths in the Svaddenipun 2 – model. Shear strain concentrations in the metarhyolite above the shear zone occurs at the same location as in the corresponding Svaddenipun 1 – model. The dip angle of the strain-concentration surface in upper metarhyolite is around 35°. Note the substantial amount of strains occurring below shear zone along SSR search area boundary.

Figure 7.10: Deviatoric stresses in the Svaddenipun 2 – model with critical shear zone parameters corresponding to a FOS of 0,995. Simulated deviatoric stresses values (MPa) in metarhyolite at a distance of 0,1 meter from shear zone/metarhyolite boundary is shown.

Figure 7.11: Maximum shear strain plot for FOS 1,0 with Svaddenipun 2 – model and partially saturated conditions. No indications of increased shear strain at elevations around 750 m.a.s.l.

Figure 7.12: Shear strain plot (left) and major principal stress plot (right) for Svaddenipun 3 – model with shear zone strengths corresponding to a critical FOS of 1,05.

Figure 7.13: Relationship between shear zone peak friction angle and corresponding FOS for the Svaddenipun 3 – model setup.

Figure 8.1: Stereoplot with comparison between field measurements and LiDAR measurements.

Figure 8.2: Illustrate incorrect surface recognized by the scanner. This may result from several effects; both from snow cover smoothing, and resolution of scanner.

Figure 8.3: Relationship between cohesion and friction angles for back-calculations of failures in rock slopes represented by the different numbers. The critical shear zone strength composition from the different Svaddenipun model setups is marked. Figure modified from Wyllie and Mah 2004.

List of tables

Table 1.1: Registered historical events at Svaddenipun.

Table 2.1: Resolution measures for Optech ILRIS-3D scanner. (Table from Sturzenegger and Yan et al 2007)

Table 2.2: Show matching parameters for the two LIDAR-Scans. RMS values less than 2 indicate a good match.

Table 3.1: Properties of limit equilibrium method. (Table modified from Broch and Nilsen 2001, and Stead and Eberhardt et al 2006)

Table 3.2: Properties of continuous and discontinuous numerical methods. (Table modified from Stead and Eberhardt et al 2006)

Table 5.1: SSR convergence parameters.

Table 5.2: Hoek-Brown parameters representing the Svaddenipun metarhyolite.

Table 5.3: Different literature values used as input for E_m for the metarhyolite. GSI and D values for Svaddenipun are selected based on recommendations in RocData manual and are discussed in Chapter 5.3.2.

Table 5.4: Poisson's ratio for rhyolite.

Table 5.5: Input parameters for Svaddenipun metarhyolite and shear zone. Shear zone ϕ and cohesion values are found in Grøneng 2010.

Table 5.6: kn and k_s parameters.

Table 5.7: Properties of fracture set K1 used as input in numerical model.

Table 5.8: Initial input parameters for metarhyolite and shear zone.

Table 5.9: Key properties of fracture set K1 used as input in numerical model.

Table 5.10: Variation of metarhyolite input parameters in parametric study. To avoid unrealistic values for the $\pm 30\%$ strength analysis, the values of GSI, D and ϕ_r for joints are set to reasonable values instead of exact calculations. m_i and MR are set to maximum and minimum recommended values for metarhyolite according to RocData user manual. Metarhyolite E_m is calculated from Equation 5.5.

Table 7.1: Mohr-Coulomb input parameters for shear zone in Svaddenipun 1 – model. Left: calculations with shear zone parameters corresponding to Åknes sliding plane, and resulting FOS. Right: Shear zone input values leading to critical stability state represented by FOS close to 1,0. For this model setup, c was remained constant and ϕ was varied until failure occurred. Differences between dry and partially saturated conditions are highlighted.

Table 7.2: Mohr-Coulomb input parameters for shear zone in Svaddenipun 2 – model. Left: calculations with shear zone parameters corresponding to Åknes sliding plane, and resulting FOS. Right: Shear zone input values leading to critical stability state represented by FOS close to 1,0. For this model setup, ϕ was remained constant and c was varied until failure occurred. Differences between dry and partially saturated conditions are highlighted.

Table 7.3: Mohr-Coulomb input parameters for shear zone in Svaddenipun 3 – model. Left: calculations with shear zone parameters corresponding to Åknes sliding plane, and resulting FOS. Right: Shear zone input values leading to critical stability state represented by FOS close to 1,0. For this model setup, c was remained constant and ϕ was varied until failure occurred. Differences between dry and partially saturated conditions are highlighted.

Abbreviations

Expression	Explanation	Expression	Explanation
<i>FOS</i>	Factor of safety	<i>RMS</i>	Root mean square
<i>SSR</i>	Shear strength reduction	<i>CAD</i>	Computer –aided design
<i>SRF</i>	Strength reduction factor	<i>GIS</i>	Geographical information system
<i>LiDAR</i>	Light detection and ranging	<i>GSI</i>	Geological strength index
<i>FEM</i>	Finite element model	<i>JCS</i>	Joint compression strength
<i>NGI</i>	Norwegian geotechnical institute	<i>JRC</i>	Joint roughness coefficient
<i>NGU</i>	Norwegian geological survey	<i>UCS</i>	Uniaxial compression strength
<i>DEM</i>	Digital elevation model	<i>m.a.s.l</i>	Meter above sea level
<i>FDM</i>	Finite difference model	<i>K1</i>	Main fracture set 1
<i>BEM</i>	Boundary element method	<i>K2</i>	Fracture set 2
<i>UDEC</i>	Universal distinct element code	<i>K3</i>	Fracture set 3

Nomenclatures

Expression	Explanation	Expression	Explanation
σ_h [Mpa]	Horizontal stress	τ [Mpa]	Shear stress
σ_v [Mpa]	Vertical stress	c [Mpa]	Cohesion
σ_1 [Mpa]	Tensile strength	c_{peak} [Mpa]	Peak cohesion
σ_{ci} [Mpa]	Uniaxial compression strength for intact rock	c_r [Mpa]	Residual cohesion
σ_n' [Mpa]	Effective normal stress	c_i [Mpa]	Instantaneous cohesion
σ_n [Mpa]	Normal stress	ϕ [°]	Friction angle
σ_1 [Mpa]	Major stress	ϕ_{peak} [°]	Peak friction angle
σ_3 [Mpa]	Minor stress	ϕ_r [°]	Residual friction angle
σ_1' [Mpa]	Major effective stress	ϕ_a [°]	Active friction angle
σ_3' [Mpa]	Minor effective stress	ϕ_i [°]	Instantaneous friction angle
E_m [Gpa]	Rock mass deformation modulus (Young's modulus)	s	Material factor Hoek-Brown criteria
E_i [Gpa]	Intact rock deformation modulus	a	Material factor Hoek-Brown criteria
G_m [Gpa]	Rock mass shear modulus	m_b	Hoek-Brown rock mass material constant
G_i [Gpa]	Intact rock shear modulus	m_i	Hoek-Brown intact material constant
k_n [Gpa]	Joint normal stiffness	D	Disturbance factor Hoek –Brown criterion
k_s [Gpa]	Joint shear stiffness	MR	Modulus ratio ($E_i=MR \cdot \sigma_{ci}$)
ϵ_z	Axial strain	ν	Poisson's ratio
ϵ_x	Strain in x-direction	f	Trial factor for SSR analysis
ϵ_y	Strain in y-direction	γ [kN/m ³]	Specific weight

Chapter 1: Introduction

1.1 Background

The topography of Norway includes numerous of large and steep valleys excavated over the last several glaciations. Such valleys often represent a scenic and beautiful view appreciated by the local population and the many tourists, but in some cases they may also represent threatening hazards with the potential of creating devastating rock slope failures. A potential large-scale slope instability has been detected at Svaddenipun, Rjukan, along the southern slope of the Vestfjord – Valley (Dahlgren and Sletten et al 2004, NGI 2009). The site consists of hard brittle rocks and is located directly above the town centre of Rjukan. The municipality of Tinn have assigned the Norwegian Geotechnical Institute to carry out a slope stability investigation. This thesis is a contribution to this work, by investigating the potential of large-scale failure through use of numerical modelling technique and a LiDAR (Light Detection And Ranging laser) analysis of the slope. Due to the severe consequences of a potential failure, it is assumed that a slope stability investigation will give valuable input to the hazard assessment of the area.

1.2 Structure of the thesis

In the introduction chapter, the purpose of this thesis is described, and then a description of the Svaddenipun site is given based on completed investigations. *Chapter 2* describes background theory and processing of the Svaddenipun LiDAR data. The general methodology for rock slope analysis is summarized in *Chapter 3*, before *Chapter 4* presents analytical techniques applied in the Svaddenipun analysis. *Chapter 6* and *7* presents the results of the LiDAR scanning and numerical modelling; results are discussed in *Chapter 8*. Finally a hazard assessment based on the findings is presented in *Chapter 9*, including a discussion on further recommended investigations. *Chapter 10* presents the thesis conclusion.

1.3 Aims and scope

The objective of this thesis is, as described in the assignment description on the first page, to carry out a slope stability analysis of the Svaddenipun slope. The author completed a preliminary investigation, including site investigations in 2009, and this master thesis is a continuation of this work. The main elements of the thesis are processing of LiDAR data collected by Loftesnes 2009 and numerical finite element modelling of the slope. Through analysis of LiDAR data, structures controlling slope stability may be detected and form a basis for discussing failure potential and comparison to field data. The main goal of the numerical modelling is to determine the critical shear strength within the present shear zone governing the Svaddenipun slope stability. Critical shear zone strength is here defined as the shear zone strength parameters applied to the model, which result in a factor of safety (FOS) of 1,0. By evaluating the obtained critical shear zone strength, the probability of failure may be discussed. Detection of the most likely failure surface may reveal useful information on kinematic slope conditions and release volumes, and are thus also vital for stability assessment. In order to achieve the aims of the thesis, the following tasks are completed:

- *Processing and interpretation of LiDAR data to obtain information on fracture orientations. Compare LiDAR results to field measurement results.*

- *Finite element analysis of the slope using the Shear Strength Reduction (SSR) method. This will give the FOS, critical shear zone material strengths and the most likely location of the failure surface.*
- *Parameter study to investigate uncertainties in input parameters and their effect on stability. Main emphasis is put on detecting shear zone parameters corresponding to a critical stability situation with FOS close to 1.*
- *Introduction of piezometric line in numerical model, to study effect of water.*
- *Assessment of slope stability based on results and existing knowledge and recommendations of further investigations.*

In the thesis description on the first page, the study of run-out lengths is mentioned as a possible task. RocFall simulations of run-out lengths are relevant only for smaller individual blocks and cannot be applied for the slope as a whole. Based on the available time, the main focus in this thesis is chosen to be on large-scale stability of the slope; therefore run-out calculations and discussion on probability for smaller rockfall events are excluded. This decision is made in collaboration with the main supervisor. Empirical run-out lengths for large-scale failure at Svaddenipun are conducted in Loftesnes 2009.

1.4 Available software and site specific literature

The following data has been made available and form a basis for the analysis:

- *Topographic maps of Svaddenipun made available from the community of Tinn.*
- *Numerical modelling Software Phase² 7.009 including user manuals from Rocscience.*
- *Software RockData 4.008 from Rocscience including user manuals.*
- *Software Dips 5.108 from Rocscience including user manuals.*
- *LiDAR processing software Polyworks including user manuals from InnovMetric.*
- *Software Parser and Matchview from Optech for preprocessing of LiDAR data.*
- *Loftesnes 2009: Svaddenipun, Rjukan; Investigations and analysis of potential rock slope instability. Specialization project thesis at NTNU.*
- *Dahlgren and Sletten et al 2004: Skredfarekartlegging I Vestfjorddalen. NGU report 2004.023.*
- *NGI report 2009: Svaddenipun, Rjukan. Beskrivelse av mulig ustabil fjellparti med forslag til innledende overvåkning. 20071925-1*

1.5 Description of the Svaddenipun site

1.5.1 Location and topography

The investigated slope at Svaddenipun is located at Rjukan, the community centre of Tinn, in the county of Telemark. *Figure 1.1* shows the location of Rjukan in the south east of Norway.



Figure 1.1: Left: Location of Svaddenipun. Right: Topographical map over Svaddenipun. (Figure from Loftesnes 2009)

The slope rise 760 vertical metres from the town centre of Rjukan, and form the southern side of the east-west striking Vestfjord-valley (Figure 1.2). The lower part consist of talus slope, the upper section is a partially vegetated cliff face. The average dip of the upper cliff section is 57° , increasing to 66° towards the top at 1040 m.a.s.l. At the top of the slope, a 90-130 metres wide and almost flat top plateau stretches parallel to the valley side. The southern boundary of the plateau consists of a shear zone, before the terrain steepens towards the 1883 meter high Gaustatoppen in south.

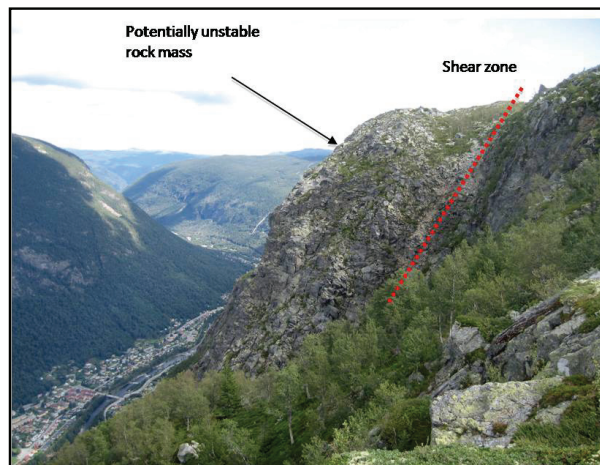


Figure 1.2: Rock slope at Svaddenipun on the southern side of the Vestfjord-valley. Town-centre of Rjukan is seen at valley floor. Photo towards east. (Figure from Loftesnes 2009)

1.5.2 Geology

Geologically, the site is located in the supracrustal Telemark-formation, and consists of a metarhyolite rocks. Main structural lineaments consist of syn- and anticlines with axis striking NNE and NNW. Locally around Rjukan, faults and fractures are oriented more parallel to the Vestfjord-valley.

1.5.3 Historical events

Several rockslides and rockfalls have occurred at Svaddenipun in historical time, this is clearly visualized by the presence of an approximate 1,5 million m^3 talus in the lower section of the slope. Table 1.1 summarize the registered events reported in Dahlgren and Sletten et al 2004. In addition to this, smaller rockfalls have been reported more frequently, indicating that the slope is active.

Table 1.1: Registered historical events at Svaddenipun.

Year	Release volume	Damage
1927	Unknown	Damage on forest and fields. Blocking of river causing flood.
1934	Unknown, but small	Did not reach valley floor.
1964	Several 10 000 m ³	Damage on road and a warehouse. One block reached residential backyard.

1.6 Completed investigations and preliminary findings

1.6.1 Background

The author have previously conducted a preliminary study of the Svaddenipun site (Loftesnes 2009). In addition to this the Norwegian Geological Survey (Dahlgren and Sletten et al 2004), and the Norwegian Geotechnical Institute (NGI 2009) have carried out preliminary investigations on behalf of the municipality of Tinn. All work includes field investigation at the top plateau and fieldwork by Loftesnes 2009 also included a field investigation in parts of the slope face. The completed investigations form the basis for the stability analyses conducted in this master thesis. Based on Dahlgren and Sletten et al 2004, NGI 2009 and Loftesnes 2009, a summary of the preliminary findings and interpretations are presented in the following sections. A more extensive description of the Svaddenipun site is given in Loftesnes 2009.

1.6.2 Confinement of the potential instability

Figure 1.4 shows a structural geological map of the Svaddenipun site including assumed boundaries of the potential instability. The main controlling structure is an approximately 15 meter thick shear zone stretching E-W, parallel to the valley and slope face. This zone has a dip of 53° to the north. No sign of daylighting of the zone was observed in the slope face during fieldwork, and it is thus assumed to be planar throughout the slope. The western margin of the potential instability is the daylighting of the shear zone, while the eastern lateral release structure is suggested to be along an observed depression, concurring with the easternmost registered open fractures at the top plateau. The eastern boundary is however more unclear. Field investigations have not detected a clear indication of the location of the instability toe, but it is suggested to be at the transition between the cliff face and the talus slope at 725 m. a. s. l. Based on observations the potential instability is divided into three sections, A, B and C with increasing indication of movement towards west (Figure 1.3).

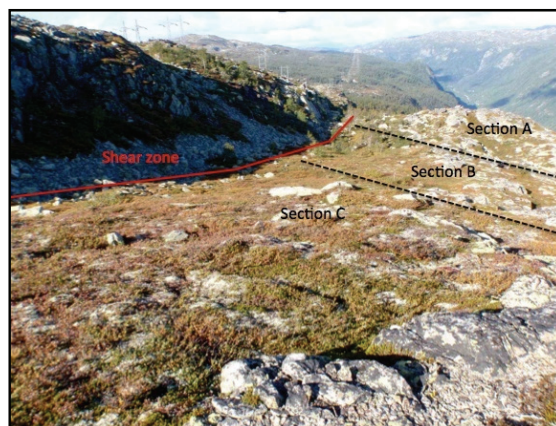


Figure 1.3: Top plateau at Svaddenipun. Southern shear zone is seen in the left of the photo along the shadow margin. Subdivision of the plateau is made along black dotted lines where depressions strike SW-NE into the valley slope. Photo taken towards west.

(Figure from Loftesnes 2009)

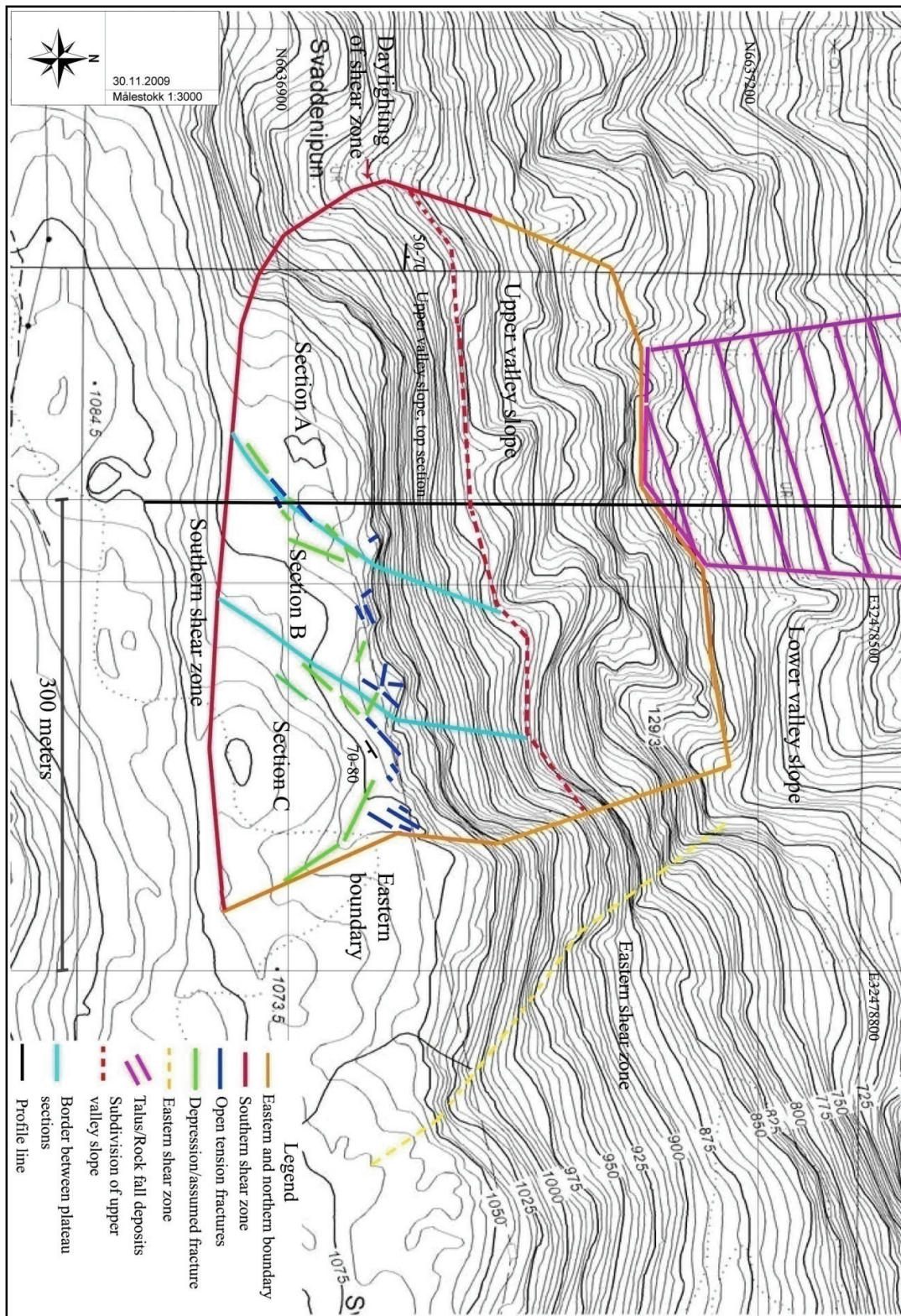


Figure 1.4: Structural geological map over Svaddenipun with confinements and subdivision of area into sections. Black line shows the profile line used for the numerical modelling in this thesis. (Figure from Loftesnes 2009)

1.6.3 Discontinuities and controlling structures

Discontinuities are a key rock mass property regarding slope stability, as failure tends to follow fractures and weak layers. The shear zone constitutes the most important structure controlling stability; dipping parallel valley slope although no daylighting of the zone is observed. In addition, two main and one less clear fracture sets are detected in the fieldwork at the site (*Figure 1.5*). Main fracture set K1 follow sub parallel to valley slope with average dip/dip direction 62/006. This is slightly steeper than dip of the shear zone and the average slope face (*Figure 1.6*). A second fracture set is dipping to the southeast with average dip/dip direction 63/123, and a third but unclear cluster of fractures are dipping to the northwest. All fracture sets show variations in both orientations and properties.

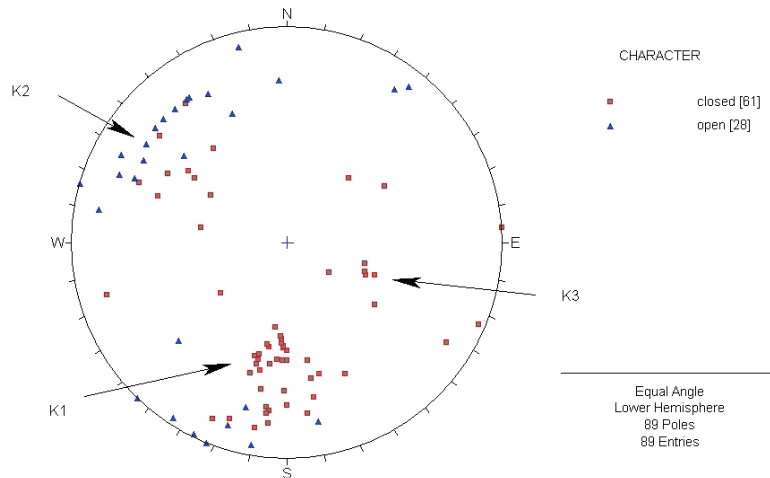


Figure 1.5: Stereoplot of all field measurements at Svaddenipun. Distinction between open and closed fractures is given. Fracture set K1 and K2 is clear, set K3 have only a few observations. (Figure from Loftesnes 2009)

At the frontal part of the top plateau, numerous open, steeply dipping, fractures are registered with lengths more than 30 meters and openings up to 4 meters (*Figure 1.6*). Some fractures have registered deformations of up to 2,5 cm over 8 years (NGI 2009). Two sets of open fractures are apparent although variations occur; K1 with average dip/dip direction 78/014, and K2 with dip/dip direction averaging 72/128.



Figure 1.6: Left: Open fracture at edge of top plateau. Right: K1 fractures parallel to valley slope in upper section of the potential instability. (Figures from Loftesnes 2009)

1.6.4 Mechanical properties

The metarhyolite present at Svaddenipun shows varying degree of foliation, from non-existing to well developed and sub-parallel to valley slope. Schmidt hammer field test indicate a σ_c for intact rock of 181 Mpa. The main fracture set K1 has a weighted average joint roughness coefficient (JRC) of 3,23.

1.6.5 Kinematic analysis and preliminary stability assessment

Kinematic analysis shows that both planar, wedge and toppling failure is theoretically possible at different scales within the slope. Kinematic mechanisms also vary in different slope sections. In Section C, toppling fractures are present, while planar and wedge failure is more probable in Section A and B. Small-scale events, such as rockfalls and smaller rockslides are highly probable throughout the entire slope. For the total stability at Svaddenipun, a planar failure along the shear zone and/or fracture set K1 seems like the most probable failure scenario. The shear zone itself does however not daylight in the slope face, and a second failure surface is needed for a total collapse of the slope. This surface may be present as a second, not observed, fracture set or as degradation of rock bridges connecting several K1 fractures.

The different failure mechanisms within the slope, also leads to internal variation in the total stability. The majority of the sliding plane is assumed to follow the shear zone, observed creep along shear zone have already reduced shear strength of this failure surface. Observations indicate that Section A has had more displacement along shear zone, leading to the impression that this section has the lowest stability. A tension crack separating Section A and B may act as the eastern lateral surface, allowing Section A to fail. Whether creep is an ongoing or remnant process along the shear zone is not clear.

Preliminary estimations of release volumes suggest a release of the most probable Section A would include a volume of 1,9 million m^3 . A total collapse of the whole slope would include a volume around 10 million m^3 . Empirical relationships suggest that a volume of only 800 000 m^3 would have a run out length that would cross the entire Vestfjord – valley and impact large parts of the town centre at Rjukan. This includes schools, kindergartens, roads and residential areas. Consequences of a slope failure would therefore be devastating although preliminary investigations have failed to detect critical signs of instability.

Chapter 2: LiDAR scanning

2.1 Introduction

Structural mapping detects important information on kinematic conditions within potentially unstable rock slopes, and it may provide key input to numerical analysis of potential hazardous areas (Sturzenegger and Stead et al 2007). As pointed out by Kemney and Norton et al 2008, there is a need for a new and more precise tool for landslide detection, evaluation and management in steep, inaccessible slopes. Where field observations are difficult or impossible, different forms of remote sensing could be a precise evaluation method for gaining key information on slope stability. Light detection and ranging (LiDAR) is an increasingly used mapping tool for description of morphology and geological structures of rock slopes (Sturzenegger and Stead 2009). LiDAR is an optical remote sensing technology that uses a laser pulse to detect the distance and the angle to a reflecting surface. LiDAR scanning was conducted on the Svaddenipun slope in October 2009. This chapter gives a presentation of the LiDAR method, and the scanning procedure and data processing for the Svaddenipun slope. Due to the limited existing literature of the Polyworks processing procedure with respect to slope stability analysis, a rather extensive description of the method is given.

2.2 Description of Light Detect And Ranging (LiDAR) technique and the application in rock slope investigations

2.2.1 Description of the LiDAR method

The LiDAR technique has gained popularity in a wide range of engineering problems over the recent years, and may be applied in industrial surveys, city planning, infrastructure scanning, mine planning and slope mapping- and stability assessment (Optech 2009 a). The LiDAR technique is in principle the same as for RADAR; the LiDAR instrument transmits light out to an object, a proportion of this light is then reflected back to the instrument, and the travel time is registered (Martin et al 2007). From this, the distance and angle to the reflected surface is calculated, and as millions of pulses with a short spacing are sent out, a cluster of points (point clouds) with coordinates are gathered. The shape of the scanned object is then determined (Collins and Kayen 2006). Both aerial and terrestrial LiDAR are available.

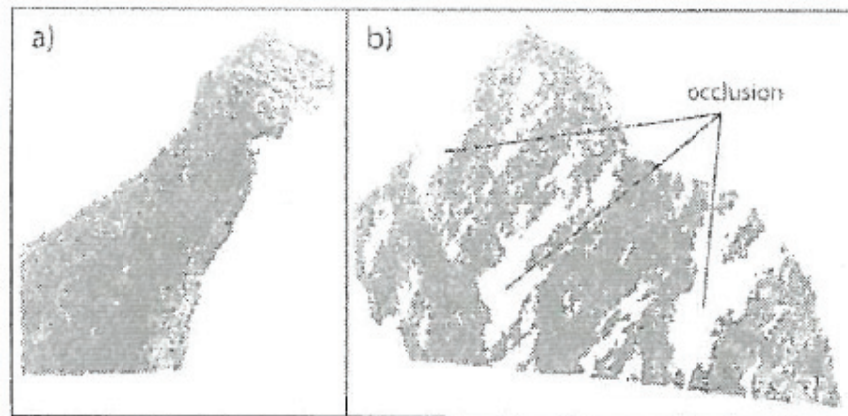
2.2.2 Applications

By processing the point cloud, surface models may be obtained giving highly accurate digital elevation models (DEM), with a resolution of 10 cm when scanning at a 500-meter distance (Sturzenegger and Stead et al 2007). Foreign objects such as vegetation or buildings may be removed so that the actual terrain surface is represented. This may then be used as input for numerical modelling. LiDAR is suitable for identifying slope instabilities and tracking rapid topographic changes. A scan creates a permanent record of the slope at a given time, and multiple scans may be taken on the same location at different times to identify volume changes and deformation patterns within the slope (Sturzenegger and Stead 2009). In this way the frequency and magnitude of the potential hazard may be evaluated (Janeras et al 2004). A LiDAR scan is highly useful for analyzing discontinuities within a slope. Fracture surfaces are detected by creating best-fit planes between adjacent points in the point cloud. Geometrical properties such as spatial location, orientation, persistence and roughness can be obtained. Compared to structural mapping in accessible outcrops in the slope, LiDAR structural mapping

covers larger sections of the slope and are thus more statistical representative. In addition, LiDAR scanning is performed at a much larger scale, giving more representative information on structures made by constrained joints, which controls the large-scale stability of the slope (Sturzenegger and Stead 2009).

2.2.3 Limitations and uncertainties

Despite the recent technology development regarding laser scanning techniques and the usefulness of such tools there are challenges that must be carefully considered when performing LiDAR-scans (Sturzenegger and Yan et al 2007). The rock mass reflectivity is controlled by a number of factors such as roughness and brightness of the scanned object in addition to its orientation relative to the scanners line-of-sight. Bright and wet surfaces typically give less reflection resulting in a less detailed point cloud due to scattering and absorption of the laser beam (Sturzenegger and Yan et al 2007). The number of reflected points also drops with increasing distance to the object. Occlusion and orientation bias reduce the number of sampled points in a scan. A rock face cannot be completely sampled from a single scanning location, and *Figure 2.1* illustrates the effect of occlusion.



*Figure 2.1: Illustrates the influence of occlusion on laser scanning measurements. a) Point cloud of a rock slope as seen from the laser scanner position. b) Point cloud of the same slope rotated using processing software showing occluded or hidden zones.
(Figure from Sturzenegger and Yan et al 2007)*

Orientation biases must also be dealt with when performing scans of slopes. First, the orientation of the rock slope with respect to the orientation of the major fracture sets may create inaccuracies (*Figure 2.2 a*). The orientation of the horizontal and the vertical line-of-scan with respect to the main fracture sets will also create a bias (*Figure 2.2 b and c*). If only single scans are completed on a rock slope, fracture surfaces may be hidden and missed on the scan, while others may be overrepresented. This phenomenon together with occlusion shows the importance of conducting several scans with different horizontal and vertical angles to the slope (Sturzenegger and Yan et al 2007).

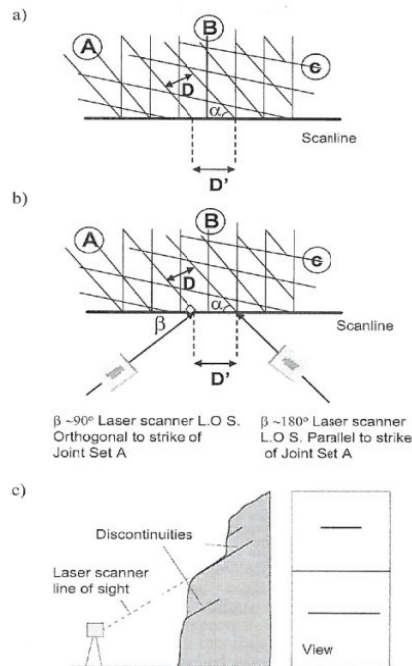


Figure 2.2: Illustration of the three forms of orientation bias. a) Rock slope orientation relative to discontinuity sets A, B and C (Terzaghi bias), b) horizontal line of sight of laser scanner with respect to rock slope (azimuth bias), c) shows discontinuity traces when line of sight is sub parallel of discontinuity set. (Figure from Sturzenegger and Yan et al 2007)

Another source of error is created by the resolution properties of the scanner. The resolution is the minimum distance between measured points, and is controlled by laser beam width, the spot spacing and distance to the scanned object (Lichti 2004). Table 2.1 give resolution measures for the Optech ILRIS-3D scanner used at Svaddenipun. The EIFOV parameter is a combined measure for effective instantaneous field of view and it defines the maximum resolution that may be obtained for a certain distance (Lichti 2004).

Table 2.1: Resolution measures for Optech ILRIS-3D scanner.
 (Table from Sturzenegger and Yan et al 2007)

Range	Angular sampling interval	Laser beam width	EIFOV
m	mm	mm	mm
5	0.13	12.85	11.0
20	0.52	15.40	13.2
50	1.30	20.50	17.7
100	2.60	29.00	25.0
200	5.20	46.00	39.8
500	13.00	97.00	84.2
800	20.80	148.00	128.6

Truncation errors in laser scanning occur when rock surfaces are too small to be measured. For a surface to be accurately measured, its dimensions have to be significantly greater than the resolution of the scanner. According to Sturzenegger and Yan et al 2007, the level of detail that can be sampled is dependent of the rock mass texture. With a GSI – value (Geological strength index) less than 40 the laser scanner is not effective in determining major fracture sets.

Due to the fact that only a proportion of a fracture surface is visible in the slope face, the measured length and persistence of discontinuities are often underestimated.

Since several uncertainties are related to the LiDAR method, this method should whenever possible be used in conjunction with other investigation techniques.

2.3 Scanning purpose and procedure at Svaddenipun

A ground based LiDAR investigation was carried out at Svaddenipun on October 13-14, 2009 (Figure 2.3). The author and Martina Böhme from the National Geological Survey of Norway (NGU) performed the scanning. An ILRIS – 3D scanner from the Canadian company Optech was used. This has a theoretical maximum range of 1500 meters, but the practical limit is found to be around 800 meters. It scans at a rate of 2000 points per second with specified range and position accuracies at 100 meters of 7 mm and 8 mm respectively. The scanner creates a point cloud, where each point consists of 3D-point coordinates and an intensity value (Sturzenegger and Yan et al 2007).



Figure 2.3: LiDAR positions (Left) and ILRIS-3D scanner at location 5 (Right). Locations 1-4 are in the valley floor and location 5 and 6 are at the top plateau. (Figure from Loftesnes 2009)

The main goals for the scanning were to extract structural geological data and to build a good terrain model of the slope including creating a digital elevation model (DEM). In addition to this it was also believed that the scans could serve as number one in a series of measurements that could detect ongoing deformations within the slope. Information on fracture spacing and roughness was not expected due to the long scanning range, The achievement of the goals is discussed in *Chapter 8*.

A total number of 7 scans were carried out, 5 from different location in the valley floor and 2 from the top plateau. The steep topography and large distances limited the number of good scanning locations. The locations in the valley floor were chosen to try to get scans from different horizontal angles, but due to the long range to the top of the slope, the horizontal spacing between locations are relatively low. As pointed out by Sturzenegger and Yan et al 2007, laser scanning point clouds undertaken from the valley floor at an elevation angle of 30-40° to a rock slope, with fracture sets dipping out of the slope may be subject to major occlusion and orientation bias. Since the scans from the valley floor falls into this category, Sturzenegger and Yan et al 2007, argues that one should try to place the scan line looking down on the slope whenever possible. Therefore two scans were performed from the top plateau,

scanning slightly downwards into the slope. GPS positions for the scanning locations were gathered together with the orientation of the scanner. Information on scanning locations is given in *Appendix 1*. An external photo from a Canon D450 camera attached on top of the scanner was taken at each location. According to Böhme 2009, this was to secure a higher-resolution picture than the one provided by the internal camera in the scanner.

The conditions for scanning were suboptimal due to an approximately 10 cm snow cover and a large distance (up to 1200 m) to the slope.

2.4 Processing of data

2.4.1 Methodology

A LIDAR-scan metafile consists of a point cloud that has to be processed in several different software's before the relevant output information is obtained.

For the Svaddenipun analysis this involved the following tasks:

- *Pre-processing by calibrating the point cloud to a digital photo and creating a file format that is readable for the main processing software PolyWorks.*
- *Filtering of the point cloud by removal of vegetation and irrelevant points.*
- *Georeferencing the scans with a digital elevation model (DEM).*
- *Creating and extracting structural planes representing rock mass discontinuities.*

The main processing software used on the Svaddenipun scans is the software *PolyWorks 11* from the company *InnovMetric*.

The following sections give an overview of the completed processing procedure, including a description of different software used. Additional information on input parameters and setup choices are given in *Appendix 2*.

2.4.2 First inspection of the scanned files

A total of 7 scans from 6 locations were performed at Svaddenipun. After a short pre-processing procedure, each of these was visually inspected in the software PifEdit from InnovMetric to get a first impression of the results. From the inspection it was obvious that the quality of the scans conducted from the valley was low due to large distance (up to 1200 meters), snow cover and orientation bias. Since the valley scans had limited reflection, the goal of creating a terrain model of the Svaddenipun slope was not achieved. Instead the focus was turned to extract structural information on discontinuities in the inaccessible top section of the slope and compare this to mapped structures. Therefore only Scan 6 from location 5 (*Figure 2.3*) and Scan 7 from location 6 at the top plateau were processed with the aim of getting structural data. There was a section between the two scans with no reflection; therefore the two scans are treated separately throughout the processing work. However the procedure for the two scans was almost identical.

2.4.3 Creating input files for PolyWorks

Some pre-processing was necessary before Scan 6 and Scan 7 could be imported to PolyWorks. First the scans were opened in the software Parser, provided by the company Optech. The Parser converts a compressed metafile (raw-data) from ILRIS-3D scans, to several different

formats that may be processed by CAD, GIS or other modelling software (Optech 2006 a). Step one was to create an 8-bit intensity file (IXF-file) from the point cloud. This was then opened in software from Optech named Matchview. This is an ILRIS-3D utility for aligning range data with digital colour photos (Optech 2006 b). Here the IXF-point cloud was calibrated with the digital photo taken from the digital camera attached on top of the scanner. By comparing pixels on the grey-scaled IXF-file and the digital photo, identical points were identified, paired and coupled (*Figure 2.4*).

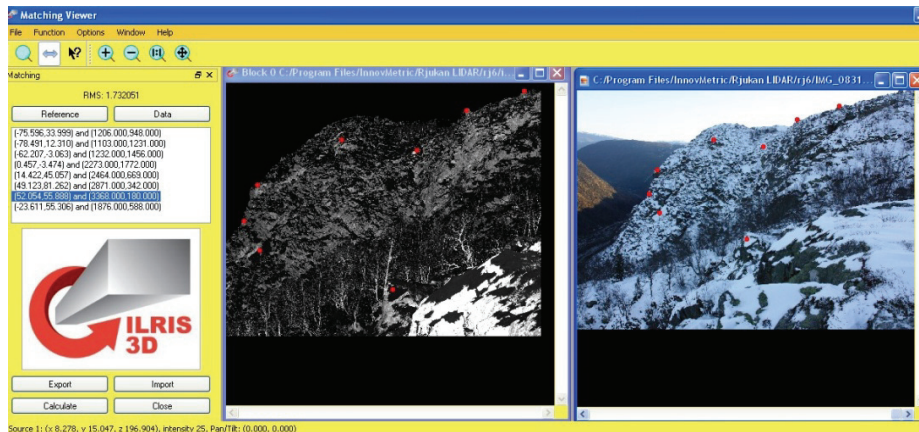


Figure 2.4: Screenshot of Scan 6 in the software Matchview during calibration of the IXF-point cloud file to a digital photo. Red marks represents identical points on scan and photo.

The number of point pairs and the RMS (Root Mean Square Error) for the matching procedure is given in *Table 2.2*. According to Optech 2006 b; a RMS value less than 2 indicate a good alignment between photo and point cloud, and both scans were thus successfully calibrated. As output from Matchview, a camera calibration file including boresight angles, camera position, and camera distortion corrections was created.

Table 2.2: Show matching parameters for the two LIDAR-Scans.

RMS values less than 2 indicate a good match.

Scan number	Scan 6	Scan 7
Number of matching pairs	8	7
RMS-Value	1,73	1,96

The next step in the processing was to use Parser to couple the camera calibration file and the 8-bit IXF file into a 24-bit coloured PolyWorks Binary Format file (PIF-file). By doing this the point cloud was given a colour and it was easy to evaluate whether points represented reflection from snow, trees or rocks. The program PifEdit, a part of the PolyWorks software package was then used to clean the scans. Trees, bushes and irrelevant points were erased manually and thoroughly in both scans, reducing the size of the files and making them easier to work with. The filtered files were then ready for processing in PolyWorks (*Figure 2.5*).

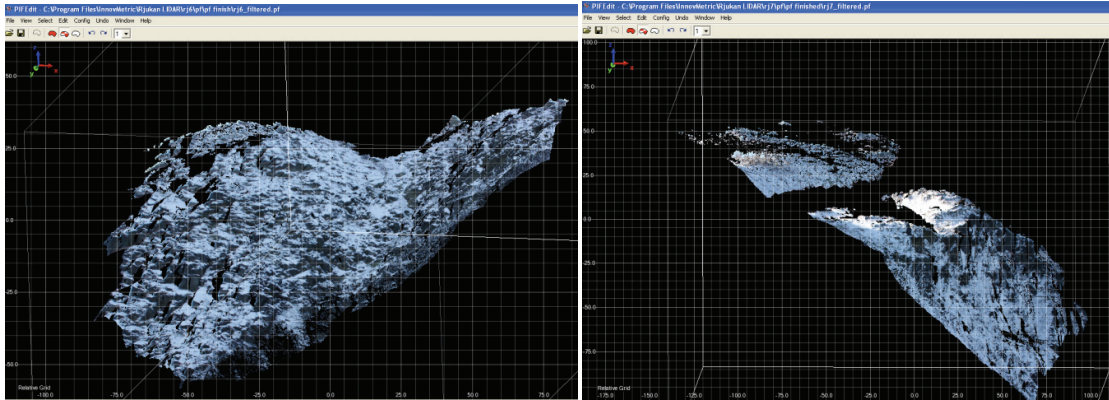


Figure 2.5: Screenshots from software pif-edit showing Scan6 (Left) and Scan7 (Right). Point cloud calibrated to digital photo makes detection of soil free surfaces easier. Effect of occlusion is shown in right scan.

2.4.4 Georeferencing data in PolyWorks

PolyWorks is one of the most used point cloud processing software in the industrial world, and it has a wide range of applications (InnovMetric 2005). It is an ideal tool for surveying and recording information from rock slope sites. The PolyWorks workflow for surveying purposes consists of the processes given in Figure 2.6 (InnovMetric 2005). Polyworks is built up as a workspace consisting of several modules performing different tasks. In the Svaddenipun analysis the modules IMAlign and IMInspect are used.


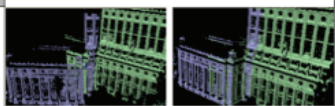


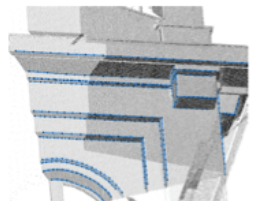

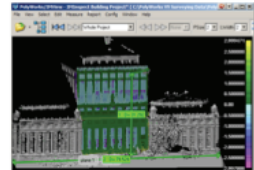
Process	Module	
Acquiring Point Cloud Data		
A. Scan the scene	 IMAlign	
B. Align the scans		
C. Geo-reference the scans		
Measuring Point Cloud Data		
A. Survey the scene	 IMInspect	 automatically extracted feature lines and measurements 
Load the aligned scans as the data object. Align the data to a global coordinate system. Then extract features, generate sections, take measurements, etc. A report can be created for each operation. Format and export detailed report items.		
B. Share/view the measurement project	 IMView	

Figure 2.6: Workflow for surveying purposes and the different modules that are applied to each task in PolyWorks. The module IMView is not used. (Figure from InnovMetric 2005)

Georeferencing the scans using a 5-meter DEM were carried out in the IMAlign module and the process is described in the following. For details regarding choice of input and calibration parameters see *Appendix 2*.

First the filtered point cloud (PIF file) was imported and the GPS-position of the LiDAR was entered. The DEM was then imported as a georeferenced point cloud from a text file with X, Y and Z coordinates. To increase processing speed, the size of the DEM file was reduced, so that only the relevant section of the slope was included. Points representing the same location on the DEM and the scan were then coupled to calibrate the scan and the DEM using the “*N-Point pair alignment function*”. 3 and 4 identical pairs were made for scan 6 and 7 respectively. To minimize errors, the function “*Best fit alignment and comparison*” was applied. This function search for point cloud points in a given maximum distance from the DEM and iterates the process until convergence is reached. Convergence was established with max search distance of 0,5 meter for Scan 6 and 1 meter for Scan 7. According to Böhme 2010 this is a good match. Next an error map showing inaccuracies in the georeferencing process was obtained (*Figure 2.7 and 2.8*).

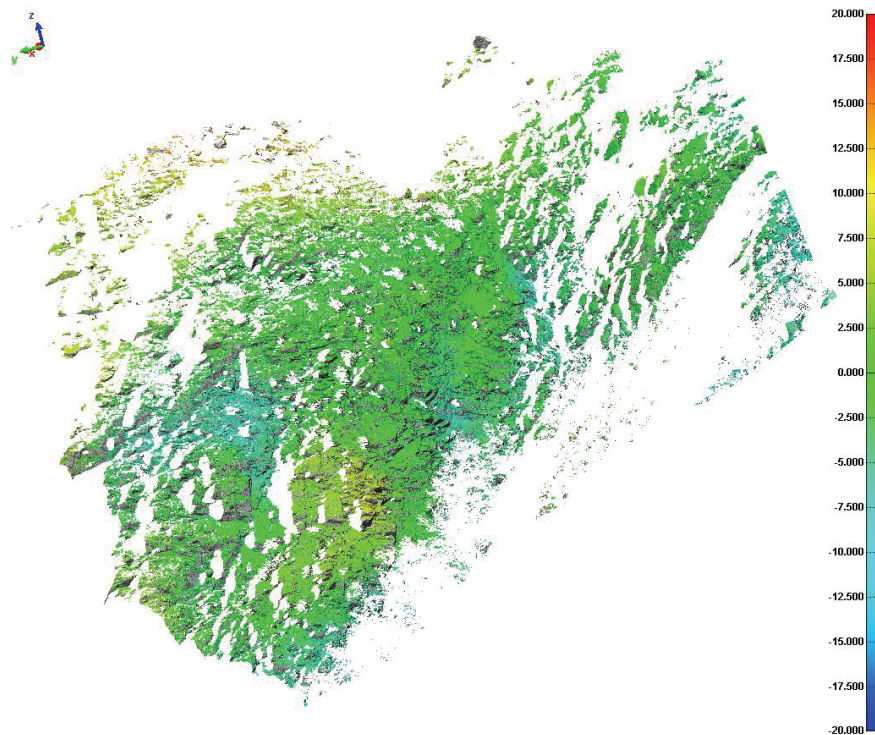


Figure 2.7: Error map of Scan 6. Show deviations between DEM and point cloud in meters, Green values indicate zero deviation. Positive value indicates that point cloud is situated on top (outside) of DEM, negative values indicate that point cloud is situated under (inside).

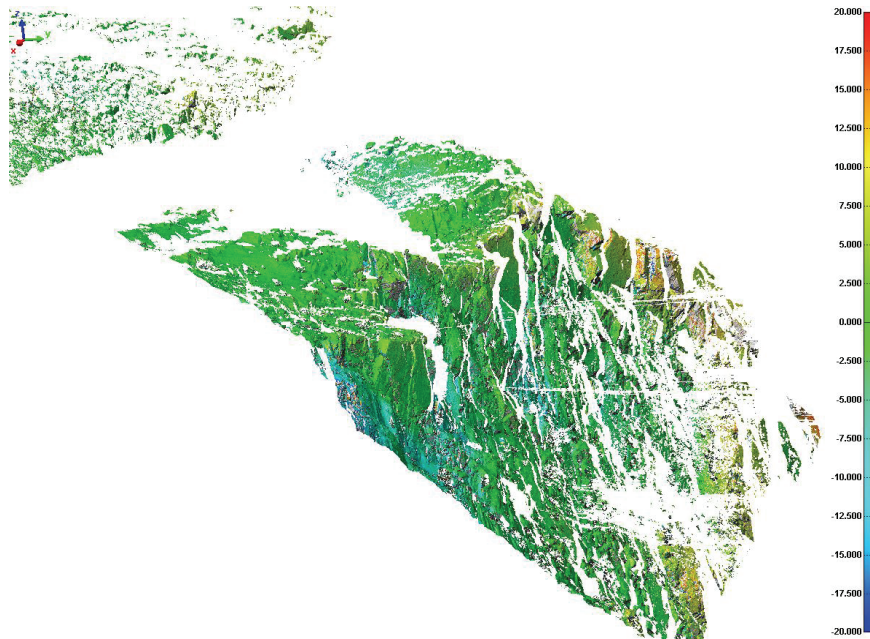


Figure 2.8: Error map of Scan 7. Show deviations between DEM and point cloud in meters, Green values indicate zero deviation. Positive value indicates that point cloud is situated on top (outside) of DEM, negative values indicate that point cloud is situated under (inside).

Most deviations are less than 10 meters, particularly in the areas of main interest in the cliff face. Some areas in the periphery have up to 20-meter difference. According to Oppikhofer 2010, results are good considering the type of information that is to be extracted from the scans (orientation data only), and the 5-meter inaccuracy of the DEM itself. As discussed in a subsequent chapter, other sources of error are expected to be considerably larger.

2.4.5 Extracting structural data in PolyWorks

After the scans were georeferenced, the IMAlign project was imported to the PolyWorks module IMInspect. Scan 6 was imported as a “*huge data file*”. This feature is suitable for inspecting large point clouds. The scan is divided into user-defined grids, and by choosing the areas of interest, only parts of the point cloud are inspected at the same time, and the need for computer memory is reduced (InnovMetric 2005). The IMAlign file for Scan 7 however was so large that it could not be opened as a “*huge data file*”, and was imported without corrections. The working unit in IMInspect was millimetres so conversion into meters for both scans also had to be carried out. The next step was to create planes that represent discontinuities in the rock mass (Figure 2.9 and 2.10). This was done by the option “*create plane*” in IMInspect, by using the “*point fit*” method. This feature let you select points on an assumed fracture surface and the program then uses the least square approach to find the best fitted plane (InnovMetric 2009). The number of planes that was created was 84 for Scan6 and 59 for Scan 7.

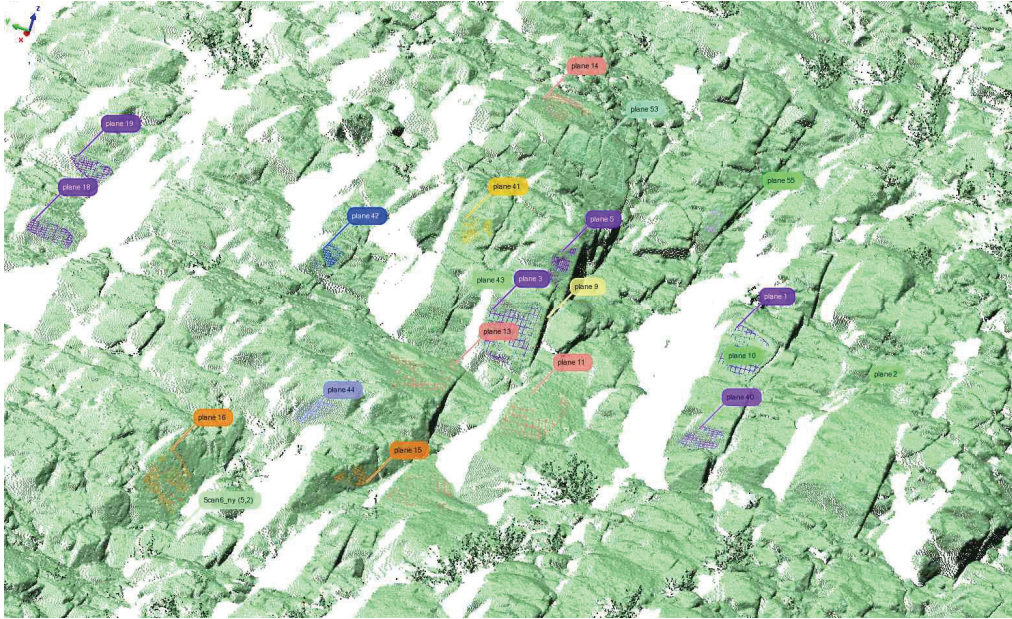


Figure 2.9: Screenshot IMInspect from a section of Scan 6. Marked planes are shown.

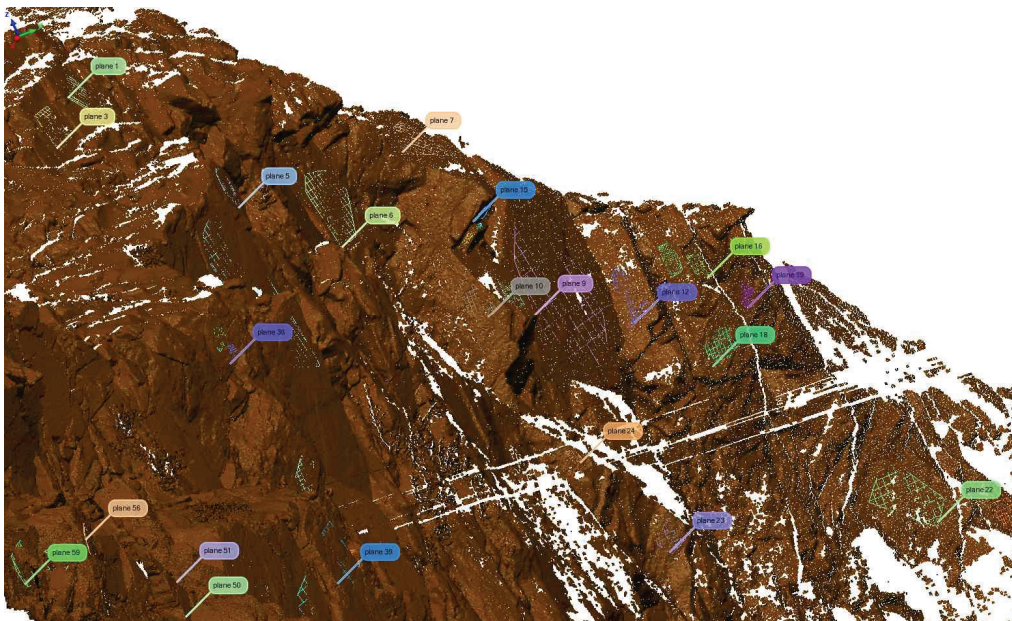


Figure 2.10: Screenshot IMInspect from a section of Scan 7. Marked planes are shown.

When selecting planes a thorough comparison to the photos from the locations was performed to ensure that the marked planes represent actual snow-free fracture surfaces in the rock slope. To limit uncertainties, no snow-covered planes were selected.

The final step in the PolyWorks processing was to extract the information on orientation of the selected planes. The azimuth system in PolyWorks does not correspond to the standard coordinate system used in geotechnical engineering, and angles with respect to X, Y and Z-axes must therefore be converted. A macro feature developed by NGI was used to convert and extract dip and dip/direction for the surfaces. The results were finally imported to the software Dips from Rocscience, allowing stereoplots to be created.

Chapter 3: Methodology for rock slope stability analysis

3.1 Introduction

A large number of different methods are applied to rock slope stability analyses, and they may be subdivided by several different classification systems. The choice of method should always be based on the available geological information, and whenever possible, several methods should be applied to the same problem to get independent results. According to Nilsen and Palmstrøm 2000, stability analysis of rock slopes follows a three-step procedure:

- 1: *Definition of the potential stability problem (including kinematic analysis)*
- 2: *Quantification of input parameters*
- 3: *Calculation of stability*

For the analysis of Svaddenipun, step 1 is described in Loftesnes 2009, while step 2 and 3 are the focus in this thesis. For the calculation of stability, a number of different techniques may be applied including the following (Nilsen and Palmstrøm 2000):

- *Empirical analysis*
- *Limit equilibrium methods*
- *Numerical analysis*
- *Physical models*
- *Probabilistic methods*

Stability analysis may also be divided into analytical or empirical analysis. Analytical approaches are based on calculations or modelling, while empirical methods are based on experience and comparison to other case studies (Nilsen and Palmstrøm 2000). *Figure 3.1* gives an overview of different analytical methods and their subgroups.

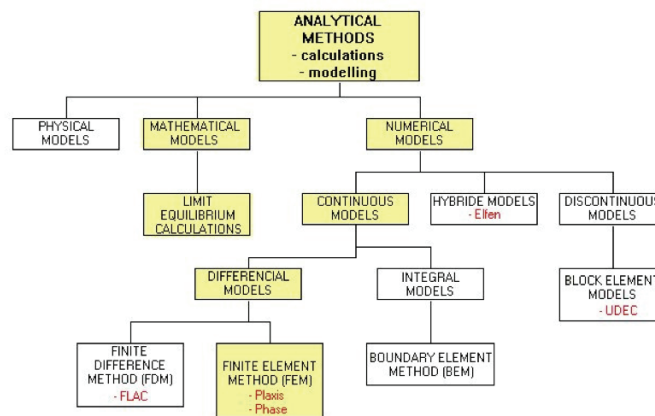


Figure 3.1: Flowchart shows different analytical methods for slope stability analysis. Different commercial codes are given in red. (Figure modified from Nilsen and Palmstrøm 2000)

The choice of analysis method should be based on the geological conditions and particularly the present failure mechanisms in the rock slope. Result of analysis from different methods is sensitive to the complexity of the failure surface within the slope (*Figure 3.2*). Traditional kinematic and limit equilibrium analysis are applied to problems including simple translational shearing along defined sliding surfaces (Stead and Eberhardt et al 2006). For complex failure

surfaces including a stepped failure surface and degradation of intact rock, numerical methods, both continuous and discontinuous may be applied. If also rotational mechanisms are present the application of hybrid models are useful.

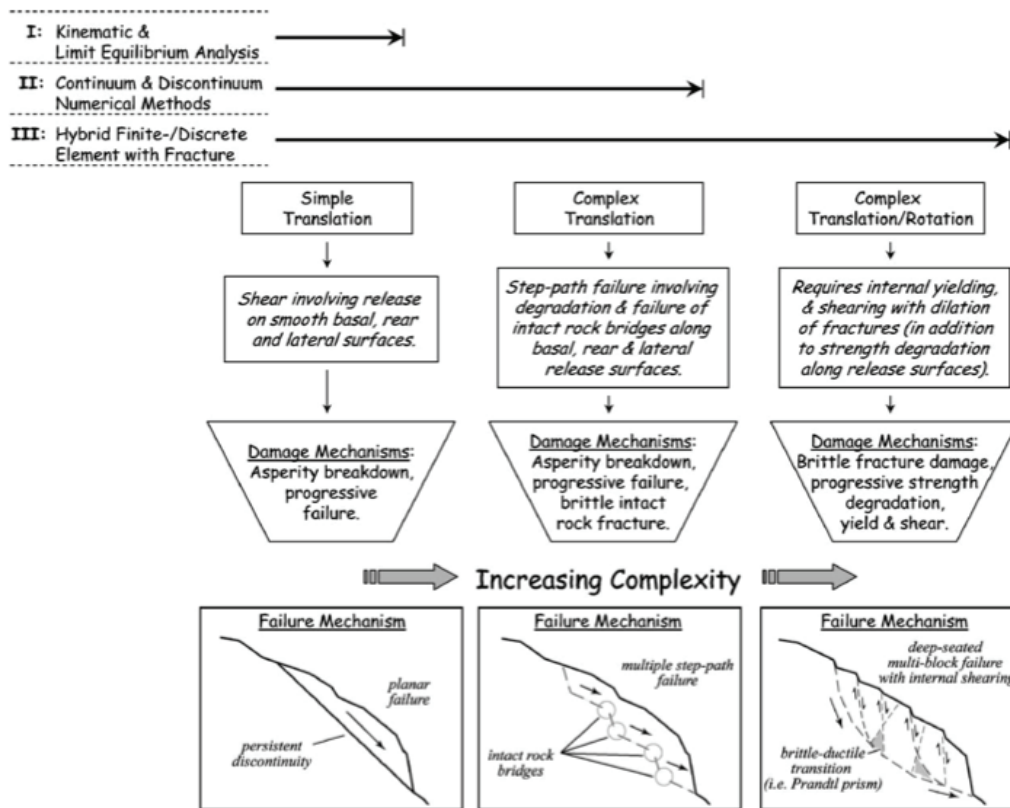


Figure 3.2: Flowchart for different levels of slope stability analysis showing which failure mechanisms they may be applied to. (Figure from Stead and Eberhardt et al 2006)

A short introduction to the two most frequently used analytical methods in slope stability analyses is presented in the following sections.

3.2 Limit equilibrium analysis

Limit equilibrium methods (LEM) are mathematical methods and have traditionally been the most common tool for rock slope stability calculations. Most commonly, it has been a deterministic analysis but lately much available software also incorporate probabilistic techniques to this method (Stead and Eberhardt et al 2006). The LEM-approach determines the FOS along a critical failure surface, given as the ratio between the material strength and the shear stress acting on the surface (Coduto 2007). Theoretically, failure occurs when driving forces (gravity and water pressure) overcome resisting forces (friction and cohesion) over the entire length of the failure surface. A prerequisite for a successful limit equilibrium analysis is the definition of the critical failure surface. After this is established, most FEM methods divide the failure mass into a number of slices in such a way that the bottom of each slice is considered to be a straight line consisting of a homogenous material (Figure 3.3).

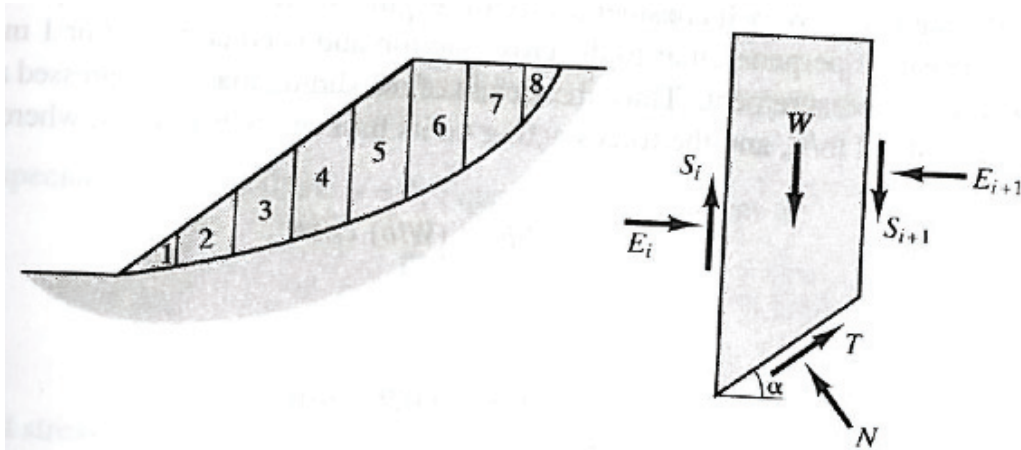


Figure 3.3: Subdivision of a slope into a number of slices. Right figure show sum of forces acting on one slice. (Figure from Coduto 2007)

The sum of forces acting on each slice is then calculated. Problems with more than one slice are statically indeterminate and simplifying assumptions must be introduced to overcome this problem. This leads to several variants of the LEM's such as the Bishop, Janbu and Morgenstern-Prince methods (Coduto 2007)

The limit equilibrium method is already a popular tool for slope stability analysis and has gained widespread acceptance throughout the engineering world. It is often used as a first approach to stability analysis due to its simplicity and easy availability through a wide range of different software. Still, limitations are involved and whenever possible, the FEM should be applied in combination with other methods such as numerical modelling to maximize advantages of both techniques. Table 3.1 summarizes properties of limit equilibrium method.

Table 3.1: Properties of limit equilibrium method. (Table modified from Broch and Nilsen 2001, and Stead and Eberhardt et al 2006)

Method	Critical input parameters	Advantages	Limitations
Limit equilibrium method	Representative geometry, material/joint shear strength, material unit weights, groundwater and external loading/support conditions.	<p>Much software available for different failure modes (planar, circular, wedge, toppling, etc.).</p> <p>Mostly deterministic but some probabilistic analyses in 2-D and 3-D with multiple materials, reinforcement and groundwater profiles.</p> <p>Suitable for sensitivity analysis of FOS to most inputs.</p> <p>Suitable for back-calculations.</p>	<p>FOS calculations must assume instability mechanisms and associated determinacy requirements.</p> <p>In situ stress, strains and intact material failure not considered. Failure occurs only along predefined weak surfaces.</p> <p>Cannot handle progressive failure trough intact rock or time- dependent creep.</p> <p>Simple probabilistic analyses may not allow for sample/data covariance.</p>

3.3 Numerical analysis

3.3.1 Numerical analysis in general

Numerical modelling is now used routinely in civil engineering and mining engineering, also in the assessment of slope stability (Stead et al 2006). The recent development on computer capacity allow more and more complex problems to be analyzed, and further development will allow huge amounts of data to be included in numerical models. Also the high availability of commercial numerical modelling codes allows such analysis to be applied to a great extent (Stead and Eberhardt et al 2006). Numerical analysis is a sub group of the analytical methods. As opposed to limit equilibrium methods, numerical models calculate the FOS without any pre-defined assumptions on location of the sliding planes (Wyllie and Mah 2004). When the slope instability is complex, numerical methods are stronger than limit equilibrium methods. By trying to represent the rock mass mechanical response to a set of initial conditions, including stresses, water levels and boundary conditions, numerical techniques have proved to be powerful tools for slope stability assessment.

3.3.2 Continuous models vs. discontinuous models

Numerical methods involve discretization of the rock mass into a number of individual elements (Nilsen and Palmstrøm 2000). Each zone is given a material model with specific properties; this could be either pure elastic or elastic-plastic. Based on these properties, the magnitudes and directions of stresses for all nodal points are calculated. The zones may be connected together making a continuous model, or separated by discontinuities allowing slip and separation between blocks. Such models are termed discontinuous (Wyllie and Mah 2004).

Continuous models are the most used numerical analysis tools. The rock slope is treated as a continuous medium consisting of a number of elements connected together. In most slope stability problems, fracturing plays an important role, and this must be included also in continuous models. Discontinuities are therefore represented explicitly, and treated as special cases, by introducing joint elements of zero, or very thin, thickness between continuum bodies. They can have elastic or elasto-plastic response to stresses exceeding the discontinuity strength (Hammah and Yakoub et al 2007). Continuous models are subdivided into the following categories (*Figure 3.1*):

- *Differential models such as Finite Element Method (FEM) or Finite Difference Method (FDM).*
- *Integral methods, such as the Boundary Element Method (BEM)*

Discontinuous models on the other hand are based on a method designed to analyze discontinuum, and treats continuum behaviour as a special case. This model can handle a large number of discontinuities, by dividing the domain into blocks that may be either deformable or rigid (Wyllie and Mah 2004). The individual blocks are interacting along their boundaries. Where the rock slope stability seems governed by movement along joint-bounded blocks or intact rock deformation, discontinuum discrete-elements are suitable. The most used discontinuum model is the distinct-element code UDEC. *Table 3.2* compare continuous models and discontinuous models and highlight advantages and limitations.

Table 3.2: Properties of continuous and discontinuous numerical methods. (Table modified from Stead and Eberhardt et al 2006)

Method	Critical input parameters	Advantages	Limitations
Continuum modelling (DEM, FDM)	Representative slope geometry; constitutive criteria (e.g., elastic, elasto-plastic, creep, etc.); groundwater characteristics; shear strength of surfaces; in situ stress state.	<p>Allows for material deformation and failure, including complex behavior and mechanisms, in 2-D and 3-D with coupled modelling of groundwater.</p> <p>Can assess effects of critical parameter variations on instability mechanisms.</p> <p>Can incorporate creep deformation and dynamic analysis.</p> <p>Some programs use imbedded language (e.g., FISH) to allow user to define own functions and subroutines.</p>	<p>Users should be well trained, experienced, observe good modelling practice and be aware of model/software limitations.</p> <p>Input data generally limited and some required inputs are not routinely measured.</p> <p>Sensitivity analyses limited due to run time constraints, but this is rapidly improving.</p>
Discontinuum modelling (DEM, DDA)	Slope and discontinuity geometry; intact constitutive criteria (elastic, elasto-plastic, etc.); discontinuity stiffness and shear strength; groundwater and in situ stress conditions.	<p>Allows for block deformation and movement of blocks relative to each other.</p> <p>Can model complex behavior and mechanisms (combined material and discontinuity behavior, coupled with hydro-mechanical and dynamic analysis).</p> <p>Able to assess effects of parameter variations on instability.</p> <p>Some programs use imbedded language (e.g., FISH) to allow user to define own functions and subroutines</p>	<p>As above, experienced users needed.</p> <p>General limitations similar to those listed above.</p> <p>Need to simulate representative discontinuity geometry (spacing, persistence, etc.).</p> <p>Limited data on joint properties available (e.g., joint stiffness).</p>

Chapter 4: Stability analysis of the Svaddenipun slope

4.1 Introduction

As described in *Chapter 1.3* the aim of the Svaddenipun stability analysis is to detect the location of the failure surface and evaluate FOS for different critical shear zone material strengths. The analytical technique that is assumed to fulfil the investigation aims in a best possible way for the Svaddenipun slope is a numerical finite element model using the shear strength reduction method (SSR). In this chapter the chosen approach is presented and justified. Then the methodology for the Svaddenipun numerical analysis is presented.

4.2 Finite Element Method

4.2.1 FEM in general

The finite element method is the most widespread numerical analysis tool in geotechnical engineering (Hammah and Yakoub et al 2007). For slope stability analysis, this method has not received too much attention until recently (Hammah and Yakoub et al 2006). The finite element code is a continuum model and it is suited to analyze a broad range of problems, including complex geometries, stress simulations and material behaviour (Rocscience 2004). The rock mass is considered as a continuum, and divided into a finite number of elements with intersecting nodes. From this element mesh, forces and displacements are calculated for each node giving output stresses and displacements. The main advantages of the FEM are the ability to handle multiple materials in a single model, combined with the possibility to accommodate non-linear material responses, and the ability to involve complex geometries. FEM codes can however not model large strains and do not allow the detachment of individual blocks (Hammah and Yakoub et al 2007).

4.2.2 Shear Strength Reduction Analysis (SSR)

In slope stability evaluations the most popular analytical investigation method has been the determination of the factor of safety. FOS is determined as the ratio of the actual shear strength to the minimum shear strength required to prevent failure (Wyllie and Mah 2004). The shear strength reduction technique introduced by Zienkiewicz et al 1975, computes the FOS by reducing the shear strength parameters until failure occurs. This technique uses finite element or finite difference codes to run a series of simulations with increasing trial factors for safety (f). Actual shear strength properties such as cohesion (c) and friction angle (ϕ) are reduced for each simulation according to the following equations:

$$c_{trial} = \left(\frac{1}{f}\right) \cdot c \quad [Equation 4.1]$$

$$\phi_{trial} = \arctan\left(\frac{1}{f}\right) \cdot \tan\phi \quad [Equation 4.2]$$

The trial factor f is systematically increased until the slope fails. This is represented as the point where the numerical solution does not converge, and the reduction value, termed as the strength reduction factor (SRF), equals the factor of safety (FOS). The approach is best described for materials following the linear Mohr-Coulomb strength criteria, but also the non-linear generalized Hoek-Brown criteria may be used (Hammah and Yakoub et al 2005). The procedure for determining the critical strength reduction factor is as follows:

Step 1: Develop a finite element model of the actual slope including geometrical parameters, material deformation and strength properties. Compute the model and extract the maximum total deformation.

Step 2: Increase the trial factor (f) according to a pre-defined algorithm and calculate factored Mohr-Coulomb material parameters from Equations 4.1 and 4.2. Apply the new strength values into the slope model and re-compute the maximal total deformation.

Step 3: Repeat Step 2 with systematic increments of f until the finite element model reaches non-convergence and becomes numerically unstable. The value of f where this occurs is the factor of safety for the slope.

Lack of convergence indicates that for the chosen strength parameters, the stress- and displacement distributions that satisfy the equations of equilibrium cannot be established. This leads to a rapid increase in deformations. As long as an appropriate number of iterations and tolerance criterion are selected, non-convergence for the model acts as a reasonable indicator for slope failure (Hammah and Yakoub et al 2007).

The shear strength reduction method (SSR) has several advantages over other analytical techniques, including the limit equilibrium method. The method may be easily used in all FEM software. It can be explicitly expressed both in terms of principal-, and shear-normal stresses. It is thus a simple, but reliable method (Hammah and Curran et al 2004). A major advantage of the method is that no a priori assumption of the shape and location of the failure surface is needed, since this is determined by the calculations and shown as concentrations in shear strain. In this way the responsible failure mechanism may be addressed. There are also no prior assumptions regarding inclinations and locations of inter-slice forces in the model. As opposed to limit equilibrium methods, numerical models always satisfy translational and rotational equilibrium (Wyllie and Mah 2004). Furthermore the SSR technique is capable of modelling progressive failure and deformations due to given stress situations (Hammah and Curran et al 2004).

4.3 Analysis method chosen for the Svaddenipun slope

Based on the described aims of the stability analysis in combination with available methods in the thesis description, the chosen approach for the Svaddenipun slope is a FEM–SSR analysis. Due to the uncertain location and complexity of the failure plane, this technique is found useful for the analysis and chosen over the limit equilibrium method, where a failure surface must be defined prior to analysis. This is in accordance with *Figure 3.2*, showing that numerical methods are suitable for complex, stepped failure mechanisms. From a practical point of view, the chosen FEM software Phase² is commercially available, and both the NGI and the NTNU have a user's licence, so it was easy to obtain. Due to the high uncertainty of the shear zone input parameters, a parameter study is carried out. This is assumed to be an acceptable alternative to a probabilistic analysis in a LEM model and, and due to the high uncertainties in input parameters, it is not believed that the accuracy of results would be better with advanced probabilistic simulations.

4.4 Finite element numerical modelling with Phase²

4.4.1 About Phase²

The numerical modelling of Svaddenipun is carried out using the finite element software Phase² from the company Rocscience. Phase² is a 2D elasto-plastic stress analysis program that may be applied to a wide range of engineering problems including:

- *Underground or surface excavations in soil/rock including support elements.*
- *Groundwater seepage analysis.*
- *Slope stability analysis with the Shear Strength Reduction (SSR) method.*

The program allows multi-stage models to be created and analyzed, and several material models may be applied including the Mohr-Coulomb and Hoek-Brown criteria's. Material models are mathematic relations between stresses and strains that try to represent the real material properties found in the rock/soil. The finite element model also includes the ability to include rock joints, these may be created discrete, or trough statistical models (Rocscience 2010 a). For the slope stability analysis at Svaddenipun the shear strength reduction technique is applied to obtain simulations of critical FOS, location of the failure surface, and the failure mechanism. A detailed description of the Phase² features is given in Rocscience 2010 c.

4.4.2 Choosing the optimal numerical method

Numerical modelling is a common used tool trying to represent the reality in the best possible way. However the results will never represent the exact conditions in a rock slope or around an excavation. The different numerical methods have both advantages and disadvantages, and they should be applied with caution and high level of expertise. Different methods are suited for different ground conditions and type of problem.

FEM–SSR analysis for rock slope stability has proved to produce similar results as limit equilibrium methods (Hammah and Curran et al 2004). According to Rocscience 2004, SSR–analysis is particularly useful when several modes of failure are present. This is assumed to be the situation at Svaddenipun since no simple planar sliding along shear zone seems likely. Calculating areas of high shear strain detects the most probable failure surface location. Although FEMs generally cannot include large deformations, the SSR approach may be useful since deformations are generally small prior to failure (Hammah and Yakoub et al 2007). In SSR–analysis there is no need to calculate large strains since it is assumed that the critical strain values detected by the SSR – method represents the slope at the point of failure. If the slope reaches initial failure, this will result in a total collapse, and the exact amount of strain is not important. The ability of modelling progressive failure through intact rock, combined with simulations of *in situ* stresses including groundwater also favours the use of FEM–SSR method.

One question that arises when FEM is used in slope stability analysis is the handling of discontinuities in the rock mass. FEM models do not have the same ability as distinct element methods to simulate large displacements along fractures. Still the FEM numerical tool chosen for the Svaddenipun analysis have the opportunity to include jointing. Introduction of joints in FEM increase the degrees of freedom and may lead to numerically unstable solutions (Hammah and Yakoub et al 2007). Therefore the jointed area at Svaddenipun was reduced to contain only the most critical sections.

4.4.3 Methodology for Phase² numerical analysis, and subdivision of model setups

Two different analytical techniques were made available for the stability analysis in the thesis assignment; limit equilibrium analysis using software Slide, or finite element modelling with SSR analysis in Phase². The first step in the modelling process was thus to choose the optimal method for this analysis. After choosing Phase², a literature study and tutorial training was conducted to learn the software. Then the geometrical model was constructed and boundary conditions evaluated before input parameters for the different materials were obtained. Both field data and reference literature was used.

The next step in the modelling was the simulations of the different model setups. A total of 35 individual simulations were performed in 3 different steps, and the modelling procedure is described in the following:

- 1 *“Svaddenipun 1 – model” setup:*
The first calculations were performed with the initial, most probable estimates on strength parameters for metarhyolite and K1 fracture set. Shear zone parameters was found from literature study of the Åknes rock slope, western Norway. Due to the importance, but high degree of uncertainty regarding the shear zone properties, it was soon discovered that assessment of exact values for this zone was inexpedient. Thus the focus of the numerical analysis shifted towards a parameter study approach (see Chapter 5.8). This included variations of shear zone strength properties until critical SRF – values of 1,0 were obtained, representing the transition from stable to unstable slope conditions. In this way the critical shear zone parameters and their probability of appearance could be discussed. After completing the search for critical SRF – values for the dry slope, a piezometric line was added to the models. All model calculations were then repeated to simulate conditions with partially saturated conditions, and a search for critical saturated shear zone parameters was conducted. All relevant Phase² – files are listed in Appendix 3 and included in Appendix 8. Files from this first part of the simulations are named Svaddenipun 1 – files. File names in the Appendices also include the shear zone strength parameters and the water conditions for the specific model.

- 2 *“Svaddenipun 2 – model” setup:*
Next, simulations with 30% reduced metarhyolite and K1 fracture set strength parameters were performed, both with literature – based (Åknes) shear zone parameters and with a search for the critical shear zone strength values. Calculations both with dry- and partially saturated slope conditions were performed. This model setup is named “Svaddenipun 2” – model, and relevant files are listed in the Appendices.

- 3 *“Svaddenipun 3 – model” setup:*
Finally, simulations with 30% increased metarhyolite and K1 fracture set strength parameters were performed, both with literature – based (Åknes) shear zone parameters and with a search for the critical shear zone strength values. Calculations both with dry- and partially saturated slope conditions were performed. This model setup is named “Svaddenipun 3” – model, and relevant files are included in the Appendices.

After completing the calculations, results were presented and interpreted. The final task was then to discuss slope stability based on the findings.

Chapter 5: Svaddenipun model setup and input parameters

5.1 Introduction

This chapter describes the construction of the numerical model in Phase². All input parameters are presented and evaluated in addition to a presentation of the model setup in Phase². A complete overview of the type of analysis carried out and the applied input parameters can be found in the Info-viewer included in each Phase² file in *Appendix 8*.

5.2 Slope model

5.2.1 General settings

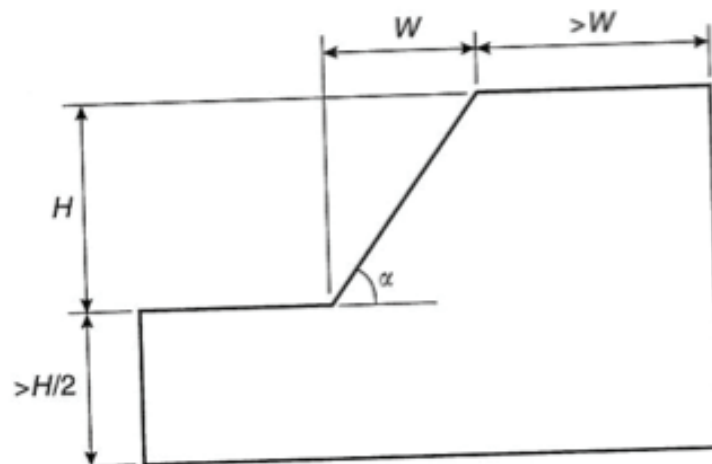
The conducted Phase² finite element analysis is a single stage plain strain analysis with a Gaussian type solver. Stresses are simulated with maximum 500 iterations and with tolerance set to 0,001, using absolute energy as convergence criteria.

5.2.2 Geometry

The numerical analysis is carried out using a 2D cross section profile along the steepest section of the slope. The location of the profile is given in *Figure 1.4*, and crosses trough Section A, that is assumed to have the highest probability of failure. The profile lies perpendicular to the valley slope, fracture set K1, and the shear zone. The profile rises from valley floor to the top plateau located around 1130 m.a.s.l. The profile was constructed manually from a 5-meter elevation map.

5.2.3 Boundary conditions

The far-field boundaries of the model are chosen based on recommendations by Wyllie and Mah 2004 presented in *Figure 5.1*.



*Figure 5.1: Recommendations for size of numerical model to avoid boundary effects.
(Figure from Wyllie and Mah 2004)*

Based on recommendations in Rocscience 2010 c, all boundary elements are fixed both in horizontal and vertical directions, except along the slope surface. This is free to move in both directions.

5.2.4 Shear Strength Reduction setup

By default, the SSR analysis search for the global critical strength reduction factor within the entire model. By selecting a defined SSR search area, the possibility of detecting the SRF from an area not of interest within the model is excluded. SSR may only be applied to plastic materials, and when the SSR area is chosen, all elements outside the area is defined as elastic. Only materials inside the SSR area are considered to be plastic and may fail (Rocscience 2010 c). The main focus of the Svaddenipun stability analysis is concentrated to the upper half of the slope. The SSR-search area where shear strength reduction analysis is carried out is thus defined from the section recognized by the transition from talus slope to cliff face at around 725 m.a.s.l., to the top of the slope. Failure within the slope is also assumed to occur along the shear zone or in the overlying metarhyolite.

In addition to the search area of the SSR analysis, several parameters influence on the convergence of the analysis, and thus whether the slope will fail or not. According to Hammah and Yacoub et al 2006 such parameters include:

- *The type of stopping criterion.*
- *The tolerance value of the stopping criterion.*
- *The number of iterations allowed before a solution is defined as non-convergent.*

Based on findings in Hammah and Yacoub et al 2006, the following parameters were chosen for the Svaddenipun model (*Table 5.1*):

Table 5.1: SSR convergence parameters.

Stop criteria	<i>Square root energy</i>
Tolerance value	<i>0,001</i>
Maximum number of iterations	<i>500 (increased from 300 compared to Hammah and Yacoub et al 2006)</i>

5.2.5 Mesh setup

According to Hammah and Yacoub et al 2006, the use of a 6 node triangular mesh is suitable for slope stability analysis. Rocscience 2004 supports this statement, where the use of a 6 noded triangular mesh gave the closest agreement with similar LEM – calculations. Hammah and Yacoub further argue that number of mesh elements has a minor impact on computed factor of safety. Based on this the mesh generated for the Svaddenipun model uses a 6 noded uniform triangular mesh with approximate number of elements set to 800. This is also in accordance with recommendations in Rocscience 2010 c.

5.3 Slope materials and failure criterion

5.3.1 Introduction

The Svaddenipun slope model consists of two different lithologies; the metarhyolite and the shear zone. Several failure criteria are common in rock slope stability analysis and the choice of the correct material failure criterion is vital for the results of the numerical simulation. The most known and accepted criteria's are the linear Mohr-Coulomb criterion and the empirical and non-linear Hoek-Brown criteria. In the following sections, the different materials and their corresponding failure criterion for the numerical modelling are described.

5.3.2 Metarhyolite

Metarhyolite is the major lithology present within the Svaddenipun slope. To reduce computation time, the metarhyolite is divided into a plastic and elastic region, where only the sections in the upper part of the slope close to valley surface are subjected to a plastic analysis. This is done based on methodology found in Grøneng 2010, and focus in the model is thus concentrated to the upper slope shear zone and the surrounding jointed rock mass. Material parameters for the metarhyolite are based on field data and Hoek-Brown classification system. These parameters are then converted to Mohr-Coulomb before applied in Phase².

Generalized Hoek-Brown criterion for metarhyolite

The generalized Hoek-Brown failure criterion has gained popularity and acceptance through applications in a large number of projects around the world (Hoek and Carranza-Torres et al 2002). The empirical criterion may be expressed as

$$\sigma'_1 = \sigma'_3 + \sigma_{ci} \left(m_b \frac{\sigma'_3}{\sigma_{ci}} + s \right)^a \quad [\text{Equation 5.1}]$$

where

- σ'_1 and σ'_3 are major and minor effective principal stresses
- σ_{ci} is uniaxial compressive strength for the intact rock
- m_b is the Hoek-Brown constant for the rock mass given by the relationship $m_b = m_i e^{\left(\frac{GSI-100}{28-14D}\right)}$ where GSI = Geological strength index, D is disturbance factor, and m_i is Hoek-Brown constant for intact rock mass.
- s and a are material constants depending on the rock mass characteristics expressed as $s = e^{\left(\frac{GSI-100}{9-3D}\right)}$ and $a = \frac{1}{2} + \frac{1}{6} \left(e^{-GSI/15} - e^{-20/3} \right)$

In order to use the Hoek-Brown criterion for estimating strength and deformability of rock masses the following parameters must be determined (Hoek 2000):

- Uniaxial compressive strength (σ_{ci}) of intact rock.
- Value of Hoek-Brown constant for intact rock pieces (m_i).
- Geological Strength Index value (GSI -value) for the rock mass.
- Disturbance factor D depending upon the degree of disturbance due to blast damage and stress relaxation. D varies from 0 for undisturbed in situ rock to 1 for disturbed rock mass.

According to Hammah and Curran et al 2004, the non-linear Hoek-Brown criterion is more suitable for predicting failure of rock masses compared to the Mohr Coulomb criterion. This is mainly due to its non-linearity and the ability to represent more accurate values at high and low stress condition. In the Svaddenipun slope, low stresses are expected due to the low overburden of the rock mass.

The Hoek-Brown criterion assumes isotropic rock masses, and should be used with caution whenever rock masses are structurally controlled by only one fracture set (Hoek 2000). Figure 5.2 show guidelines for when the criteria should be used. The metarhyolite is governed by three fracture sets, however the set K1 is assumed to have a major influence on large-scale stability. Hoek-Brown criterion may in this way be suboptimal, however the Hoek-Brown material model includes a quantification of rock mass properties, this increases the reliability compared to direct application of other material models. An alternative material model using intact rock

properties would result in to optimistic parameters and the Hoek-Brown criterion is chosen for the metarhyolite.

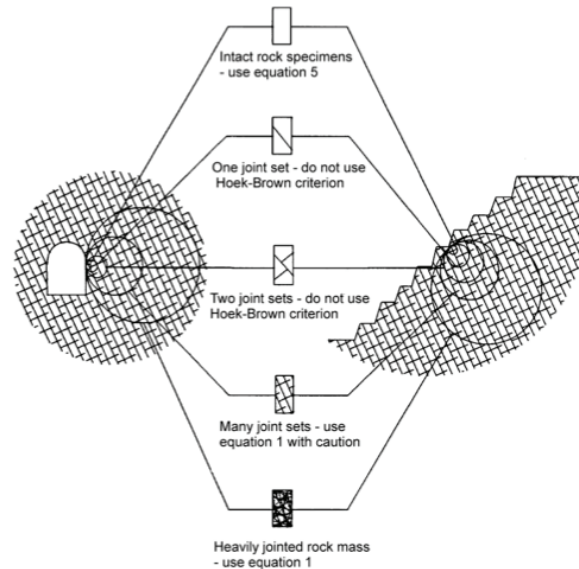


Figure 5.2: Guidelines for using Hoek-Brown material model for different rock masses. Equation 1 referred to in the figure is the same as Equation 5.1 in the text above. Equation 5 referred to in the figure 5 is the same as to Equation 5.1 in the text above with $a=0,5$. (Figure from Hoek 2000)

Hoek-Brown parameters for metarhyolite

Hoek-Brown parameters for the Svaddenipun slope were chosen based on field measurements and guidelines given in Software RocData from Rocscience and are listed in Table 5.2. The geological strength index (GSI) is used to describe the materials. The metarhyolite is assumed to have a blocky structure with good surface conditions. Hoek Brown parameters m_i and MR are average rhyolite values found in RocData user manual. The disturbance factor D expresses the mechanical stresses that a rock mass have been exposed to during history. The factor is mainly used related to mechanical excavation by humans related to tunnel blasting or open pit slope mining. The Rock mass at Svaddenipun may however also have been exposed to mechanical disturbance during the last glaciations. According to RocData manual a D -value of 0,7 may be applied to slopes that have undergone smooth blasting. The effect of ice at Svaddenipun is assumed to be less than this, and after discussion with the main thesis supervisor, D -value for the metarhyolite is set to 0,5.

Table 5.2: Hoek-Brown parameters representing the Svaddenipun metarhyolite.

Parameter	Metarhyolite
σ_{ci} [Mpa]	181
m_i	25
GSI	65
D	0,5
MR	400

Conversion of metarhyolite parameters from Hoek-Brown to Mohr-Coulomb criterion

The most frequently used failure criterion in geotechnical engineering is the classical Mohr-Coulomb failure envelope introduced by Coulomb in 1773, and most numerical software can apply this criterion for slope stability analysis. The criterion describes the linear relationship between normal and shear stresses at failure along a rock surface expressed as:

$$\tau = c + \sigma_n \cdot \tan \phi \quad [\text{Equation 5.2}]$$

where

- τ = shear stress
- c = cohesion
- σ_n = normal stress
- ϕ = friction angle of the material

Application of the Hoek-Brown criterion in FEM – SSR analysis is not straightforward. The non-linear criteria induce difficulties in finding closed form equations for the factored Hoek Brown parameters, and the computation time is significantly increased (Hammah and Curran et al 2004). This problem may, according to Hoek and Carranza-Torres et al 2002, however be overcome by calculating a Mohr-Coulomb failure envelope equivalent to the Hoek-Brown model and use this in the modelling. In the Svaddenipun analysis this approach is used, and conversion from Hoek-Brown to a linear Mohr Coulomb failure envelope is carried out using the software RocData.

The main challenge when converting Hoek-Brown parameters into Mohr-Coulomb is to obtain relevant values for ϕ and c . In order to get a realistic fit, a good estimation of the present σ_n values in the rock mass is vital (Hoek 2000). Friction parameters are highly dependent on the normal stress situation, and calculation errors may be introduced if ϕ and c are not adjusted to the acting stress conditions (Nilsen 2000). *Figure 5.3* shows the linear fitting process where a linear Mohr-Coulomb line is placed tangent to the Hoek-Brown curve at the acting σ_n value. An estimate of σ_n is calculated for the upper shear zone/metarhyolite boundary, this is at the deepest level where failure in intact metarhyolite is assumed to occur. Along this material boundary the overburden is relatively constant, and despite the fact that some increase in stress situation is expected with decreasing elevation, σ_n is assumed to have constant values along this boundary. σ_n is thus calculated from a mean overburden of 50 meters using the following relationship:

$$\sigma_n = \cos \theta \cdot \gamma z \quad [\text{Equation 5.3}]$$

where

- θ = dip of shear zone (53°)
- γ = specific weight of metarhyolite ($0,026 \text{ MN/m}^3$)
- z = depth from slope surface (50 m)

This gives a normal stress along the upper shear zone boundary of 0,8 Mpa. The function “Instantaneous Mohr-Coulomb sampler” in the software RocData was then used to obtain c_i and ϕ_i for the given σ_n .

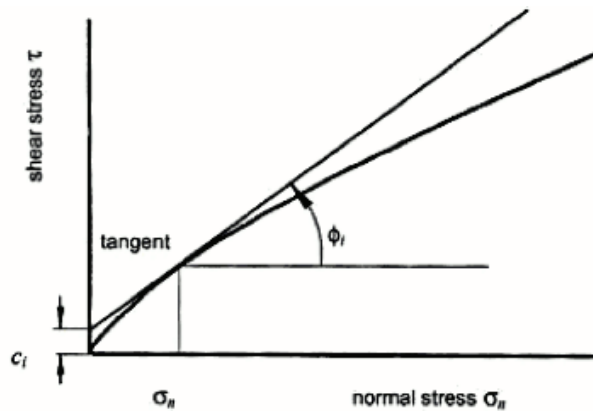


Figure 5.3: Linear fitting of the Mohr-Coulomb failure criterion to the curved Hoek-Brown line. Definition of the instantaneous cohesion c_i and friction angle ϕ_i for a specific value of σ_n . (Figure from Hoek 2000)

5.3.3 Shear zone

The Svaddenipun shear zone constitute a small part of the slope, still it is vital for the stability situation. Due to the inaccessibility of the slope, mapping of this zone is not carried out, resulting in significant uncertainty regarding shear zone strength properties. As described both in Grøneng 2010 and Laws and Eberhardt et al 2003 a shear zone is likely to contain several types of materials in different ratios. The observed displacements of several meters along the shear zone reduce probability of high content of intact rock. The shear zone material is thus assumed to consist of heavily fractured metarhyolite with some rock bridges. High content of fines and potentially also clay with swelling properties cannot be excluded.

Due to the high uncertainties regarding shear zone properties, focus of the numerical analysis is shifted towards a parameter study approach (see Chapter 5.8). This includes variations of shear zone strength properties until critical FOS close to 1,0 is obtained, representing the transition from stable to unstable slope conditions. In this way the critical shear zone parameters and their probability of appearance could be discussed.

Despite the expected variations in composition, the shear zone is modelled as a 10 meter homogeneous layer. This is to overcome the difficulty of representing a discontinuous rock mass in a continuous model. The extent of the zone is also unclear and to simulate a worst case scenario the shear zone is continuous through the entire slope. The shear zone is modelled with constant thickness and a dip angle of 53° , and thus no daylighting will occur within the slope. The applied failure criterion for the shear zone is also affected by the uncertainty regarding material composition. Due to the high potential appearance of fines, including clay material, and the uncertain homogeneity of the 10 meter thick shear zone, the Mohr-Coulomb criterion is chosen over the Hoek – Brown material model.

Grøneng 2010 present the shear strength parameters used in a SSR analysis for an assumed sliding plane at the Åknes rock slope in western Norway. This slope has several similarities to the Svaddenipun slope. Both locations have the similar slope scale with failure within a large glacial valley slope. Lithologies at both locations include highly competent brittle rocks, and failure is assumed to occur along weaker layers within these hard rocks. The strength estimations at Åknes are also based on a comprehensive investigation program including field mapping, lab test of sliding plane material and core drillings. The Åknes input parameters are

therefore well documented and more reliable than any estimation carried out at Svaddenipun. In addition to simulations with varying shear zone parameters, the different Svaddenipun model setups are therefore also calculated with Åknes shear zone properties gathered from Grøneng 2010. The applied ϕ and c represent shear zone properties resulting in FOS of 1,04 for the Åknes SSR calculations. This also gives the opportunity to carry out a comparison between the two slopes.

5.4 Rock mass parameters for metarhyolite and shear zone

5.4.1 Young's modulus and Poisson's ratio

The Young's elasticity modulus of an intact rock sample (E_i) relates the strain-response to an applied stress, and is defined by Hooke's law as

$$E_i = \sigma_z / \varepsilon_z \quad [Equation 5.4]$$

where

- $\sigma_z =$ axial stress
- $\varepsilon_z =$ axial strain

The deformation modulus of rock masses (E_m) is an important parameter for the description and calculation of stresses and deformations in rock slopes. Derivation of this parameter involves some uncertainties, and the modern practice is to estimate it from rock mass classification systems using empirical relationships (Romana 2002). According to Wyllie and Mah 2004, a relationship that relates E_m to the Hoek-Brown failure criteria can be expressed as follows:

$$E_m = \left(1 - \frac{D}{2}\right) \sqrt{\frac{\sigma_{ci}}{100}} 10^{\left(\frac{GSI-10}{40}\right)} [in Gpa] \quad [Equation 5.5]$$

Myrvang 2001 suggests that a reasonable estimate for rock mass modulus is:

$$E_m = 0,5 \cdot E_i \quad [Equation 5.6]$$

No laboratory tests have been carried out on the Svaddenipun metarhyolite and input values for E_m are based on empirical relationships and literature study (Table 5.4). Equation 5.5 and 5.6 are used for conversion, and the applied Svaddenipun E_m is averaged from the different values in Table 5.3. Average value of E_m is 15,2 Gpa. This is considered as relatively low compared to expected values, but is found according to the equations given above and is therefore the best estimate possible.

Table 5.3: Different literature values used as input for E_m for the metarhyolite. GSI and D values for Svaddenipun are selected based on recommendations in RocData manual and are discussed in Chapter 5.3.2.

Location	Lithology	σ_{ci} [Mpa]	GSI	D	E_i [Gpa]	E_m [Gpa]	γ [kN/m ³]	Converted to E_m using
Svaddenipun	Meta-rhyolite	181 ***	65	0,5		24		Equation 5.5
Moflåt, Rjukan	Rhyolite	186*			21*	10	26*	Equation 5.6
Nore l, Rødberg	Meta-rhyolite					10 **		
Mår, Rjukan	Rhyolite				34*	17	26*	Equation 5.6

*Collected from Myrvang 2001 ** Collected from Hope and Palmstrøm et al 1997 ***Collected from Loftesnes 2009

Shear zone E_m for the Svaddenipun slope is estimated from reference literature due to the lack of field data. Shear zone properties are assumed to show significantly lower values than the metarhyolite, and the E_m found for the Åknes sliding plane in Grøneng 2010 is thus used as a starting value. E_m is related to rock mass strength in general, and for the parameter study, deformation modulus is chosen in relation to changes in ϕ and c .

Rock masses exposed to stresses and compression in one direction will also show lateral strain (Myrvang 2001). This effect is defined as the Poisson's ratio:

$$\nu = -\frac{\varepsilon_x}{\varepsilon_z} = -\frac{\varepsilon_y}{\varepsilon_z} \quad [\text{Equation 5.7}]$$

where ε_x , ε_y and ε_z are strains in different directions.

Input value of Poisson's ratio for metarhyolite is set to 0,17; this is averaged from values found in literature presented in Table 5.4. Due to the assumed properties of the shear zone, the ν value for the shear zone is expected to be higher and is set to the default Phase² value of 0,3.

Table 5.4: Poisson's ratio for intact rhyolite.

Lithology	ν	Reference
Rhyolite, Moflåt Rjukan	0,14	Myrvang 2001
Rhyolite Mår, Norway	0,19	Myrvang 2001
Siliceous Rhyolite, Nevada	0,17	Lutz and Hickman et al 2010

The main use of rock mass deformation modulus and Poisson's ratio in numerical modelling is in the calculation of deformations. In the Svaddenipun analysis however, the main focus is detection of a failure surface and the FOS. According to Hoek 2000, deformation of good quality rock masses is mainly controlled by strength properties of discontinuities, and E_m and ν is assumed only to have a minor influence on the FOS and stability at Svaddenipun.

5.4.2 Tensile strength

Rock masses may have a significant tensile strength, but due to the purpose of the analyses of investigating critical failure states, low values are applied. By using Hoek-Brown material model, a more realistic estimate on tensile strength is obtained compared to the Mohr-Coulomb criterion. Tensile strength for the metarhyolite is obtained from the Hoek-Brown parameters in RocData, and the value is 0,4 Mpa. Due to the expected weak material, and the aim of the investigations of detecting critical shear zone strengths at slope failure, shear zone is assumed to have zero tensile strength.

5.4.3 Dilation angle

The dilation relates the volume increase within a rock due to shearing. Shearing results in normal displacement that must be accompanied by volume increase of the rock (Rocscience 2010 c). Dilation angle increase with rock strength, and range between zero and ϕ . In heavily fractured rocks, shearing does not lead to volume increase and dilation is neglected. According to Hammah and Yacoub et al 2006, the angle of dilation does not have significant influence in slope stability problems due to the general low confinement stresses. The measured JRC value for the metarhyolite at Svaddenipun indicate little roughness and the volume increase due to shear displacement is believed to be limited. In the heavily disturbed shear zone fractures will

probably be filled with finer materials, and shear displacement is not expected to lead to significant dilatancy. Based on this, dilation angle is set to zero for both materials.

5.4.4 Specific weight

Based on values in *Table 5.3*, γ for the metarhyolite is set to 26 kN/m^3 . Due to more jointing than for intact metarhyolite γ for the shear zone is reduced to 24 kN/m^3 .

5.4.5 Peak vs. residual shear strength

Both Mohr-Coulomb and Hoek-Brown failure criteria's uses peak shear strength to describe failure within rock masses. *Figure 5.4* show a shear test carried out on a discontinuity surface, and the following stress/deformation curve. At small displacements the specimen behaves elastically, and shear stress increase linearly. After initial failure along the surface the residual shear strength is lower than the peak shear strength (Wyllie and Mah 2004).

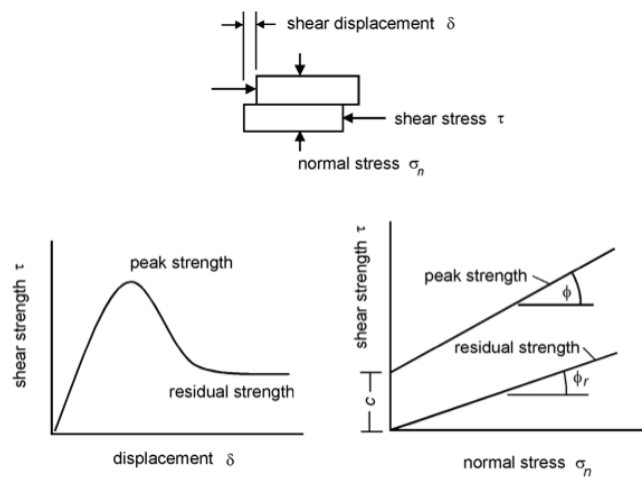


Figure 5.4: Upper and lower left: Laboratory test of shear strength along a discontinuity surface and the related stress/deformation curve. Lower right: Mohr plot of peak and residual shear strength. Figure from Hoek 2000.

In the Svaddenipun model residual values for Barton-Bandis friction angle is found as described in *Chapter 5.5.2*. For the residual values for ϕ and c in the Mohr-Coulomb criterion, some assumptions have been made. After initial failure along a sliding surface, the cohesion that used to connect the grains on both sides of the fracture are reduced, or completely removed. The initial shearing has also crushed down some of the surface asperities that originally contributed to cohesion. An approach where identical peak and residual friction values are used would therefore not reflect the actual mechanisms within the failing rock mass. The area of main interest is where the local failures that lead to the total collapse of the slope are located. This location does not necessarily coincide with the location of the first failure (*same as peak failure*), and residual values become important in simulating this. In *Figure 5.4* residual friction is lower than peak friction and residual cohesion is zero. According to Lu 2010 it is unrealistic to assume zero cohesion after initial failure for the numerical model. Based on recommendations from Lu 2010, the residual value for cohesion is reduced to 50% of peak value, and residual friction angle is reduced to 90 % of the peak value.

5.4.6 Summary of input parameters for metarhyolite and shear zone

The methodology described above results in the input parameters to the numerical model of the Svaddenipun slope. Initial shear zone ϕ and cohesion parameters are found in Grøneng 2010, and are not applied in the critical shear zone strength parameter search. Values are given in Table 5.5.

Table 5.5: Input parameters for Svaddenipun metarhyolite and shear zone. Shear zone ϕ and cohesion values are taken from Grøneng 2010.

Material	Metarhyolite	Shear zone
c_{peak} [Mpa]	1,8	0,92
c_r [Mpa]	0,9	0,46
ϕ_{peak} [°]	66	36
ϕ_r [°]	59	32
σ_f [Mpa]	0,4	0
E_m [Gpa]	15	6
ν	0,17	0,3
Dilation	0	0
γ [kN/m ³]	26	24

5.5 Discontinuities

5.5.1 Implementing discontinuities in Phase² model

The presence of discontinuities, and particularly their orientation and properties has a major influence on slope stability (Wyllie and Mah 2004). Although the Phase² 7.0 is a continuum code, it allows joint networks to be included in the analysis. Fracture set K1, that is assumed to have significant influence on the stability at Svaddenipun is thus included in the model. Due to long computation time when applying fractures to the entire model, only the metarhyolite section close to the slope surface includes joints. Fractures are not included in the shear zone, since the rock mass is assumed to be heavily jointed and crushed, and the reduced strength parameters applied to this zone incorporates weakening due to rock mass jointing. Fracture set K2 is neglected due to the perpendicularity to the profile of investigation, and set K3 have an uncertain appearance and is excluded from the 2D analysis.

5.5.2 Barton-Bandis criterion for shear strength of discontinuities

According to Nilsen and Palmstrøm 2000, the appearance and properties of discontinuities are the key factor controlling slope stability. The shear strength of discontinuities is vital for the failure potential and minor change in shear strength may give large change in total stability, enhancing the importance for a good estimation of this parameter.

An empirical method for determining the peak shear strength for a discontinuity surface is given by Barton and Bandis 1990. According to this, joint surface strength and the normal stress acting on the discontinuity surface govern the shear strength of an unfilled joint. A prerequisite is rock-to-rock contact between fracture walls and no infillings (Wyllie and Mah 2004). The shear strength τ is then defined as:

$$\tau = \sigma'_n \cdot \tan \left[JRC \cdot \log_{10} \left(\frac{JCS}{\sigma'_n} \right) + \phi_r \right] \quad [Equation 5.8]$$

where:

$$- \quad \sigma'_n = \text{Effective normal stress}$$

- JRC = Joint roughness coefficient
- JCS = Joint surface compressive strength
- ϕ_r = Residual friction angle

For fresh, unweathered joints ϕ_r = basic friction angle. When the stress level is high compared to rock strength, the ratio JCS/σ_n - ratio is small, and the shear strength is mainly governed by residual friction angle. At low stress levels, the JCS/σ_n – ratio is high resulting in a high influence of the roughness on the peak shear strength (Wyllie and Mah 2004). The Barton-Bandis shear strength criterion for the K1 fractures at Svaddenipun may be applied directly in the Phase² model.

Barton-Bandis criteria are used in the Svaddenipun numerical model to describe the properties of the fracture set K1. The necessary input parameters are the following:

- JRC = Joint Roughness Coefficient
- JCS = Joint Compressive Strength
- ϕ_r = residual friction angle
- σ_n = effective normal stress
- Joint Normal Stiffness
- Joint Shear Stiffness

JRC and JCS

Loftesnes 2009 collected JRC and JCS parameters for fracture set K1. Average weighted value for joint roughness coefficient was 3,23. According to classification given in Singh and Goel 2006 this value corresponds to a rough planar surface. Scaled joint compression strength from Schmidt-hammer tests averaged 181 Mpa. For fresh unweathered joints, the $JCS=\sigma_{ci}$, and this is assumption is used in this analysis. *Table 5.3* show similar σ_{ci} -vaulegathered from a nearby location. The number of samples is quite small, but these values are used as input values for the fractures in the slope model due to the lack of better estimates.

ϕ_r

Estimations of ϕ_r are made from measured dip angle of K1 – sliding surfaces in the Svaddenipun slope. Numerous such surfaces were observed along the slope face, with an average dip angle of 50°. If no water and ice were present at the time of these failures, the observed angle may be used as an estimate of the active friction angle (ϕ_a). Failure is likely to have been influenced by at least water, but this would lead to the fact that the *real* ϕ_a was higher at time of failure. The observed sliding planes may thus represent a conservative estimate of ϕ_a , from where ϕ_r may be found using *Equation 5.9*:

$$\phi_{observed} \approx \phi_a = \left[JRC \cdot \log_{10} \left(\frac{JCS}{\sigma_n} \right) + \phi_r \right] \quad [Equation 5.9]$$

Equation 5.9 is identical to the expression for ϕ_a given in Barton-Bandis *Equation 5.8*. Solved with respect on ϕ_r with the given normal stress and fracture parametres the resulting ϕ_r is 42°. This value might seem a little too high, but it is the most accurate estimate based on field measurements, and thus used for the numerical analysis.

Joint stiffness

Joint normal- and shear stiffness parameters for the K1 fracture set was estimated according to Rocscience 2010 c, and may be expresses by the following equations:

Joint normal stiffness: $k_n = \frac{E_i \cdot E_m}{L(E_i - E_m)}$ [Equation 5.10]

Joint shear stiffness: $k_s = \frac{G_i \cdot G_m}{L(G_i - G_m)}$ [Equation 5.11]

where

- E_m and G_m are rock mass modulus and rock mass shear modulus
- E_i and G_i are intact rock modulus and intact rock shear modulus
- L is mean joint spacing set to 5 meters

Calculations for estimation of G_m and G_i are given in Appendix 5, and values for k_n and k_s are given in Table 5.6.

Table 5.6: k_n and k_s parameters.

K_n	k_s
6 Gpa/m	2,6 Gpa/m

5.5.3 Statistical appearance of fracture set K1

Properties of fracture set K1 are presented in Loftesnes 2009, and model input values are based on these findings. However some modifications have been made. Spacing of fractures tends to increase with depth below the slope surface, and the observed 1-meter mean spacing for the K1 fractures was increased to 5 meters. This also speeds up computations significantly. To account for uncertainties within fracture properties, a statistical distribution function for these parameters is applied in the Phase² model and presented in Table 5.7. When the fractures are created, the program identifies the location of the first joint randomly. Persistence parameter in Phase² is not the same as in structural geology; here it is defined as L1/L2 in Figure 5.5.

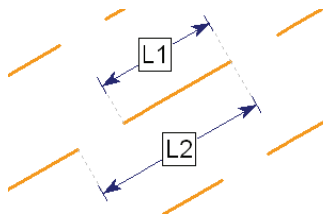


Figure 5.5: Definition of discontinuity persistence as L1/L2 in Phase².
Figure from Rocscience 2010 c.

Table 5.7: Properties of fracture set K1 used as input in numerical model.

Property	Value		
Joint model	Parallel statistical		
Dip	62		
Spacing	5 m	Normal distribution	St.dev: 1 meter
Length	8 m	Normal distribution	St.dev :2 meter
Persistence	0,5	Normal distribution	St.dev: 0,1 meter
Joint end condition	Open at boundary, material and surface contact		

5.6 Stresses

According to Wyllie and Mah 2004, the role of *in situ* stresses has traditionally been neglected in slope stability analysis. The reasons for this may be the use of LEMs that cannot include stress analysis, or the fact that most slope failures are gravity driven, limiting the effects of

in situ stresses. For many rock slope problems, stresses are also largely unknown; stress estimations are therefore difficult. According to Panthi and Nilsen 2005, *in situ* stress situation have considerable influence on the rock deformation and hence the slope stability. Numerical models, such as Phase² have the ability to calculate and evaluate stresses, highlighting the advantages of finite element analyses.

The stress state at Svaddenipun has not been measured. Valley excavation from previous glaciations has however created a redistribution of stresses along the slope. A staged, numerical model could be used to simulate the elastic rebound and stress redistribution by glacial melt, but the thickness of ice that have been present in the area is not known, making such simulation inexpedient. The effect of glacial unloading is also assumed to be small compared to the initial removal of rock overburden, reducing relevance of glacial unloading simulations. The presence of lateral release of the potential instability in west, and the fractured shear zone in south, lead to the assumption that high horizontal stresses cannot be transferred into the potential instable area. The eastern extent of the potential instability may however go through solid rock, still it is assumed that only gravitational stresses are present in the critical section of the slope, and horizontal stresses result from the gravitational component of the vertical stress, expressed in Myrvang 2001 as:

$$\sigma_h = \frac{\nu}{1-\nu} \sigma_v \quad [Equation 5.12]$$

For the metarhyolite that constitute the majority of the Svaddenipun slope this results in a stress ratio of $\sigma_h=0,2 \cdot \sigma_v$. This relationship is applied in both horizontal directions. The ratio is low for Norwegian conditions, but horizontal stresses, at least in the analyzed plane, are expected to be low due to the short distance between the shear zone and slope surface, both contributing to stress relieve.

5.7 Water

Water is together with the presence and properties of discontinuities assumed to be the major parameter controlling slope stability, and should be included in numerical analysis whenever possible (Nilsen and Palmstrøm 2000). The presence of water in a slope reduces the shear strength of the rock mass due to the decreased value of σ_n' acting on the discontinuity surfaces. In addition, water enhances erosion and weathering, and act as a driving force in near vertical tension cracks (Wyllie and Mah 2004). Conductivity of massive rocks is normally low, and major water flow follows discontinuities. Numerical modelling in Phase² includes the possibility to model responses to an applied water table, and a piezometric line is added in all relevant models of the Svaddenipun slope.

The hydrogeological situation at Svaddenipun is not studied and some assumptions have been introduced to the model. Water flow in metarhyolite is prone to follow fractures, however the connectivity of these, and hence the potential build-up of water pressure, is unclear. Considerably water pressures may however not be excluded. The composition of the shear zone also affects the hydraulic conditions within the slope. If clay minerals are present, the conductivity of the shear zone is strongly reduced and it may be close to dry. If the shear zone is brittle, with little infillings, open fractures will exist, allowing water to saturate the zone. The inability of the Phase² program to model water flow along fractures, reduces the representativeness of the actual hydrogeological conditions.

Early analysis of a water table placed along the base of the shear zone resulted in negligible change in FOS. A water table was thus placed approximately 20 meters above the shear zone/metarhyolite contact, resulting in a new σ_n' of 0,6 Mpa. This leads to an almost complete saturation of the shear zone, and this is assumed to be the worst-case scenario representing the highest possible water influence on slope stability. The water table is set to enter the valley side in the talus slope at around 500 m.a.s.l. This is in conjunction to observations by Loftesnes 2009, as no signs of daylighting springs were observed in the upper section of the slope.

The change in effective normal stresses changes the residual friction angle for fractures. This is however automatically implemented in Phase² calculations since σ_n' is included in *Equation 5.8*. The change in σ_n' also affects the conversion of metarhyolite friction parameters, from Hoek-Brown to Mohr-Coulomb criterion. Due to minor effects, adjustments were not done.

5.8 Parametric study

Parametric studies are highly important in numerical analysis. Due to the uncertainty introduced by representing rock mass properties as single values, analysis using variation in input parameters results in more realistic estimates of slope stability. Parameter studies reflect the sensitivity of the modelling results to a change in input values, and detect the most critical parameters for the stability.

One of the main uncertainties regarding the stability situation at Svaddenipun, and thus the main focus in the parameter study, are the shear zone strength properties. The majority of the sliding plane is assumed to follow this lithology, and due to the high uncertainty regarding shear zone input parameters, simulations with only one assumed strength configuration are inexpedient. A parametric study is carried out to evaluate the stability at different shear strengths. This includes variations of shear zone material properties until critical FOS – value of 1,0 is obtained, representing the transition from stable to unstable slope conditions. In this way the critical shear zone strength parameters and their probability of appearance can be discussed.

Shear zone strength parameters that influence FOS the most are assumed to be ϕ and cohesion. Remaining input parameters are more related to the magnitude of deformations, and are thus of secondary importance in the stability analysis. Since shear strength is influenced both by cohesion and ϕ , only one of the two parameters is changed at the time. It is assumed that cohesion at time of failure is low, peak cohesion is thus held constant at 50 kPa, while ϕ is varied. Some analysis results in unrealistic high values of ϕ in order to obtain a FOS – value of 1. For such model setups, ϕ is held constant at 50° and cohesion adjusted until the slope fails. E_m value is assumed to follow strength properties of the shear zone, and is thus changed in relation to changes in ϕ and c . The shear zone parameter study is carried out both for dry and partially saturated conditions.

To study the model sensitivity to metarhyolite and K1 fracture parameters, a second parameter study is conducted. Simulations with approximately 30% reduced and 30% increased metarhyolite and K1 fracture strength values are carried out. For each of these two model setups, the critical shear zone parameter study is conducted to detect critical shear strengths, leading to numerically instability indicating slope failure. Input material properties for these simulations are given in *Table 5.10*. For convenience the 30% reduced conditions are termed “*Svaddenipun 2*” configuration, and the 30% increased values are termed “*Svaddenipun 3*”

configuration. Joint spacing and persistence already has a statistical distribution and are unchanged in this parameter study. Both dry and partially saturated analysis is conducted for the *Svaddenipun 2-*, and *Svaddenipun 3 – model* setups.

Due to the uncertainty regarding initial stress conditions within the slope, some simulations with isotropic stress conditions are also conducted. In this way the change in stability with changing stress conditions can be discussed.

ϕ_r for the discontinuity set K1 is also considered as an uncertain parameter due to the limited tests carried out on metarhyolite material. Therefore some calculations with reduced ϕ_r -values are carried out.

5.9 Evaluation of input parameters and Phase² model limitations

Results of analysis are never better than model input. Numerical simulations of actual conditions within a rock slope will always be subject to errors and uncertainties deriving from input parameters, model setup or weaknesses in the numerical model itself. Awareness and detection of such limitations is important, and parameter studies are useful both by reducing uncertainties, and in detecting what parameters have the largest influence on stability.

The largest uncertainty for the Svaddenipun input parameters are the shear zone strength properties, and the potential for outcropping of this, in the lower section of the slope. The aim of the conducted parameter study is to investigate the effect of strength variations and eliminate as much as possible of the uncertainty regarding shear zone strength. The location of the shear zone in the model is based on existing field observations. A curved shear zone with daylighting within the talus covered lower section of the valley slope would change the stability assessment dramatically.

Despite the limited availability of representative literature data and knowledge of the actual slope conditions, input parameters for metarhyolite and K1 fracture set are assumed to have as good quality as possible. Still input parameters are based on either a limited number of field measurements or on reference literature, clearly introducing some uncertainty. Choice of failure criteria for the rock masses is partially based on rock mass properties, and limited knowledge of these, may also induce some uncertainty in the representativeness of the selected material models.

Hydrogeological conditions are not investigated, and the location of the water table in the model is assumed to be a worst-case scenario. According to Lu 2010 a major shortcoming with the Phase² program is that water cannot be modelled to follow joints, as the case would be in reality. Water is assumed to fill the pores within the rock, only affecting the effective stresses within the slope as a whole. This is independent of where the fractures are located and is clearly not the actual situation within the rocks.

One of the main sources of errors in the numerical model is the fact that Phase² analysis of Svaddenipun is the 2D analysis of a 3D problem. The stress situation is converted from three into two dimensions, parallel and normal to the profile plane. A basic assumption is that no shear stress or strain occurs in the out-of plane direction. Uncertainties regarding stresses, displacements and rock mass fracturing that is not parallel to the analyzed profile are thus introduced. Phase² modelling also assumes constant cross section of infinite length; this is not the actual situation at Svaddenipun.

In order to obtain realistic modeling results, the stress situation must be as correct as possible. The *in situ* stress situation is highly difficult to measure and is subject to assumptions. Stresses are however assumed to be of secondary importance regarding FOS and total slope stability, and parameter study with isotropic stress situation may reveal the sensitivity to changing stress conditions.

Different numerical techniques and software have their strengths and weaknesses, and all methods, including FEM with SSR analysis, show some unwanted effects. According to Löw 2009 the results of SSR analyses are sensitive to the location and the size of the SSR-search area. There may also be several reasons for lack of convergence of the SSR model besides just the reduction in material strength. Such reasons may be incorrect boundary conditions, or incorrect *in situ* stress situation (Krahn 2007).

5.10 Summary of input parameters for Svaddenipun slope model

5.10.1 Input parameters for the initial model (Svaddenipun 1 – model)

Table 5.8 show the initial input values for metarhyolite and shear zone materials. Table 5.9 show initial parameters for K1 discontinuity properties. Spacing, length and persistence of discontinuities are remained constant throughout the parameter study.

Table 5.8: Initial input parameters for metarhyolite and shear zone.

Material	Metarhyolite	Shear zone	Comment
σ_t [Mpa]	0,4	0	RocData estimations based on Hoek-Brown parameters
c_{peak} [Mpa]	1,8	0,92	Metarhyolite value based on Hoek-Brown criterion, Shear zone based on Grøneng 2010.
c_r [Mpa]	0,9	0,46	50% of peak value
ϕ_{peak} [°]	66	36	Metarhyolite value based on Hoek-Brown criterion, Shear zone based on Grøneng 2010.
ϕ_r [°]	59	32	90% of peak value
E_m [Gpa]	15	6	From Equation 5.5 based on Hoek-Brown parameters
ν	0,17	0,3	From literature study
Dilation	0	0	See discussion Chapter 5.4.3
γ [kN/m ³]	26	24	From literature study

Table 5.9: Key properties of fracture set K1 used as input in numerical model.

Property	Value	Comment
JCS	181	From Barton-Bandis criteria. Values based on Loftesnes 2009
JRC	3,2	
ϕ_r [°]	42	
k_n [Gpa]	6	Calculations shown in Chapter 5.5.2 and Appendix 5. Based on E_m for metarhyolite
k_s [Gpa]	2,6	
Dip [°]	62	Loftesnes 2009
Spacing [m]	5	Adjusted from Loftesnes 2009
Length [m]	8	Loftesnes 2009
Persistence	0,5	Default value in Phase ²

5.10.2 Input parameters for the parametric study

The parameter study involved a 30% increase/reduction of initial metarhyolite and K1 discontinuities parameters, in addition the variation of shear zone parameters until a FOS close

to 1,0 was obtained. Table 5.10 summarizes the metarhyolite and K1 fracture parameters; the different input parameters for the shear zone strengths are given in Appendix 7.

Table 5.10: Variation of metarhyolite input parameters in parametric study. To avoid unrealistic values for the $\pm 30\%$ strength analysis, the values of GSI, D and ϕ_r for joints are set to reasonable values instead of exact calculations. m_i and MR are set to maximum and minimum recommended values for metarhyolite according to RocData user manual.

Metarhyolite E_m is calculated from Equation 5.5.

	30%reduction in strength parameters “Svaddenipun 2– model”	30%increase in strength parameters “Svaddenipun 3– model”
Hoek Brown parameters	Metarhyolite	Metarhyolite
σ_{ci} [Mpa]	125	235
GSI	40	80
D	0,6	0,3
m_i	20	30
MR	300	500
E_m [Gpa]	4,4	73
Mohr-Coulomb parameters		
σ_t [Mpa]	0	1,5
c_{peak} [Mpa]	0,48	6,4
c_r [Mpa]	0,24	3,2
ϕ_{peak} [°]	55	70
ϕ_r [°]	50	63
Dilation angle	0	0
Barton Bandis parameters		
JCS	125	235
JRC	2,2	4,2
ϕ_r [°]	30	50
k_n [Gpa]	1,8	28,8
k_s [Gpa]	0,8	4,6

5.10.3 Phase² Svaddenipun model

Figure 5.6 presents a screenshot of the completed model in Phase².

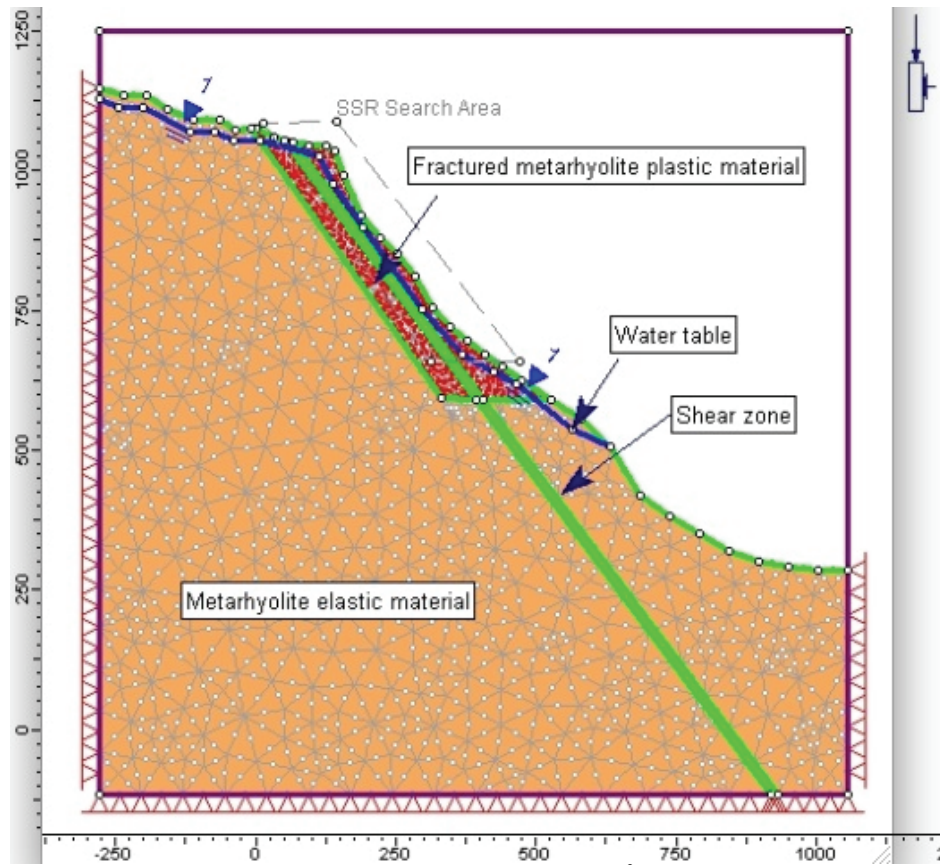


Figure 5.6: Screenshot of completed model built in Phase² used for the numerical analysis.

Chapter 6: Results from LiDAR survey

6.1 Introduction

Based on the scanning procedure and the methods for processing LiDAR point clouds described in previous chapters, discontinuity orientations from the Svaddenipun slope were successfully obtained. Scanning of the inaccessible parts of the slope reveals vital information on discontinuity pattern for the slope as a whole, as opposed to results from field measurements at specific outcrops. In this chapter, contour- and stereoplots on discontinuity pattern obtained from the LiDAR survey is presented.

6.2 Fracture orientations detected in LiDAR survey

Figure 6.1 show stereoplot for both scans. All the registered discontinuities from Scan 6 are within Section A of the slope, while Scan 7 contains measurements from both section A, B and C (Figure 1.4). The different scans show different fracturing pattern, the 84 discontinuities extracted from Scan 6 has numerous of fractures dipping towards SE (K2) but also a set dipping steeply to the north (K1) and one to the NW (K3). On Scan 7 however the pattern of the 59 fractures is more scattered showing a clear K1-set and then many scattered fractures dipping steeply from NE to SE.

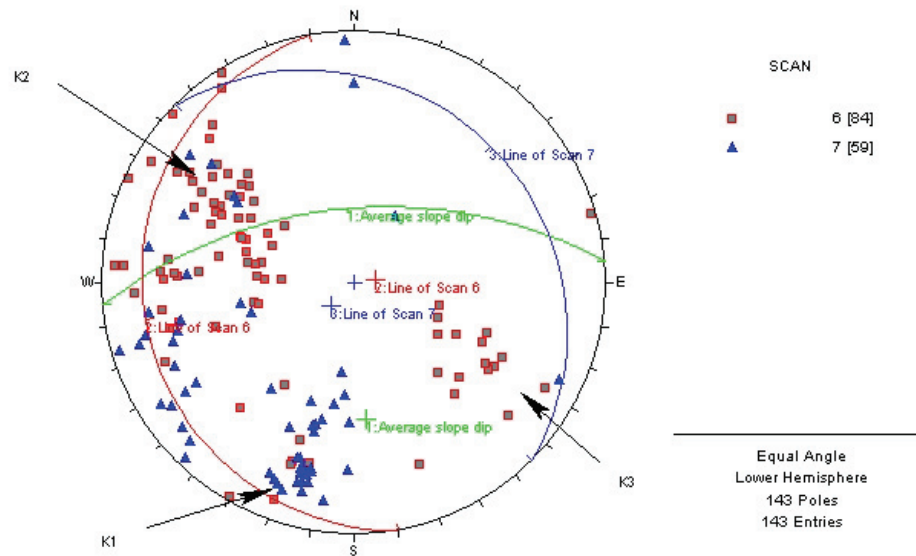


Figure 6.1: Stereoplot for 143 discontinuities found on LiDAR Scan 6 (red) and Scan 7 (blue). The scanning direction for both scans is shown in red and blue lines. Green line shows average slope dip.

Figure 6.2 show contourplots for all 143 discontinuities collected from the two LiDAR scans. This plot visualizes the amount of clustering in fracture orientation, and the contours represent the statistical concentrations of the poles calculated using a Fisher distribution method. A statistically significant cluster should have Fisher concentrations above 6%, while a concentration of 4-6% represent a marginally significant cluster (Rocscience 2010 b). Fracture

set K1 show a highly significant cluster, so does fracture set K2. K3 and a steep, eastern-dipping set show marginally significance.

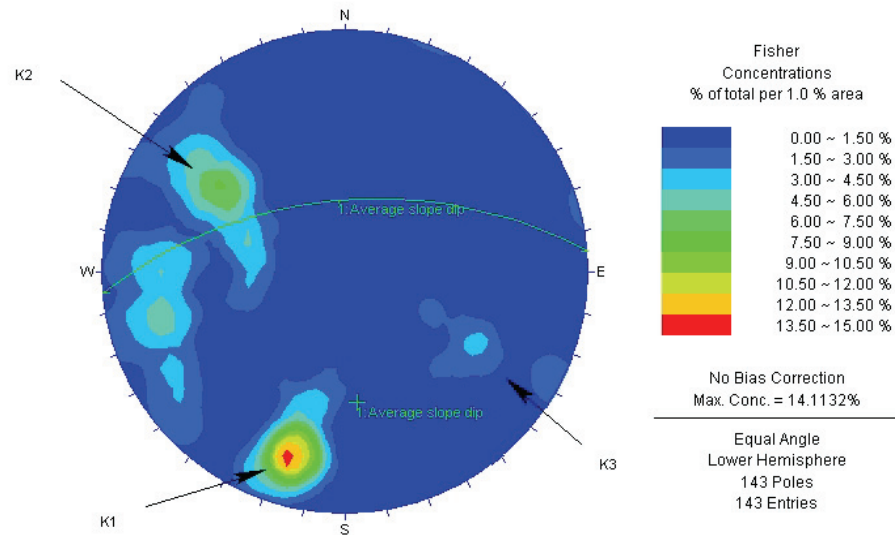


Figure 6.2: Contourplot for 143 discontinuities from LiDAR scans with Fisher concentrations.

When orientation measurements are made, a bias is introduced in favour of those features, which are perpendicular to the direction of surveying. To avoid this bias a Terzaghi-weighing may be used (Rocscience 2010 b). The orientation of the scanned rock surface varies, and Terzaghi weighing would thus not give more accurate results. Therefore an unweighted contourplot is used. Separate stereo- and contourplots for each of the scans are given in Appendix 6.

Chapter 7: Results from Phase² modelling

7.1 Introduction

This chapter presents the most relevant results from different model setups in the SSR stability analysis in Phase². Results are described in 3 different sections, corresponding to the subdivision of the Phase² files based on metarhyolite and K1 fracture strength parameters described in *Chapter 4.4.3(Svaddenipun 1-, 2-, and 3 – model setup)*. Within each section, results both with shear zone parameters corresponding to assumed Åknes sliding plane, and the values corresponding to a critical shear zone strength, indicating failure of the slope model are presented. All sections include results both from dry and from partially saturated slope conditions. A complete list of all relevant models is presented in *Appendix 3*, and the corresponding Phase²-files are included in *Appendix 7*.

7.2 Calculations with initial strength parameters for metarhyolite and K1 discontinuities (Svaddenipun 1 – model)

7.2.1 Introduction

Table 7.1 shows the input parameters for shear zone strength properties and resulting FOS for the *Svaddenipun 1 – configuration* within the slope. In the following sections the results are presented for the different shear zone input parameters.

Table 7.1: Mohr-Coulomb input parameters for shear zone in Svaddenipun 1 – model. Left: calculations with shear zone parameters corresponding to Åknes sliding plane, and resulting FOS. Right: Shear zone input values leading to critical stability state represented by FOS close to 1,0. For this model setup, c was remained constant and ϕ was varied until failure occurred.

Differences between dry and partially saturated conditions are highlighted.

	<i>Åknes shear zone parameters</i>		<i>Reduced strength corresponding to FOS close to 1,0</i>	
	<i>Dry slope</i>	<i>Partially saturated slope</i>	<i>Dry slope</i>	<i>Partially saturated slope</i>
$E_m [Mpa]$	6000	6000	1000	1000
$\phi_{peak} [^\circ]$	36	36	9	15
$c_{peak} [Mpa]$	0,92	0,92	0,05	0,05
FOS	1,7	1,5	1,01	1,00

7.2.2 Calculations with shear zone parameters corresponding to Åknes sliding plane

Dry slope conditions

Critical FOS for the *Svaddenipun 1 – model* with shear zone parameters corresponding to the Åknes sliding plane in Grøneng 2010 is 1,70. Due to the expected rapid increase in strain after critical SRF is reached, and in order to visualize a clear pattern, *Figure 7.1* shows maximum shear strain at FOS of 1,71. Majority of shear strain occurs along the shear zone. At elevation close to 750 m.a.s.l., around 25 meters above the transition from talus to cliff face, there is an area with increased shear strain stretching from the shear zone through metarhyolite reaching the slope face. This region also shows the highest deviatoric stresses within the slope (defined as principal stress minus mean stress), and dip angle of the strain concentration-line trough metarhyolite is around 20°. Exact displacement values are not relevant for this analysis, since main emphasis in the SSR method is put on detecting the critical limit where the displacements

increase above a threshold value, indicating total collapse of the slope. Displacement results are thus excluded from the analysis.

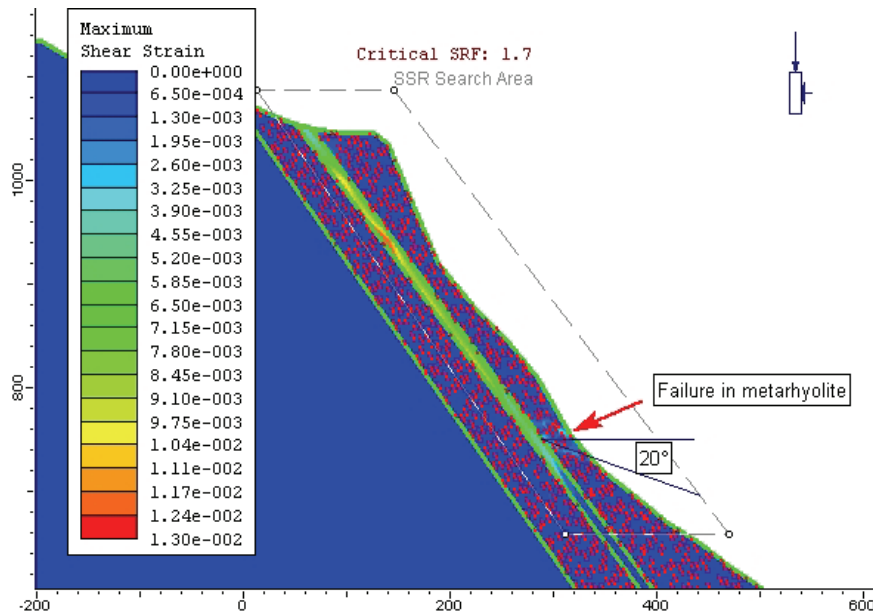


Figure 7.1: Maximum shear strain in the Svaddenipun – 1 model with Åknes sliding plane properties for the shear zone. Critical FOS is 1,70, figure show situation at FOS=1,71. Red lines represent K1 fractures.

Partially saturated slope

Introduction of water to the simulation with initial strength parameters reduces FOS from 1,7 to 1,5. The maximum shear strain occurs not only along, but also under the shear zone towards the boundary of the SSR – search area. This is shown in Figure 7.2. The metarhyolite region around 750 m.a.s.l shows the same increased shear strain values as the dry slope model, major effective stresses are here reduced to half the dry slope conditions.

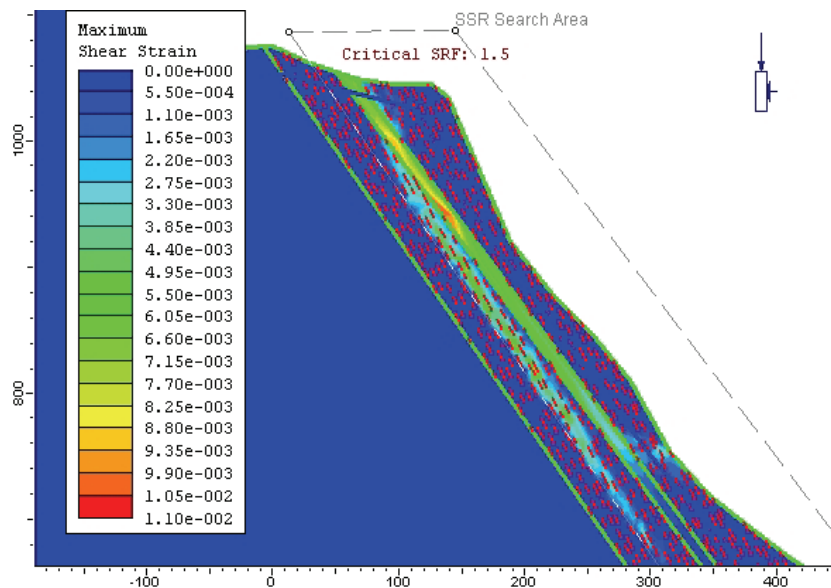


Figure 7.2: Maximum shear strain in the partially saturated Svaddenipun – 1 model with Åknes sliding plane properties for the shear zone.

7.2.3 Result of critical shear zone strength calculations

Dry slope

In the parametric study the shear strength of shear zone was reduced to a certain value in order to obtain a critical FOS close to 1,0. For the *Svaddenipun 1-model* setup, the shear zone critical strength values corresponding to such conditions are given in *Table 7.1*. Shear zone input values and corresponding FOS for all *Svaddenipun – 1* simulations carried out are given in *Appendix 7*. *Figure 7.3* shows maximum shear strain plot with shear zone parameters corresponding to a critical FOS of 1,01 for this model configuration. Most of the shear strain occurs along the shear zone, and in the metarhyolite around 740 m.a.s.l. Approximate dip angle of a line through the shear strain concentration in metarhyolite is 30° (*Figure 7.3*). The cross sectional area with a baseline constituted by the highest shear strain values in *Figure 7.3* is approximately $14\,700\text{ m}^2$. With a cross width of Section A in *Figure 1.4* of approximately 150 meters, the release volume would be 2,2 million m^3 . A failure along the total 350-meter long shear zone in *Figure 1.4* would include a total volume of 5,15 million m^3 .

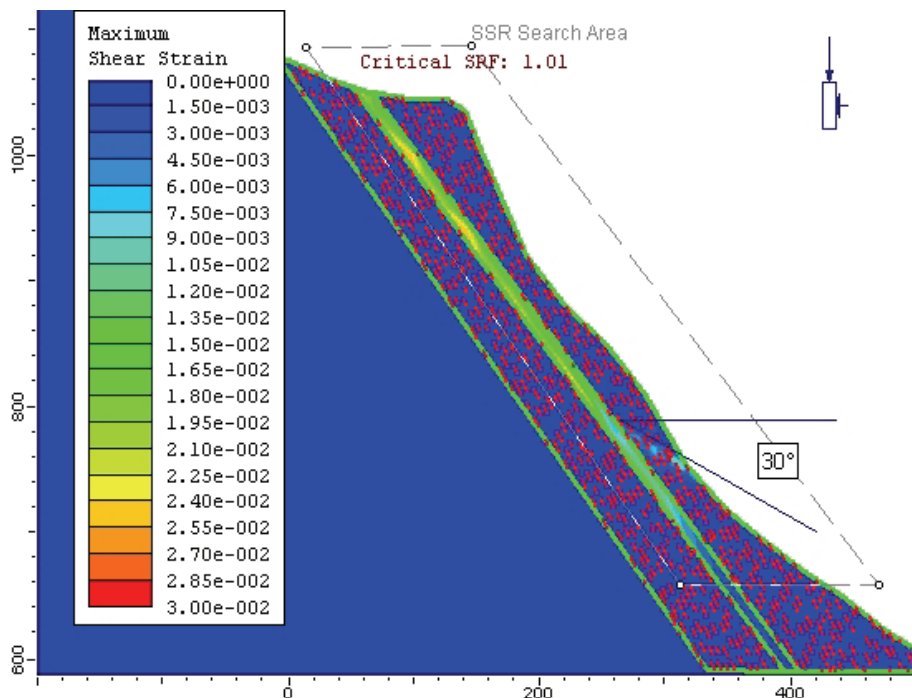


Figure 7.3: Shear strain plot for reduced shear zone properties corresponding to critical SRF (1,01) for Svaddenipun 1 – model. The plot is presented for a SRF of 1,02 to illustrate where the failure plane is likely to be located. Cross sectional area of the upper slope lying above the shear zone and the 30° -line trough metarhyolite is around $14\,700\text{ m}^2$.

Maximum stresses and deviatoric stresses in the shear zone are low, while the overlying metarhyolite experience a significant stress concentration both in major and deviatoric stresses in the area around 750 m.a.s.l. Major stress values exceeds 10 Mpa in this region. *Figure 7.4* show the major principal stress plot for the FOS=1,01 calculation. Here the maximum normal stress along a K1 joint surface is also marked, the location of this fracture is in the area with largest major stress.

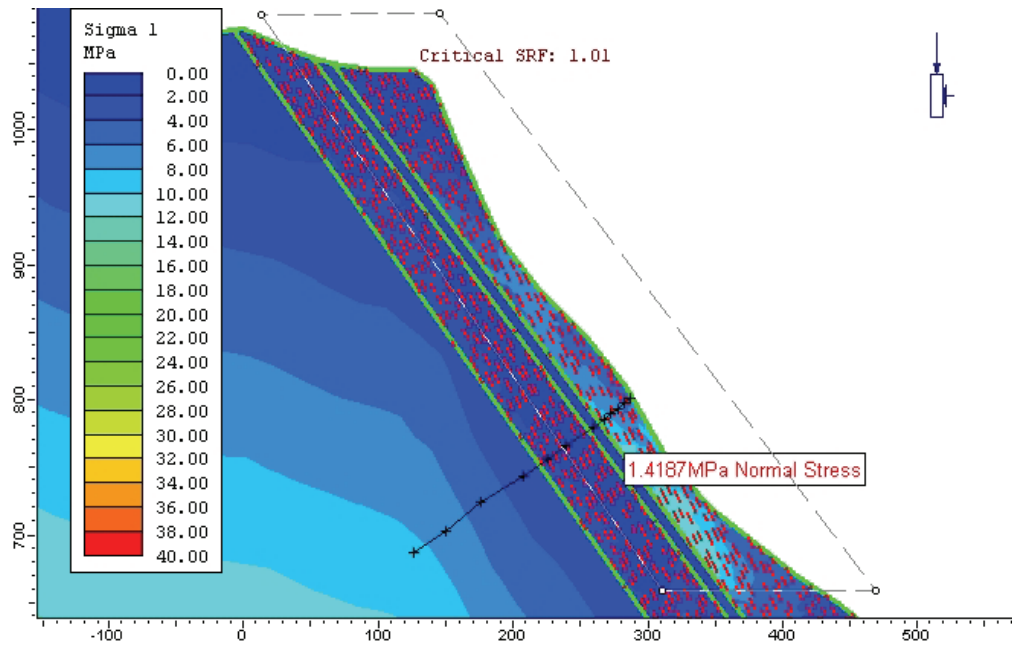


Figure 7.4: Major stress distribution for Svaddenipun 1 – slope model with critical shear zone parameters corresponding to SRF value of 1,01. Black dotted line shows location of stress plot values given in Figure 7.5. Maximum normal stress value along a K1 joint surface is given in red (1,4 MPa), and the location of this fracture is in the area with highest major stress.

σ_1 and σ_3 values along the profile in Figure 7.4 are presented in Figure 7.5. Maximum stresses decrease towards the slope surface, with lowest values in the shear zone. A dramatic increase in σ_1 -value occurs on the contact between the weak shear zone and the overlying metarhyolite, around 700-800 m.a.s.l. Towards slope surface σ_1 stresses decrease again. σ_3 values are negative, but less than σ_1 far away from the slope surface where overburden is highest, before they gradually increase to maximum values in the shear zone. Also σ_3 decrease towards valley slope.

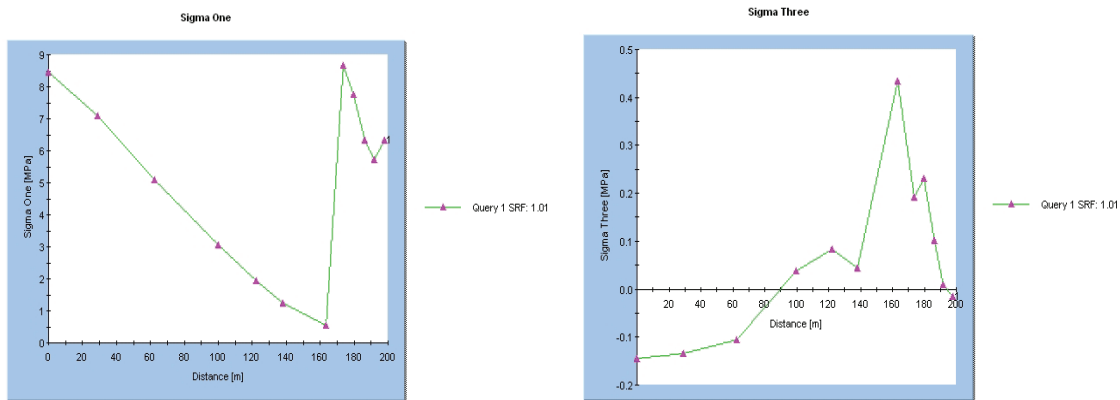


Figure 7.5: σ_1 (left) and σ_3 (right) graphs along marked line in Figure 7.4. Horizontal axis value increases towards slope surface. σ_1 values decrease towards shear zone, before a large increase in region close to slope surface. σ_3 show highest values in shear zone

Due to the high uncertainty of the initial stress condition, a simulation with isotropic stresses was conducted for the Svaddenipun 1– model with critical shear zone strength. All parameters

except σ_v / σ_h ratio was left unchanged, resulting in a decrease in FOS from 1,01 to 0,98. Figure 7.6 shows deviatoric stress plot in the area with the highest stress concentrations around 700 m.a.s.l., both for the initial and the isotropic stress simulations. As can be seen, deviatoric stresses are relatively similar, with a slightly higher value for isotropic stress conditions. Peak values for initial deviatoric stress conditions are around 10 MPa, while the peak value for isotropic stress distribution is around 11 MPa. Magnitude of major stress is similar for both models, while metarhyolite shear strain concentration is marginally lower for the isotropic stress conditions.

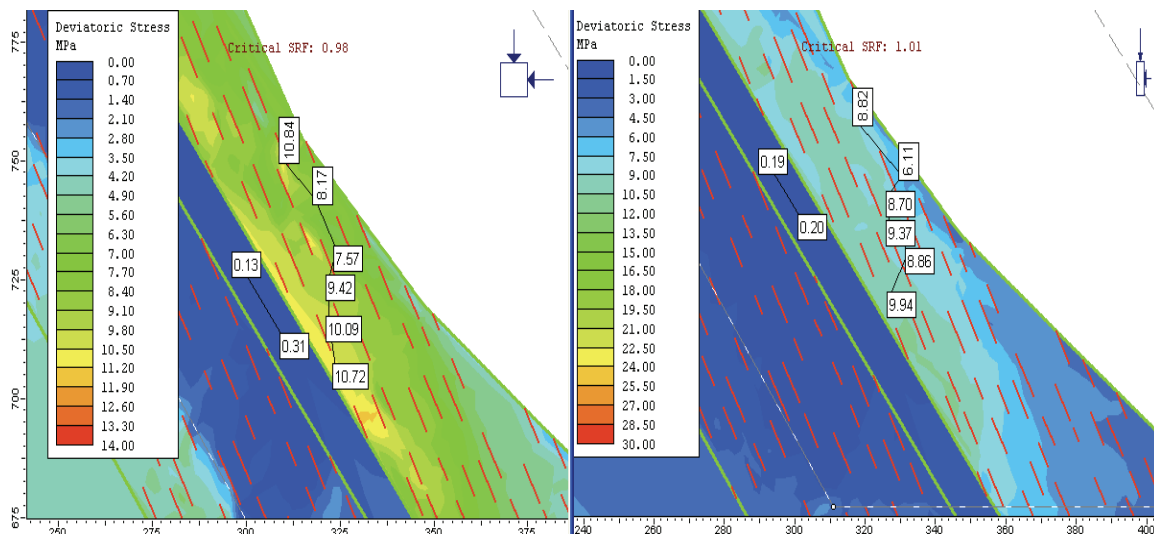


Figure 7.6: Deviatoric stress plots for isotropic stresses (left) and initial stress conditions (right) for critical shear zone strength in the Svaddenipun 1 – model. Numbers indicate the magnitude of deviatoric stresses at critical FOS close to 1,0.

Some uncertainty regarding ϕ_r for Barton-Bandis fracture set K1 was discussed in Section 5.8. Therefore a simulation with reduced ϕ_r value was conducted to see whether this uncertainty affect slope stability calculations or not at the actual strength situation. ϕ_r for K1 fractures was reduced from 42° to 30° while all other parameters were remained constant. The calculated FOS showed an increase from 1,01 to 1,04.

Partially saturated slope

The critical conditions (FOS=1) for partially saturated slope with Svaddenipun 1– model setup is obtained with a peak friction angle of 15° for the shear zone material. This is an increase from 9° for the dry slope conditions. Maximum shear strain pattern is similar to the pattern in Figure 7.3 for the dry slope conditions at FOS of 1,01. Stress conditions for partially saturated conditions show the same pattern as for the dry slope (see Figure 7.4) with slightly reduced effective stress values beneath the water table. Figure 7.7 shows relationship between friction angle and FOS for all simulations with Svaddenipun 1 – model setup. A linear relationship can be seen both for dry and partially saturated slope conditions, still dry slope conditions show higher sensitivity to changing ϕ_{peak} .

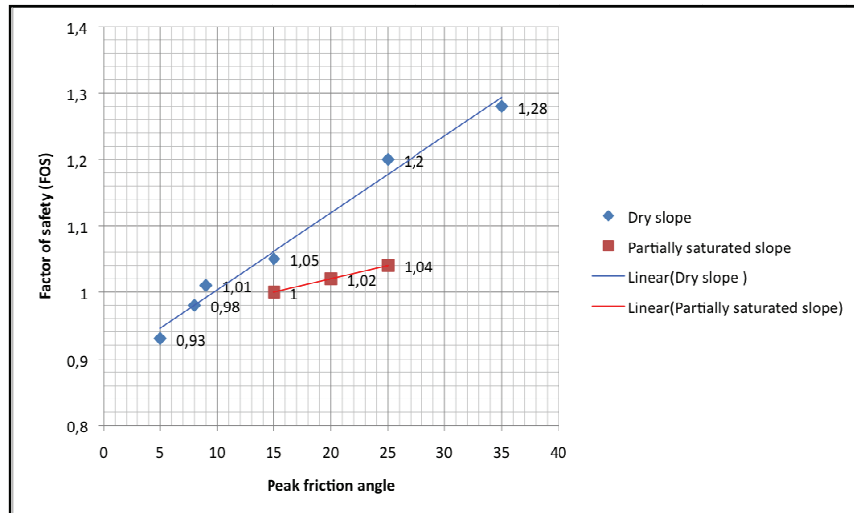


Figure 7.7: Peak friction angle and corresponding FOS for dry (blue) and partially saturated (red) analysis of Svaddenipun 1 – model setup. FOS values are listed next to each point in plot. A linear relationship between friction angle and FOS is clear, although sensitivity to changing friction angle is different for the two cases.

7.3 Calculations with 30% reduced strength parameters for metarhyolite and K1 discontinuities (Svaddenipun 2 – model)

7.3.1 Introduction

Table 7.2 shows the input parameters for different shear zone strength properties and resulting FOS for the Svaddenipun 2–model within the slope. For this model setup, strength values for metarhyolite and K1 fractures have been reduced 30%. This results in a low strength ratio between critical shear zone parameters, and the surrounding metarhyolite, clearly affecting the results. Due to the unrealistic high values of ϕ that had to be applied in order to simulate slope collapse in the parameter study, ϕ was set to 50° and the cohesion was increased until FOS close to 1 was obtained.

Table 7.2: Mohr-Coulomb input parameters for shear zone in Svaddenipun 2 – model. Left: calculations with shear zone parameters corresponding to Åknes sliding plane, and resulting FOS. Right: Shear zone input values leading to critical stability state represented by FOS close to 1,0. For this model setup, ϕ remained constant and c was varied until failure occurred.

Differences between dry and partially saturated conditions are highlighted.

	Åknes shear zone parameters		Reduced strength corresponding to FOS close to 1,0	
	Dry slope	Partially saturated slope	Dry slope	Partially saturated slope
E_m [Mpa]	6000	6000	4000	4000
ϕ_{peak} [°]	36	36	50	50
c_{peak} [Mpa]	0,92	0,92	0,40	3,50
FOS	1,14	0,77	0,995	1,00

7.3.2 Calculations with shear zone parameters corresponding to Åknes sliding plane

Dry slope

Calculations with the dry *Svaddenipun 2– model* setup and shear zone parameters identical to those for Åknes sliding plane result in a FOS of 1,14. Maximum shear strains are small, and mostly occurring underneath the shear zone sub-parallel to fracture set K1, following the lower margin of the SSR search area (*Figure 7.8*). Only upper section of the shear zone shows some minor shear strains, and the overlying metarhyolite show no clear strain concentrations. Stresses are low with no sign of concentrations around or within the shear zone.

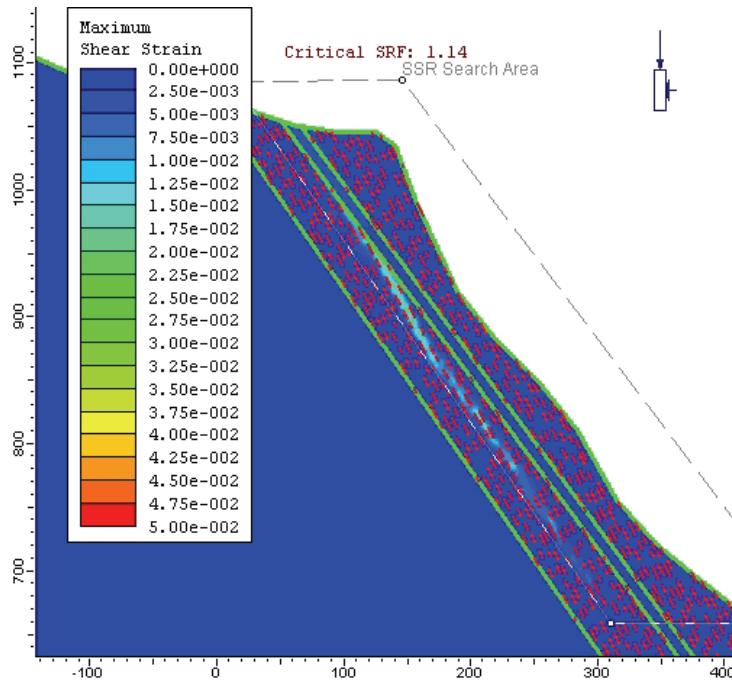


Figure 7.8: Shear strain plot for dry Svaddenipun 2 – model with Åknes sliding plane parameters applied in the shear zone. Strains occur only in upper part of shear zone and in the underlying metarhyolite along SSR search area boundary.

Partially saturated slope

When water is introduced to this model, resulting FOS is reduced to 0,77. Shear strains pattern is similar to dry slope conditions, but values are significantly higher. Some shear strain concentration in the upper metarhyolite layer at 750 m.a.s.l is also present, but the pattern is not clear. Concentration of stresses in metarhyolite above the shear zone is minimal but deviatoric stresses are a little higher than for dry slope conditions.

7.3.3 Result of critical shear zone strength calculations

Dry slope

Critical shear zone strength values resulting in a FOS of 0,995 for the *Svaddenipun 2– model* are given in *Table 7.2*, and the corresponding maximum shear strain plot is given in *Figure 7.9*. Shear strain concentrations in the upper metarhyolite layer around 775 m.a.s.l. are significant, and occur in the same area as with the *Svaddenipun 1 – model* setup. The dip angle of the zone showing increased strain is around 35°. There is also a substantial amount of shear strain along the SSR search area boundary in the metarhyolite beneath the shear zone.

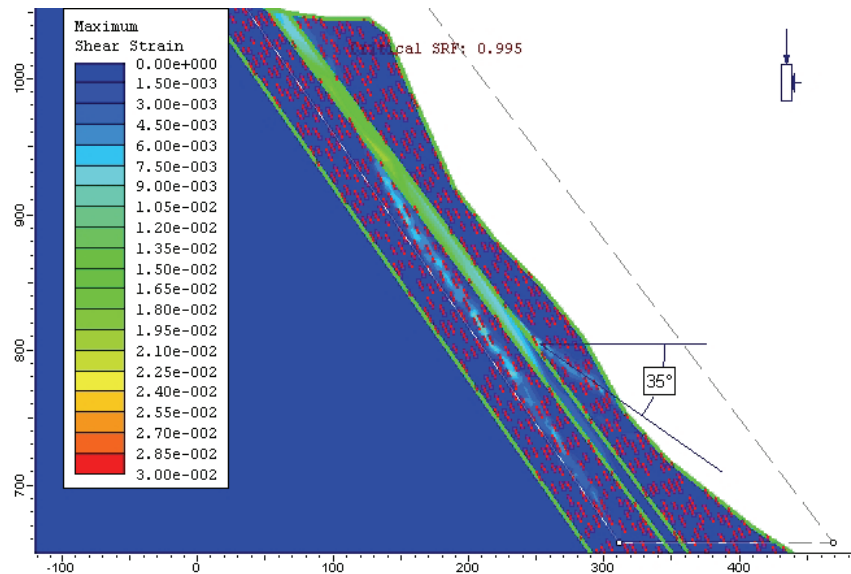


Figure 7.9: Maximum shear strain figure for critical shear zone strengths in the Svaddenipun 2 – model. Shear strain concentrations in the metarhyolite above the shear zone occurs at the same location as in the corresponding Svaddenipun 1 – model. The dip angle of the strain-concentration surface in upper metarhyolite is around 35°. Note the substantial amount of strains occurring below shear zone along SSR search area boundary.

Deviatoric stress situation for the Svaddenipun 2 – model with critical shear zone strength is given in Figure 7.10. No stress concentration in the metarhyolite above the shear zone is observed in contrast to similar calculations with Svaddenipun 1 – model setup, and stresses are generally low. Deviatoric stresses in the metarhyolite at 750 m.a.s.l are below 4 MPa. Major principal stress is below 3 MPa, and minor principal stress values are always positive, with peak values around 0,5 MPa

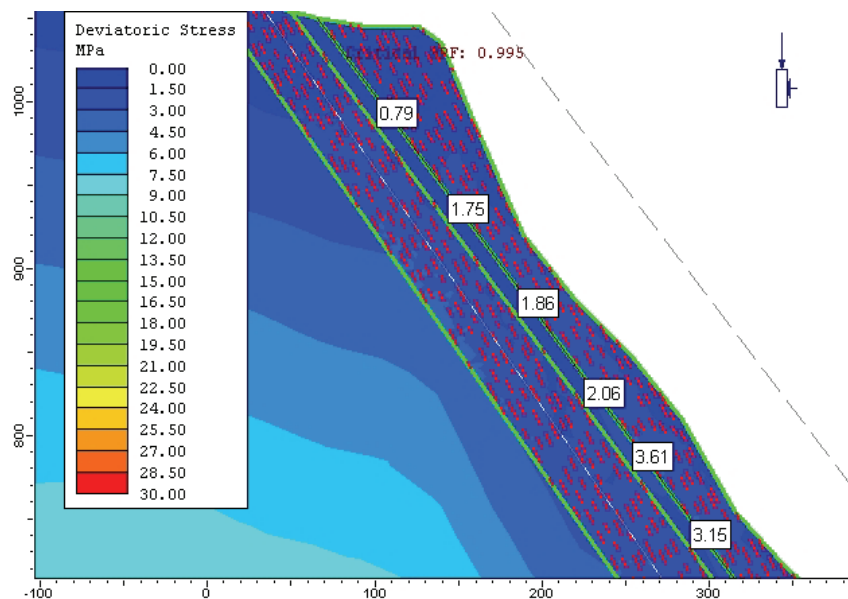


Figure 7.10: Deviatoric stresses in the Svaddenipun 2 – model with critical shear zone parameters corresponding to a FOS of 0,995. Deviatoric stress values (MPa) in metarhyolite at a distance of 0,1 meter from shear zone/metarhyolite boundary are shown.

A simulation with reduced ϕ_r for the K1 discontinuity set was carried out for the *Svaddenipun 2 – model* with critical shear strength properties. ϕ_r for K1 fractures was reduced from 30° to 25° resulting in a small decrease in FOS from 0,995 to 0,99. Shear strains, stress distribution and displacement rates for the two models are similar.

Partially saturated slope

The critical shear zone strength parameters with a partially saturated *Svaddenipun 2 – model* at FOS of 1,0 is given in *Table 7.2*. Maximum shear strain distribution for this simulation is presented in *Figure 7.11*. Shear strains in the upper part of the slope occur in the metarhyolite parallel to K1 fractures, until the influence of the SSR search area boundary forces strains to follow this line. Except for the top section, shear strain within the shear zone is small. No increase in shear strain trough the upper metarhyolite section is observed in the partially saturated analysis of the *Svaddenipun 2 – model*.

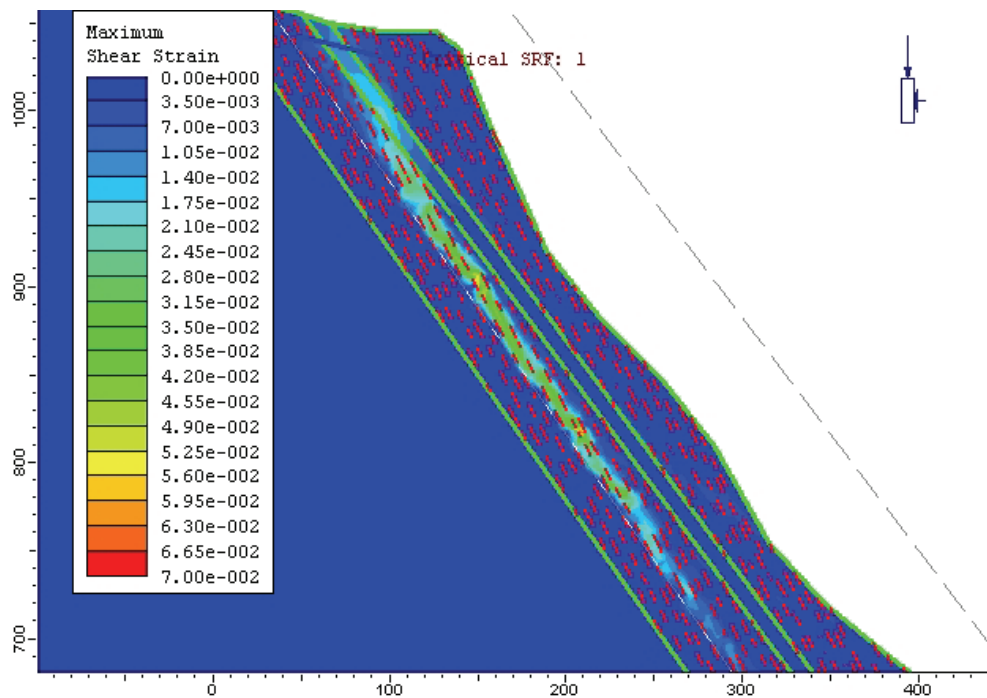


Figure 7.11: Maximum shear strain plot for FOS 1,0 with Svaddenipun 2 – model and partially saturated conditions. No indications of increased shear strain int the upper metarhyolite at elevations around 750 m.a.s.l.

There is a change in stress distribution between dry and partially saturated conditions for the critical shear zone strength calculations. For the partially saturated slope, both σ_1' and deviatoric stresses are high within the lower section of the shear zone, and low in the surrounding metarhyolite. Peak shear zone values for σ_1' and effective deviatoric stresses are approximately 10,5 and 9 MPa respectively.

7.4 Calculations with 30% increased strength parameters for metarhyolite and K1 discontinuities (Svaddenipun 3 – model)

7.4.1 Introduction

Table 7.3 shows the input parameters for shear zone strength and resulting FOS and calculated critical friction angles for the *Svaddenipun 3– model*. Here metarhyolite and K1 fractures have 30% increased strength values. In the following section the results are presented for the different shear zone input parameters.

Table 7.3: Mohr-Coulomb input parameters for shear zone in *Svaddenipun 3 – model*. Left: calculations with shear zone parameters corresponding to Åknes sliding plane, and resulting FOS. Right: Shear zone input values leading to critical stability state represented by FOS close to 1,0. For this model setup, c was remained constant and ϕ was varied until failure occurred.

Differences between dry and partially saturated conditions are highlighted.

	Åknes shear zone parameters		Reduced strength corresponding to FOS close to 1,0	
	Dry slope	Partially saturated slope	Dry slope	Partially saturated slope
E_m [MPa]	6000	6000	500	500
ϕ_{peak} [°]	36	36	5	10
c_{peak} [MPa]	0,92	0,92	0,05	0,05
FOS	3,01	2,84	1,05	1,01

7.4.2 Calculations with shear zone parameters corresponding to Åknes sliding plane

Shear zone strengths identical to the assumed Åknes sliding plane result in a FOS of 3,01 for the dry *Svaddenipun 3 – model*. Shear strain will occur along shear zone and in the overlying metarhyolite located around 750 m.a.s.l. This is similar to conditions in *Figure 7.1* for the *Svaddenipun 1– model*. The simulations also show that maximum shear strain in the metarhyolite located above the shear zone occurs in regions with concentrations both for peak and deviatoric stresses.

Partially saturated conditions for the *Svaddenipun 3 – model* have a FOS of 2,84. Both shear strain and stress patterns are similar to dry slope conditions with stress relief in the shear zone, and strain concentrations in the metarhyolite close to the slope surface at around 725 m.a.s.l.

7.4.3 Result of critical shear zone strength calculations

Dry slope

A significant reduction in shear zone strength was necessary to obtain numerically instability for the *Svaddenipun 3 – model*. Calculated FOS was 1,05 for the parameters given in *Table 7.3* with ϕ_{peak} of 5°. Shear strain occurs only within the shear zone and no sign of increased shear strain values are detected within the overlying metarhyolite, as shown in *Figure 7.12*. Stresses are low throughout the shear zone. At elevations around 750 m.a.s.l there is a large stress concentration in the metarhyolite particularly above the upper shear zone/metarhyolite boundary. Major principal stress reaches over 10 MPa, while minor principal stresses are close to zero resulting in a high deviatoric stress. Still no shear strain occurs in this area.

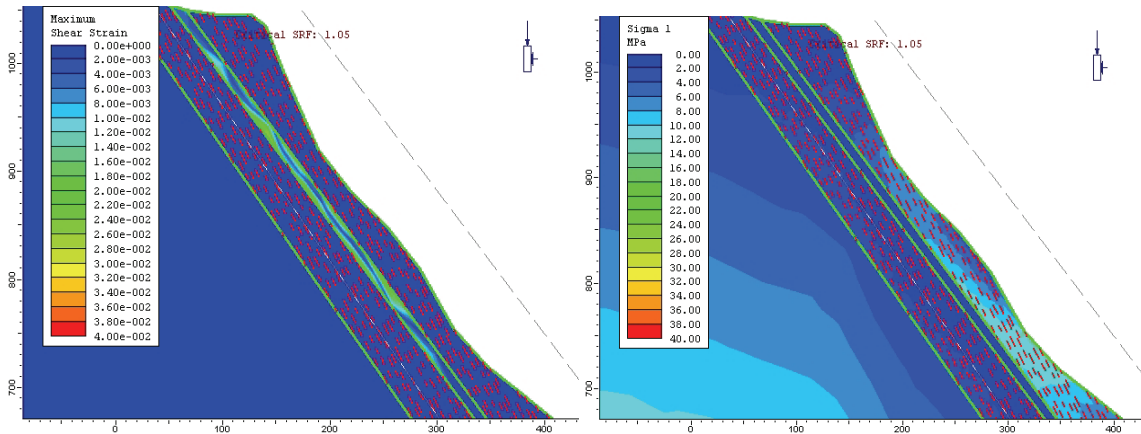


Figure 7.12: Shear strain plot (left) and major principal stress plot (right) for Svaddenipun 3 – model with shear zone strengths corresponding to a critical FOS of 1,05.

Partially saturated slope

A FOS value of 1,01 for the Svaddenipun 3 – slope conditions with included water table are obtained with a critical shear zone ϕ_{peak} of 10° . Both shear strain patterns and stress distribution concurs with the dry slope conditions. Figure 7.13 shows relationship between shear zone peak friction angle and corresponding FOS for both wet and partially saturated conditions with Svaddenipun 3 – model. A linear relationship between peak friction angle and FOS is present, and FOS is highly sensitive to small changes in friction angle value. Dry slope conditions show higher sensitivity to changes in ϕ than do partially saturated conditions.

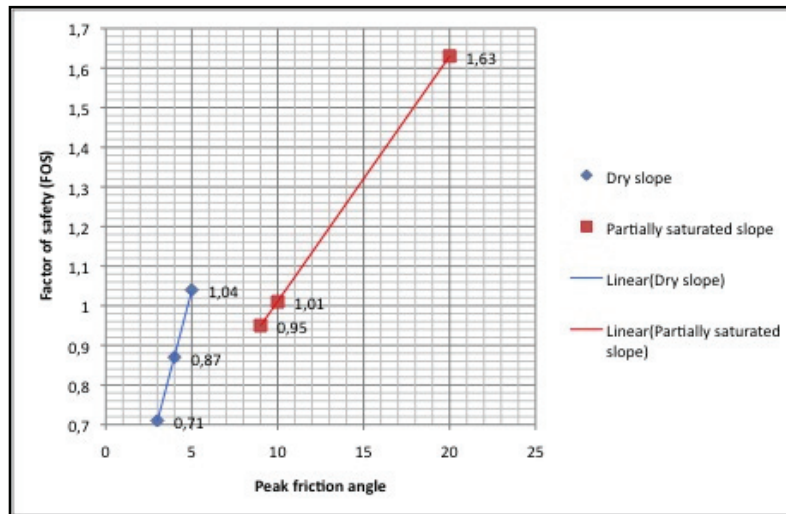


Figure 7.13: Relationship between shear zone peak friction angle and corresponding FOS for the Svaddenipun 3 – model setup.

Chapter 8: Discussion of results from LiDAR survey and Phase² modelling

8.1 LiDAR scanning

8.1.1 Achievement of scanning goals

As discussed in *Chapter 2.3*, the conditions for scanning at the Svaddenipun slope were suboptimal, and due to this, not all goals for the LiDAR survey was completed. Due to snow cover and the large distance to the upper section of the slope, and orientation bias in the lower sections, a high-resolution DEM of the slope was not obtained. Scan locations 5 and 6 are suitable for deformation measurement over time, since both the frontal cliff and reference points south of the shear zone may be included in the same scan. The collected dataset cannot be used due to snow cover. If new scans from the same locations are compared to the completed scans, the thickness of the snow layer would appear as deformations. This is obviously incorrect. Structural orientations for discontinuities were successfully obtained; this is important since surface mapping data is confirmed and validated for the whole slope.

8.1.2 Structural geological information

The purpose of the LiDAR-scanning was among others to obtain structural data for discontinuity orientations. As presented in *Figure 6.1* this was completed for 143 discontinuity surfaces. Comparison of results from LiDAR survey with the structural field mapping results reveal clear correlations between the two mapping methods. Stereoplot with measurements both from LiDAR and surface mapping are presented in *Figure 8.1*. The presence of both fractures set K1 and K2 is confirmed by LiDAR results. K1 fractures were mainly mapped in Scan 7 due to orientation bias present in Scan 6. LiDAR fractures in the K1-region on the stereoplot in *Figure 8.1*, generally show higher dip angles than field measurements. This reduces probability for daylighting fractures, extending from shear zone to the terrain surface, allowing planar sliding and total collapse of the slope. In contrast to field measurements, the scanner also recognizes a large number of K3 fractures, indicating that such set is present within the slope. Due to orientation bias, such K3 fractures only appear in Scan 6, and the set is here much clearer than in the field measurements. Scanner orientation may favour the appearance of such fractures since the line- of scanning is sub-parallel to the dip direction of the measured discontinuities. Fracture set K3 may thus be overrepresented in the scan. Its presence is still likely, and may affect the eastern lateral release of the potential instability. Compared to kinematic analysis in Loftesnes 2009, some of the LiDAR mapped K3 fractures show potential for planar or wedge failure. Due to the high dip angle, such fractures cannot create sliding planes from shear zone to the slope face, and K3 fractures is assumed to have low influence on large-scale slope stability.

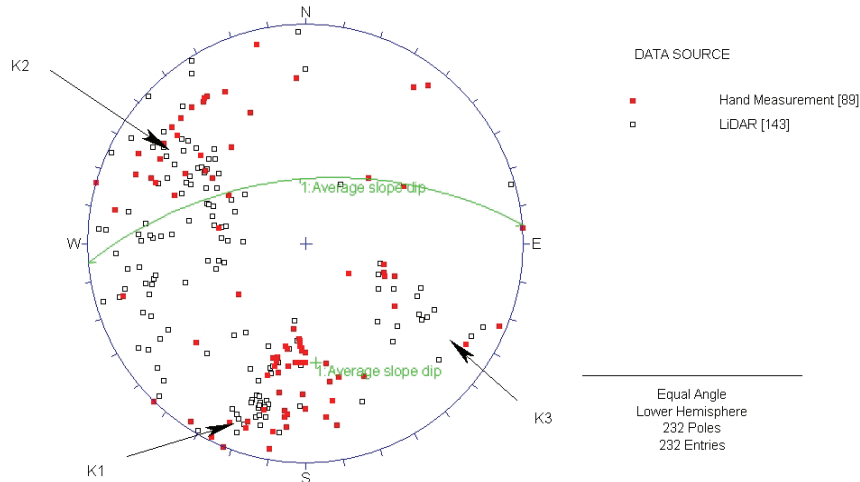


Figure 8.1: Stereoplot with comparison between field measurements and LiDAR measurements.

Structural mapping with LiDAR technique obtained information on structures from inaccessible areas that could not be reached by man. The mapped fracture planes are derived from all sections within the upper Svaddenipun slope. LiDAR results are thus more representative for the slope as a whole and not restricted to conditions at small outcrops along the periphery of the potential instability, as are the field measurements. This both confirms the field measurements and makes them representative for the whole slope. It is thus likely that all major fracture sets affecting slope stability situation have been identified. The probability of an unobserved daylighting fracture set, creating a sliding surface extending from the shear zone through intact metarhyolite to the terrain surface, is reduced.

8.1.3 Error sources

As noted in *Chapter 2*, there are some uncertainties regarding the LiDAR technique. An obvious error source in the Svaddenipun dataset is the snow cover that could possibly create surfaces that would appear as fractures in the scan (*Figure 8.2*). To avoid false mapping, the photos were carefully studied and no surfaces with snow cover were selected during the selection of fracture planes. The distance from the scanner to the rock surface was up to 300 meters for the analyzed scans, and for the 800-meter range ILRIS scanner, errors due to long distance should be minimal. Still closely spaced fractures may be interpreted wrongly as is illustrated in *Figure 8.2*. Processing and georeferencing could also introduce errors, but according to Oppikhofer 2010, this error is far less than the variability within the fracture sets and the error in hand measurements of fractures. During creation of planes in PolyWorks, attention was put on minimizing deviation between fracture surfaces and constructed planes. By following the methods described in *Chapter 2*, the overall errors from the LiDAR mapping of discontinuities are assumed to be small. The correlation between LiDAR and field measurements also indicates that errors are limited.

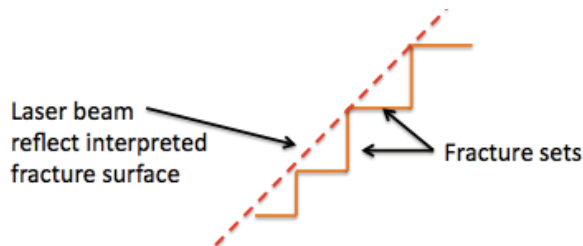


Figure 8.2: Illustrate incorrect surface recognized by the scanner. This may result from several effects; both from snow cover smoothing, and resolution of scanner.

8.2 Numerical modelling in Phase²

8.2.1 Location of the failure surface

One of the main objectives in this thesis is the detection of a potential sliding surface for a large-scale slope failure. According to Rocscience 2010 c, the areas experiencing maximum shear strain are likely to constitute the failure surface within the rock masses. By evaluating shear strain at different SRF-values, the probable sliding plane may be detected and a model of the progressive failure through intact rock may be obtained. Still it is important to mention that failure may occur along other surfaces showing less shear strains, however such failures have higher FOS and thus lower probability of occurrence. Rocscience 2004 b discusses the location of failure surfaces within rock slopes. It is stated that if a weak layer with strength properties less than 50-60% of a surrounding stronger layer is present, sliding will occur along the weak layer. Results from the vast majority of simulations show that failure will mainly occur along the shear zone as long as this has lower strength than the surrounding metarhyolite.

Most simulations also detect large shear strains and thus a daylighting failure surface, dipping 20-35°, extending from the shear zone to the terrain surface around 725-750 m.a.s.l (*Figure 7.1*). Within this area all simulations also show stress concentrations, with peak values for deviatoric stress and major principal stress. Deviatoric stresses are defined as the principal stress minus the mean stress and are an indicator of the anisotropic stress situation within a slope (Rocscience 2010 c). Development of rock mass failure and shear strain is a result of the magnitude of stress anisotropy in relation to the rock mass strength. For most models at Svaddenipun, areas of high deviatoric stresses concur with the areas showing large shear strain, confirming this relationship. This is particularly the case in the metarhyolite at elevations around 700-750 m.a.s.l where daylighting of the failing surface is assumed to take place.

In the analysis with similar strength parameters for metarhyolite and shear zone, the location of the failure surface is influenced by fracture set K1. Failure will then propagate underneath shear zone sub-parallel to fracture set K1 increasing the importance of discontinuity properties. Since shear strains are only calculated within the SSR-search area, the strains are forced to follow the lower boundary of this.

It is assumed that shear zone have significantly lower strength than metarhyolite, therefore the most likely scenario for the Svaddenipun slope will create a failure surface following the shear zone from the top plateau downwards to approximately 800 m.a.s.l, where it propagates through the overlying metarhyolite and daylights in the slope around 750 m.a.s.l.

8.2.2 Factor of safety and assessment of calculated critical shear zone strengths

The three different model setups (*Svaddenipun 1-3 models*) results in different critical shear zone strengths indicating slope failure. *Figure 8.3* show relationship between friction angle and cohesion for different slopes around the world and corresponding descriptions of the present rock masses. Descriptions are assumed to represent the average strength parameters along the whole length of the failure surface. Numbers represent back calculations of sliding plane strength parameters at different slope failures from around the world, presented in Wyllie and Mah 2004.

The calculated critical shear strength of *Svaddenipun 1* – and *Svaddenipun 3*– model plot in the lower left of this diagram with a failure surface described as weathered soft rock with clay coated slickensided joint surfaces. Recorded failures in this region of the plot have occurred in

clay shale and bentonite clay materials (Wyllie and Mah 2004). Since deformations along the Svaddenipun shear zone have occurred, the presence of such weak material within this zone may not be excluded. Its appearance throughout the entire 10 meter thick shear zone without sections showing higher strength is however unlikely. The calculated critical shear zone strength in the *Svaddenipun 1-* and *3 – models* seems unrealistic low. The actual shear zone material must thus have a higher strength, and FOS must be higher than 1 for both models. The changes in critical friction angle of 5-6° under influence of water do not affect this statement.

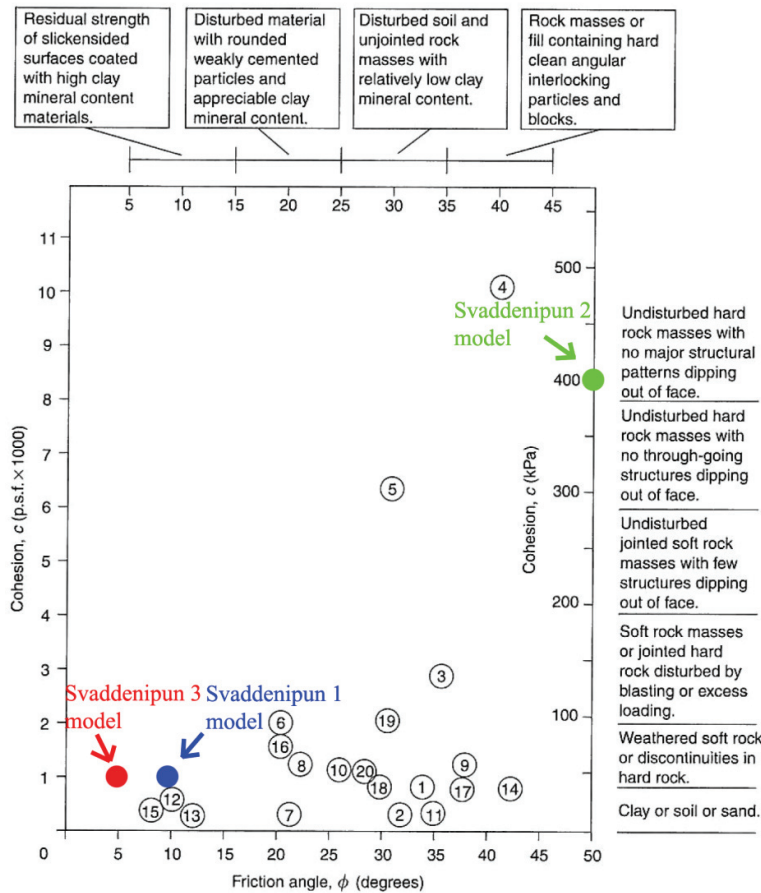


Figure 8.3: Relationship between cohesion and friction angles for back-calculations of failures in rock slopes represented by different numbers. The critical shear zone strength compositions from the different Svaddenipun models are marked.

Figure modified from Wyllie and Mah 2004.

Failure of the dry *Svaddenipun 2 – model* will occur if shear zone cohesion is under 400 kPa and ϕ , less than 50°. This corresponds to strength values slightly lower than the values for metarhyolite applied in this model. According to *Figure 8.3* such materials may be described as undisturbed hard rock without daylighting structures and with hard clean angular interlocking of blocks. The figure also shows that most reported failures have occurred at significantly lower sliding plane strengths. One of the key assumptions for the Svaddenipun analysis is that for failure to occur, the shear zone should have significantly lower strength properties than the surrounding metarhyolite. The calculated critical shear zone strength for the *Svaddenipun 2 – model* is thus regarded as much too high for the actual conditions at Svaddenipun. The model is thus not representative for the Svaddenipun slope and further discussion of this model is excluded.

From the registered slope failures in *Figure 8.3*, the lithology that seems most similar to the Svaddenipun site is number 9, a faulted rhyolite in Nevada. Cohesion values were here similar to critical *Svaddenipun 1-* and *3 – models*, and ϕ_r was around 37° . Since the critical shear zone strengths seems to be too low in the calculated *Svaddenipun 1-* and *3 – models*, properties of the faulted Nevada rhyolite may represent more realistic conditions for average shear strength along the most probable failure surface. Calculations with *Svaddenipun 1 – model* with similar cohesion, and a ϕ_r for the shear zone of 35° , similar to the Nevada rhyolite, result in a FOS of 1,28. This might be a better estimate on the strength of the most likely failure surface within the Svaddenipun slope.

8.2.3 General trends and patterns of different model setups

Stress distributions

Stress relief within the shear zone can be seen in all *Svaddenipun 1-* and *3 – models* where rock mass strength ratio between metarhyolite and shear zone is high. The weak material in the shear zone is incapable of transferring stresses, leading to redistribution of stress in the surrounding rocks, and a high stress ratio at the contact boundaries. Stress concentration is highest in the overlying metarhyolite showing peak values both in deviatoric and major principal stress in the area around 700-750 m.a.s.l. This area corresponds to the thinnest sections of the overlying metarhyolite, and as major stress direction is parallel to slope, the stress concentration should be highest in this area. Stress concentration is also highly dependent on the overburden, explaining why the maximum stresses occur at around 750 m.a.s.l and not in the narrow metarhyolite region at around 900 m.a.s.l. As already discussed there is close correlation between areas with stress concentrations and shear strain occurrence. This is due to the fact that as deviatoric stresses rise, there is an increased probability for tensile fracture propagation.

Influence of water

All models show significant reduction in stability by the introduction of water. According to *Figure 7.7* and *Figure 7.13*, FOS is more sensitive to a change in peak friction angle for dry slope conditions than for a partially saturated slope. This may be explained by the significant influence water generally has on stability, reducing the relative importance of change in friction angle. The importance of other parameters is reduced when water is present. Barton 1973 shows that normal reduction in friction angles are between $5-10^\circ$ when water is introduced on a test specimen. This is similar to the change in critical shear zone ϕ_{peak} for *Svaddenipun 1 –* and *Svaddenipun 3 – models* when the water table is added (*Table 7.1 and 7.3*). As for dry slope conditions, the critical shear zone friction angles for both model setups are assumed to be unrealistically low, also when a water table is added. This indicates that even if the actual slope is saturated, the actual shear zone strengths must be higher than those applied in the two models. The relative importance of water is thus lower than the influence of the highly varying shear zone strength parameters applied to the models.

When strength ratio between shear zone and metarhyolite is low, shear strains are not restricted to follow the shear zone, and water has a major influence on the location of the failure surface. When water is added to the *Svaddenipun 1 – model* with same shear zone strength as for the assumed Åknes sliding plane, maximum shear strain no longer occurs within the shear zone, but propagates into the underlying metarhyolite (*Figure 7.2*). This may be explained by the fact that water pressure increases towards depth, affecting the location of shear strains and rock mass failure.

Svaddenipun 1 – model

An unrealistic weak shear zone must be present to obtain critical SRF – calculations indicating slope failure in the *Svaddenipun 1– model*. Maximum shear strain, and thus the failure surface, follows the zone, until it cuts through the metarhyolite reaching the slope terrain around 750 m.a.s.l. The location of the high strains, and thus propagation of the failure surface through metarhyolite, concurs with the area showing peak deviatoric and major principal stresses. This confirms the effect that stress concentrations have on the location of high shear strains. Even though deviatoric stresses are low within the shear zone, most failure occurs here. This reflects the importance of stress/strength ratio, and not the absolute stress magnitude for each material. A significantly higher deviatoric stress is needed to induce shear strain within the metarhyolite than in the shear zone. Simulations with isotropic stress conditions show small influence on FOS and strain pattern. This is mainly due to the stress relief along the weak shear zone, preventing the expected higher horizontal stress to be transferred into the overlying metarhyolite. A reduction in deviatoric stress is thus not observed.

Svaddenipun 3 – model

Shear strain plot for the critical shear zone properties in the *Svaddenipun 3 – model* show no shear strain increase for the upper metarhyolite section, indicating that daylighting of a failure surface is improbable. The reasons for this derive from the high strength of the metarhyolite itself, and the high ratio between shear zone and metarhyolite strength. A significant shear zone reduction is needed to obtain critical FOS values leading to slope failure. The significant stress concentrations in the metarhyolite around 750 m.a.s.l, is not high enough for failure to occur in the strong rock.

8.2.4 Representativeness of initial Åknes strength parameters

The Åknes shear zone strength parameters applied in the Svaddenipun analysis correspond to a 25 cm thick sliding plane in the Åknes gneiss located 110 meters below slope surface. The material composition assumed for the Åknes failure surface consists of 60-62% unfilled joints, 35% gouge-filled joints and 3-5 % intact rock bridges, the latter highly increasing the total material strength (Grøneng 2010). The significant thickness and extent of the Svaddenipun shear zone indicate that major fracturing and crushing have occurred, resulting in a low content of intact rock. Amount of gouge filled material is expected to be significant, and presence of clay cannot be excluded. Even if stress conditions and the thickness of the Åknes-sliding plane differ from conditions within the Svaddenipun shear zone, the composition of the two zones could be similar. Thus may the calculated FOS (1,7 without and 1,5 with water) for the most likely *Svaddenipun 1 – model* with shear zone parameters corresponding to Åknes sliding zone be a reasonable estimate on the actual stability of the Svaddenipun slope. Probability of a shear zone consisting of significantly weaker material than the Åknes material is assumed to be low. The minimum FOS for the Svaddenipun slope should thus be in the same range as results from *Svaddenipun 1 – model* calculations with Åknes shear zone parameters.

Svaddenipun 3 – model with Åknes shear zone parameters show similar stress and strain patterns as *Svaddenipun 1 – model*. Since the FOS is higher, a more stable situation is present if the *Svaddenipun 3 –model* represents the actual slope conditions.

8.2.5 Reliability of results and model uncertainties

Whenever modelling results show reasonable and expected patterns, this increase the reliability of the model. The recorded shear strain patterns mainly following the weak shear zone and the thinnest section of the overlying metarhyolite is as expected. All simulations show that shear

strains occur in the section of the slope from 500 m.a.s.l and upwards along the valley slope. In this way it is clear that model size is appropriate and boundary effects may be regarded as negligible.

The strong relationship between induced stresses and the following strains are also reasonable. There is however as already discussed several difficulties in obtaining realistic stress distributions in a 2D numerical model. If the input stress distribution should be incorrect this would lead to wrong strain locations. The limited effects of *in situ* stress variations calculated for the *Svaddenipun 1 – model* indicate that stresses have minor influence on FOS and location of shear strain as long as the shear zone material has low ability to transfer stresses.

Modelling results are highly sensitive to shear zone strength properties, and the strength ratio to the surrounding metarhyolite. This is particularly the case for dry slope conditions, and it is clear that an approach trying to assess single shear zone values are inexpedient, and would lead to unreliable results. By varying the shear zone properties the reliability of the results increase, since the discussion of critical shear zone strengths may be compared to reference literature in a better way than may input parameters. The potential outcropping of the shear zone in the talus slope below 700 m.a.s.l also represents a major uncertainty.

Parametric study has reduced the probability of missing the actual conditions present in metarhyolite and K1 fracture set. The unrealistic results of the *Svaddenipun 2 – model* indicates that actual strength properties of metarhyolite and K1 fractures must be higher than those applied in this model.

The conducted parameter study on model sensitivity to reduced ϕ_r along K1 fractures, results in negligible effects on FOS. This may be explained by the fact that K1 fractures are not continuous in the model, reducing the influence of fracture strength parameters.

Chapter 9: Assessment of slope stability based on results and recommended further investigations

9.1 Introduction

The conducted stability analysis in this thesis have revealed substantial amount of information on the stability situation at Svaddenipun. Based on these findings, in addition to results from previous reports, a stability assessment of the Svaddenipun slope is given in this chapter. Uncertainties still exists, and stability assessment would change if real conditions deviate from the assumed slope model.

9.2 Assessment of slope stability based on existing knowledge

Calculated critical shear zone strengths in the different models indicate that the Svaddenipun slope is in a non-critical state with a FOS for the slope that is higher than 1. None of the critical shear zone strength calculations indicating failure are assumed to represent realistic slope conditions. As long as the models are valid, the probability for total slope failure seems small. Even if result indicate a FOS higher than 1, an instable situation cannot be excluded, particularly not on a long time scale. Hoek and Bray 1981 discuss acceptable FOS values to be around 1,3 for short-term stability, and 1,5 for long-term stability of rock slopes. A FOS of 1,28 was obtained for the most likely *Svaddenipun 1 – model* with ϕ_r –value for the shear zone comparable to an observed rhyolite failure in Nevada. FOS of 1,5 was obtained with partially saturated slope and Åknes shear zone parameters. Neither of these models can be excluded, this reflects the need for better shear zone parameter assessment and further investigations within the slope.

Structural data obtained from the LiDAR scanning both confirms field results and makes them representative for the whole slope. It is thus likely that all major fracture sets affecting the slope stability situation have been identified. Kinematic conditions within the slope are expected to be similar to findings in Loftesnes 2009, with 3 clear fracture sets. Fracture set K1, that were assumed to have major influence on kinematics and slope stability, might according to numerical modelling results influence less than shear zone strength properties and strength ratio to metarhyolite. According to LiDAR results, the probability of a fourth, unobserved, fracture set, creating a sliding surface through metarhyolite from the shear zone to the terrain surface is low. Failure through metarhyolite must thus occur as time-dependent degradation of rock bridges connecting several K1 fractures leading to a stepped failure surface. On the overall scale, this reduces probability of total slope failure, since intact metarhyolite rock bridges have significantly higher strength properties than shear zone and K1 fractures.

The most probable failure surface will follow the shear zone from the top plateau downwards to around 800 m.a.s.l, where it cuts through intact the metarhyolite and daylight in the slope around 750 m.a.s.l. Loftesnes 2009 describes that two highly crushed ridges are present in this region of the slope, and even if their processes of formation are unknown, it cannot be excluded that they relate to deformation within the rock masses in this region, due to toe compression leading to fracturing.

Minimum calculated release volumes of Section A indicate a failure of 2,2 million m^3 , this is higher than estimation in Loftesnes 2009. It is assumed that this volume is large enough to

cross the entire Vestfjord – valley (Loftesnes 2009). A total collapse along the entire shear zone length, including both Sections A, B and C in *Figure 1.4*, would involve around 5,1 million m^3 . As described in Loftesnes 2009, failure of such volumes would have severe consequences for the town centre of Rjukan.

9.3 Uncertainties

Uncertainties regarding actual slope conditions are still evident. Although the most likely kinematic slope conditions have been detected, including the location of most probable failure surface, the numerical simulations have not detected the actual FOS within the slope. The potential for large-scale instability may thus not be excluded. Stability seems governed by the shear zone, and detection of ongoing deformations may dramatically change slope stability assessment. Despite the measured opening of top plateau fractures, it is not clear whether observed displacement along shear zone result from active or remnant processes. The potential outcropping of the shear zone in the talus slope below 700 m.a.s.l also influence the stability assessment largely, and make shear zone strength properties even more vital for the slope stability. On the other hand the shear zone may in fact terminate at shallow depths close to the slope top, increasing the total stability. The long shear zone persistence along the top plateau however indicates that it extends at least to some depth.

The model response to introduction of water within the slope is clear, significantly reducing FOS or critical strength parameters needed to obtain FOS close to 1. However, as long as the shear zone strength parameters show considerable uncertainties, the influence of water is of secondary importance. First when a better estimate of the shear zone properties is obtained, a more precise location of the water table will be required in order to detect actual FOS.

9.4 Recommended further investigations

Based on the described uncertainties there is still need for increased knowledge of the Svaddenipun slope. The main uncertainty regarding the slope stability situation is the detection of ongoing deformations. As presented in Loftesnes 2009, it is important to detect whether observed displacements along shear zone are a result of active processes or not. This could be done by a new LiDAR survey with snow-free conditions from location 5 and 6, identical to the scans that are analyzed in this thesis. The 2009-scans cannot be used due to the snow cover. An alternative could be mounting of extensometers across open fractures at the top plateau, but such measurement will not detect shear zone displacement. LiDAR scanning would detect continuous deformations for the whole scanned area, and record differential movement within the slope suggesting that this method might give the best results.

Stability calculations are highly dependent and sensitive to variations in shear zone properties, and better assessment of these will improve the knowledge of the actual FOS within the slope. An important task to be conducted is thus to obtain more accurate data on shear zone material strength and the potential for outcropping of this zone in the lower sections of the slope. This is however not straightforward, since conditions along the daylighting section of the shear zone have low representativeness of the conditions at depth, where the deformations occur. By rope access from the top plateau, the steepest section of the western daylighting area, showing the assumed highest representativeness, might give useful information. The most extensive investigation would probably involve core drillings from the top plateau and throughout the shear zone; however the costs of such investigations are high.

Chapter 10: Conclusion

LiDAR scanning and numerical stability analysis of the Svaddenipun slope have revealed valuable input to the stability assessment of the Svaddenipun slope. Compared to the preliminary stability conclusions described in Loftesnes 2009, the findings in this thesis have not detected new elements that increase the hazard potential for the slope.

The following statements conclude the main findings in the Svaddenipun stability analysis conducted in this thesis:

- *Despite that not all scanning goals were completed; the conducted LiDAR investigation succeeded in detecting discontinuity patterns in the Svaddenipun slope. A high correlation with field measurements, indicate that all major fracture sets within the slope are detected. Results also show the advantages and reliability of LiDAR technique for slope stability analyses.*
- *According to LiDAR data, the presence of a daylighting fracture set in the upper metarhyolite layer, creating a failure surface from shear zone to the terrain surface is unlikely. This indicates that rock failure in metarhyolite must propagate through strong intact rock, increasing the total available shear strength along the failure surface.*
- *The FEM-SSR analysis in Phase² is found to be a useful and reliable tool for detecting locations of the failure surface and critical shear zone material strengths inducing slope failure.*
- *Results from numerical modelling show no sign of a critical stability state at Svaddenipun. None of the calculated critical shear zone strength calculations, resulting in factor of safety value close to 1, represents realistic slope conditions. Factor of safety must thus be higher than 1. For total slope failure to occur, the constructed slope models must be wrong.*
- *According to the numerical simulations, the most probable failure surface will follow shear zone in the upper slope before propagating through fractured metarhyolite until daylighting occurs. Such failure would mobilize minimum 2,2 million m³.*
- *Since no exact FOS – value is obtained; the assessment of the exact stability situation, and probability for long-term instability cannot be evaluated in detail.*
- *Modelling results show expected relationships between material strengths, stress concentrations and induced shear strains. This increase model reliability. Model show highest sensitivity to shear zone parameters, but also water has high influence on stability.*
- *Both input parameters and numerical model setup is subject to uncertainties. Conditions deviating from the assumed slope model, particularly regarding shear zone strength parameters and its potential for outcropping in the lower part of the slope would change the hazard assessment dramatically.*
- *Due to the uncertainties and large consequences of a failure of the Svaddenipun slope, further investigations are highly recommended. This includes deformation measurement to detect whether shear zone is deforming at present. If results confirm this, a more extensive investigation program for detecting better shear zone parameters should be initiated.*

Chapter 11: References

- Barton N, 1973: *Review of a new shear-strength criterion for rock joints*. Engineering geology, 7(1973). Pp 287-332. Elsevier Scientific Publishing Company, Amsterdam.
- Broch E and Nilsen B, 2001: *Ingeniørgeologi Berg*. Institutt for geologi og Bergteknikk, NTNU Trondheim. (Norwegian)
- Böhme M, 2009: *Personal comment during LiDAR scanning of the Svaddenipun slope*. October 13th 2009.
- Coduto D. P, 2007: *Geotechnical engineering, Principles and Practice*. Prentice Hall of India New Dehli. ISBN-978-81-203-2137-3.
- Collins B. D, Kayen R, 2006: *Land-Based Lidar Mapping – a New Surveying Technique to Shed Light on Rapid Topographic Change*. USGS factsheet 2006-3111. Downloaded from: <http://pubs.usgs.gov/fs/2006/3111/>
- Dahlgren S, Sletten K, Blikra L.H, Sandersen F, 2004: *Skredfarekartlegging i Vestfjorddalen*. NGU report nr.2004.023 (Norwegian)
- Grøneng G, 2010: *Stability Analyses of the Åknes Rock Slope, Western Norway*. Doctoral theses at NTNU, 2010:30.
- Hammah R. E, Curran J. C, Yacoub T, Corkum B, 2004: *Stability analysis of rock slopes using the finite element method*. Published at Eurock 2004 & 53rd Geomechanics Colloquium. Schubert (ed.)
- Hammah R.E, Yakoub T, Corkum B, Wibowo F, Curran J.H, 2007: *Analysis of block rocks slopes with finite element shear strength reduction analysis*. Published in Rock mechanics: Meeting society's Challenges and Demands – Eberhardt, Stead and Morrison (eds). 2007 Taylor & Francis Group, London. ISBN 978-0-415-44401-9. P 329
- Hammah R.E, Yakoub T, Corkum B, Curran J.H, 2006: *A comparison of finite element slope stability analysis with conventional limit equilibrium investigation*. Proceedings of the 58th Canadian Geotechnical and 6th Joint IAHC-CNC and CGS Groundwater Specialty Conferences Saskatoon, Saskatchewan, Canada, September 2005.
- Hammah R.E, Yakoub T.E, Corcum B.C, Curran J.H, 2005: *The shear strength reduction method for the generalized Hoek-Brown criterion*. American Rock Mechanics Assosiation. Anchorage Alaska June 25th - 29th 2005
- Hoek E, Bray J, 1981: *Rock Slope Engineering*. Revised 3rd edition. SPON Press Taylor and Francis Group.
- Hoek E, 2000: *Practical Rock Engineering*. Downloaded from: <http://www.rocsience.com/hoek/PracticalRockEngineering.asp>

- Hoek E, Carranza-Torres C, Corcum B, 2002: *Hoek-Brown Criterion – 2002 edition*. Proceedings of the 5th North American Rock Mechanics Symposium and the 17th Tunnelling Association of Canada: NARMS-TAC 2002, Toronto, Canada, Vol 1, page 267-273.
- Hope, Palmstrom A, Finnerud K, 1997: *Rebuilding of the 70 years old Nore 1 Power Plant*. Conference on Hydropower'97, Trondheim, Norway, pp. 631-638
- InnovMetric 2005: *PolyWorks® V9.0 User's Guide for Surveying Applications*. December 2005. InnovMetric Software Inc. 2014 Jean-Talon Nord, Suite 310 Ste-Foy, Québec, Canada, G1N 4N6.
- InnovMetric 2009: *PolyWorks/IMInspect™, Comparison and Verification Software Reference Guide Version 11 for Windows February 2009*. InnovMetric Software Inc. 2014 Cyrille-Duquet, Suite 310 Québec, Qc, Canada, G1N 4N6.
- Janeras M, Navarro M, Georgina A, Ruiz A, Wolfgang K, Tayala J, Barbera M, Lopez F, 2004: *LiDAR applications to rock fall hazards assessment in Vall De Nuria*. Presented on: 4th ICA Mountain Cartography Workshop, Vall de Nuria, Catalonia, Spain. September 30th –October 2nd 2004.
- Kemney J, Norton B, Handy J, Donovan J, 2008: *Three-Dimensional Digital Imaging for the Identification, Evaluation and Management of Unstable Highway Slopes*. Final report for Highway IDEA project 119, US Transportation research board.
- Krahn J. 2007: *Limit equilibrium, strength summation and strength reduction methods for assessing slope stability*. Published in *Rock Mechanics: Meeting Society's Challenges and Demands – Eberhardt, Stead & Morrison (eds)*. 2007 Taylor & Francis Group, London, ISBN 978-0-415-44401-9. Page 311-318
- Kveldsvik V, Einstein, H, Nilsen B, Blikra L. H, 2008: *Numerical Analysis of the 650,000 m² Åknes Rock Slope based on Measured Displacements and Geotechnical Data*. Rock Mech Rock Eng DOI 10.1007/s00603-008-0005-1.
- Laws S, Eberhardt E, Löw S, Descoedres F, 2003: *Geomechanical Properties of Shear Zones in the Eastern Aar Massif, Switzerland and their Implication on Tunnelling*. *Rock mechanics and rock engineering* 2003: 36 (4), pp 271-303.
- Lichti D.D, 2004: *A resolution measure for terrestrial laser scanners*. In proceedings: ISPRS Congress: International Archives of the Photogrammetry, Remote sensing and Spatial Information Sciences, Istanbul July 12th -23rd 2004.
- Loftesnes Kristian, 2009: *Svaddenipun, Rjukan; Investigations and analysis of potential rock slope instability*. Specialization project thesis at NTNU, Trondheim. (Norwegian)
- Lu Ming, 2010: *Personal comment*. 23.04. April 23rd 2010

Lutz S. J, Hickman S, Davatzes N, Zemach E, Drakos P, Robertson-Tait A, 2010: *Rock mechanical testing and petrologic analysis in support of well stimulation activities at the desert peak geothermal field, Nevada*. Proceedings, Thirty-Fifth Workshop on Geothermal Reservoir Engineering Stanford University, Stanford, California, February 1st -3rd, 2010 SGP-TR-188

Löv S, 2009: Notes from lecture: *Landslide Analysis ETH, Zurich: Case Study III (Preonzo)*, May 4th 2009

Martin C.D, Tannant D.D, Lan H, 2007: *Comparison of terrestrial-based, high resolution, LiDAR and digital photogrammetry surveys of a rock slope*. Published in Rock Mechanics: Meeting Society's Challenges and Demands – Eberhardt, Stead & Morrison (eds). 2007 Taylor & Francis Group, London, ISBN 978-0-415-44401-9. Page 37-45.

Myrvang A, 2001: *Bergmekanikk*. Institutt for Geologi og Bergteknikk, NTNU Trondheim. (Norwegian)

NGI, 2009: *Svaddenipun, Rjukan. Beskrivelse av mulig ustabil fjellparti med forslag til innledende overvåkning*. Report nr 20071925-1 (Norwegian)

Nilsen B, 2000: *New trends in rock slope stability analyses*. Bulletin Eng Geol Env (2000) 58: 173-178. Springer Verlag

Nilsen B, Palmstrøm A, 2000: *Engineering Geology and Rock Engineering*. Norwegian group of rock mechanics. Handbook No 2.

Oppikhofer T, 2010: *Personal comment*. March 16th 2010.

Optech, 2006 a): User Manual: *Optech ILRIS-3D Operation Manual*. Optech Incorporated Industrial & 3D Imaging Division 300 Interchange Way Vaughan, Ontario Canada L4K 5Z8. Downloaded from:

http://facility.unavco.org/project_support/polar/support/TLS/ILRIS3D_Manual.pdf

March 10th 2010

Optech, 2006 b): User manual: *ILRIS-3D Matching Viewer Guide Version 1.0 Beta 3*. Optech Incorporated Industrial & 3D Imaging Division 300 Interchange Way Vaughan, Ontario, Canada L4K 5Z8. Downloaded from:

<http://facility.unavco.org/kb/questions/44/TLS+Manual+-+Matchview+User+Manual>. March

10th 2010.

Optech, 2009 a): Downloaded from: <http://optech.ca/i3dapps-ilris.htm>. March 3rd 2010.

Panthi K.K, Nilsen B, 2005: *Numerical analysis of stresses and displacements for the Tafford slide, Norway*. Bulletin Eng Geol Env (2005). DOI 10.1007/s10064-005-0009-y.

Rocscience, 2004: *A new era in slope stability analysis; Shear strength reduction finite element technique*. Article prepared for RocNews Summer 2004.

Rocscience 2004 b: *Application of the Finite Element Method to Slope Stability*. Rocscience Inc. Toronto, Ontario, Canada 2004.

Rocscience, 2010 a): *Phase² product sheet*.

Downloaded from: <http://www.rocscience.com/products/Phase2.asp>. March 2nd 2010.

Rocscience, 2010 b): *Dips online user manual*. Downloaded from:

<http://www.rocscience.com/downloads/dips/WebHelp/DIPS.htm>. March 12th 2010.

Rocscience 2010 c): *Phase² online user manual*. Downloaded from:

<http://www.rocscience.com/downloads/phase2/WebHelp/phase2.htm>

Romana Ruiz M, 2002: *Determination of deformation modulus of rock masses by means of geomechanical classifications*. Published in Eurock 2002, ISRM International Symposium on Rock Engineering for Mountainous Regions. Funchal November 25th -28th 2002. C. Dinis da Gama and L Ribeiro e Sousa (ed).

Stead D, Eberhardt E, Coggan J.S, 2006: *Developments in the characterization of complex rock slope deformation and failure using numerical modelling techniques*.

Engineering geology 83 (2006). Pp 217-235.

Sturzenegger M, Stead D, Froese C, Moreno F, Jaboyedoff M, 2007: *Ground-based and airborne LiDAR for structural mapping of the Frank Slide*. Published in Rock Mechanics: Meeting Society's Challenges and Demands – Eberhardt, Stead & Morrison (eds). 2007 Taylor & Francis Group, London, ISBN 978-0-415-44401-9.

Sturzenegger M, Yan M, Stead D, Elmo D, 2007: *Applications and limitations of ground based laser scanning in rock slope characterization*. Published in Rock Mechanics: Meeting Society's Challenges and Demands – Eberhardt, Stead & Morrison (eds). 2007 Taylor & Francis Group, London, ISBN 978-0-415-44401-9.

Sturzenegger M, Stead D, 2009: *Close range terrestrial digital photogrammetry and terrestrial laser scanning for discontinuity characterization on rock cuts*.

Engineering Geology 106 (209), Pp 163-182.

Singh B, Goel R. K, 2006: *Tunnelling in Weak Rocks*. Chapter 7. Geo-Engineering Book Series Editor John A. Hudson FEng Imperial College of Science, Technology and Medicine, University of London, UK

Wyllie D. C, Mah C. W, 2004: *Rock Slope Engineering. Civil and Mining*. 4th Edition. Spon Press, Taylor and Francis Group.

Appendices

Appendix 1: LiDAR scanning locations

Table A1.1: Coordinates and relevant information of the processed LiDAR – scanning locations.

Location	Scan nr.	Coordinates			Scanning direction		Resolution scanner
		East	North	Elevation	Dip direction	Dip angle	
5, west of shear zone top plateau	6	32478128	6636843	1013	80	10	30mm at 150m range
6, eastern boundary of instability at top plateau	7	32478727	6637011	1045	225	15	30mm at 150m range

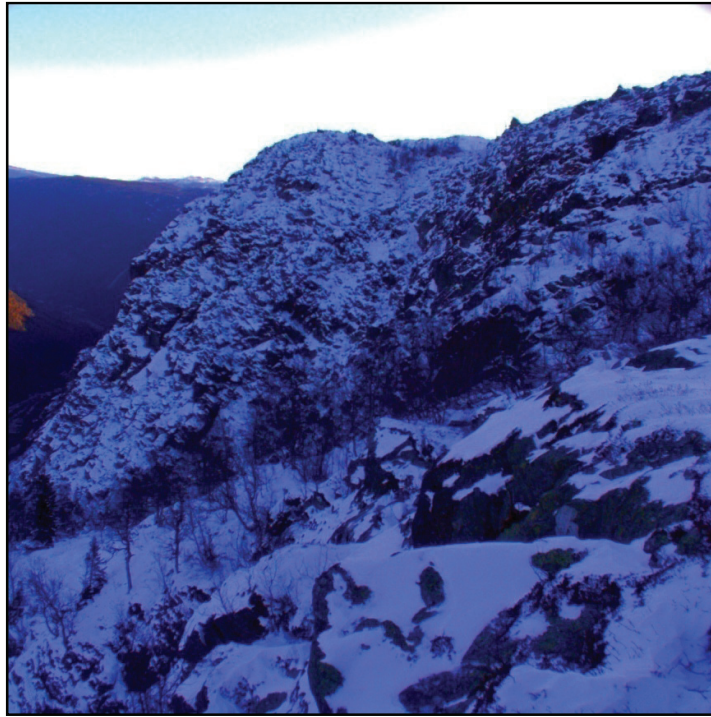


Figure A1.1: Photo of scan 6.



Figure A1.2: Photo of scan 7.

Appendix 2: LiDAR processing setup parameters

Table A2.1: Input parameters in Polyworks module IMAlign.

<i>IMAlign setup parameters</i>	<i>Scan 6</i>	<i>Scan 7</i>	<i>DEM</i>	<i>Comment</i>
<i>Number of interpolated points</i>	7428058	7916631	15498	<i>Total number of imported points in point cloud or DEM.</i>
<i>Units</i>	<i>Meters</i>	<i>Meters</i>	<i>Meters</i>	
<i>Interpolation setp [m]</i>	0,03	0,03	5	<i>Length of sides in the grid constructed when importing a point cloud or DEM. Should be similar to the resolution of the DEM or Point cloud.</i>
<i>Max angle [deg]</i>	89	89	89	<i>Angle between two neighbouring cells. Cannot be more than 90, this implies shadow and loss of points. A low value would remove vegetation from scan. High value still needed to include rock surfaces that are perpendicular to each other.</i>
<i>Max edge length [m]</i>			40	<i>Parameter to avoid that to long cells is created when two corresponding cells are sub-parallel.</i>

Appendix 3: List of all relevant Phase² files

The following table lists all the 35 relevant Phase² files used in the numerical modelling of the Svaddenipun slope. Model names correspond to the Phase² file-names on the memory stick in Appendix 8.

Table A3.1: Complete list of all relevant Phase² files used in the numerical modelling of the Svaddenipun slope.

File name	Dry	Partially saturated	Model purpose	Model setup
svaddenipun 1 dry fhi lik 5	X		Critical Shear zone property search	Svaddenipun 1
svaddenipun 1 dry fhi lik 8	X		Critical Shear zone property search	Svaddenipun 1
svaddenipun 1 dry fhi lik 9	X		Critical Shear zone property search	Svaddenipun 1
svaddenipun 1 dry fhi lik 15	X		Critical Shear zone property search	Svaddenipun 1
svaddenipun 1 dry fhi lik 25	X		Critical Shear zone property search	Svaddenipun 1
svaddenipun 1 dry fhi lik 35	X		Critical Shear zone property search	Svaddenipun 1
svaddenipun 1 dry hbestimates	X		Åknes shear zone parameters	Svaddenipun 1
svaddenipun 1 dry fhi lik 9 isotropic stressses 1	X		Isotropic stress simulationss	Svaddenipun 1
svaddenipun 1 dry fhi lik 9 bbphi lik 25	X		Reduced K1 fractures Barton Bandis ϕ_c	Svaddenipun 1
svaddenipun 1 wet fhi 15		X	Critical Shear zone property search	Svaddenipun 1
svaddenipun 1 wet fhi 20		X	Critical Shear zone property search	Svaddenipun 1
svaddenipun 1 wet fhi 25		X	Critical Shear zone property search	Svaddenipun 1
svaddenipun 1 wet		X	Åknes shear zone parameters	Svaddenipun 1
svaddenipun 2 dry reduced 30% hb	X		Åknes shear zone parameters	Svaddenipun 2
svaddenipun 2 dry reduced 30% phi 30	X		Critical Shear zone property search	Svaddenipun 2
svaddenipun 2 dry reduced 30% phi 50.fez	X		Critical Shear zone property search	Svaddenipun 2
svaddenipun 2 dry reduced 30% phi 50 c 250kpa	X		Critical Shear zone property search	Svaddenipun 2
svaddenipun 2 dry reduced 30% phi 50 c 350kpa	X		Critical Shear zone property search	Svaddenipun 2
svaddenipun 2 dry reduced 30% phi 50 c 400kpa	X		Critical Shear zone property search	Svaddenipun 2
svaddenipun 2 dry reduced 30% phi 50 c 450kpa	X		Critical Shear zone property search	Svaddenipun 2
svaddenipun 2 dry reduced 30% phi 50 c 500kpa	X		Critical Shear zone property search	Svaddenipun 2
svaddenipun 2 dry reduced 30% phi 50 c 550kpa	X		Critical Shear zone property search	Svaddenipun 2
svaddenipun 2 dry reduced 30% phi 50 c 400kpa bbphi 25	X		Reduced K1 fractures Barton Bandis ϕ_c	Svaddenipun 2
svaddenipun 2 wet reduced		X	Åknes shear zone	Svaddenipun 2

<i>30%</i>			<i>parameters</i>	
<i>svaddenipun 2 wet reduced 30% phi 50 c 1000 kpa</i>		<i>X</i>	<i>Critical Shear zone property search</i>	<i>Svaddenipun 2</i>
<i>svaddenipun 2 wet reduced 30% phi 50 c 3000 kpa</i>		<i>X</i>	<i>Critical Shear zone property search</i>	<i>Svaddenipun 2</i>
<i>svaddenipun 2 wet reduced 30% phi 50 c 3500 kpa</i>		<i>X</i>	<i>Critical Shear zone property search</i>	<i>Svaddenipun 2</i>
<i>svaddenipun 3 dry increase 30%</i>	<i>X</i>		<i>Åknes shear zone parameters</i>	<i>Svaddenipun 3</i>
<i>svaddenipun 3 dry increase 30% phi lik 3</i>	<i>X</i>		<i>Critical Shear zone property search</i>	<i>Svaddenipun 3</i>
<i>svaddenipun 3 dry increase 30% phi lik 4</i>	<i>X</i>		<i>Critical Shear zone property search</i>	<i>Svaddenipun 3</i>
<i>svaddenipun 3 dry increase 30% phi lik 5</i>	<i>X</i>		<i>Critical Shear zone property search</i>	<i>Svaddenipun 3</i>
<i>svaddenipun 3 wet increase 30%</i>		<i>X</i>	<i>Åknes shear zone parameters</i>	<i>Svaddenipun 3</i>
<i>svaddenipun 3 wet increase 30% phi 9</i>		<i>X</i>	<i>Critical Shear zone property search</i>	<i>Svaddenipun 3</i>
<i>svaddenipun 3 wet increase 30% phi 10</i>		<i>X</i>	<i>Critical Shear zone property search</i>	<i>Svaddenipun 3</i>
<i>svaddenipun 3 wet increase 30% phi 20</i>		<i>X</i>	<i>Critical Shear zone property search</i>	<i>Svaddenipun 3</i>

Appendix 4: Screenshots of RocData input parameters for metarhyolite

The following figures show screenshots from RocData software, where metarhyolite strength parameters were converted from Hoek – Brown into Mohr – Coulomb material model.

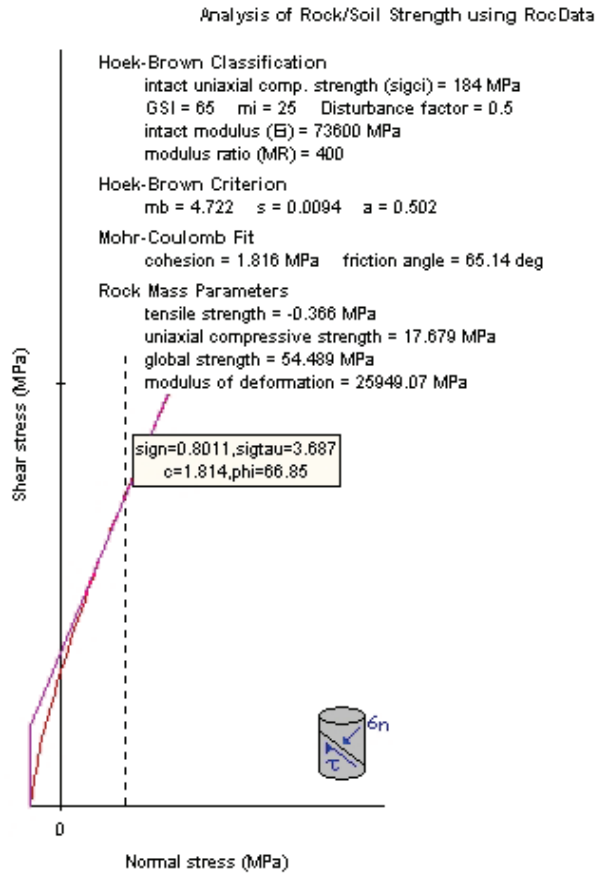


Figure A4.1: Conversion of Hoek – Brown parameters for the metarhyolite in the Svaddenipun 1 – model.

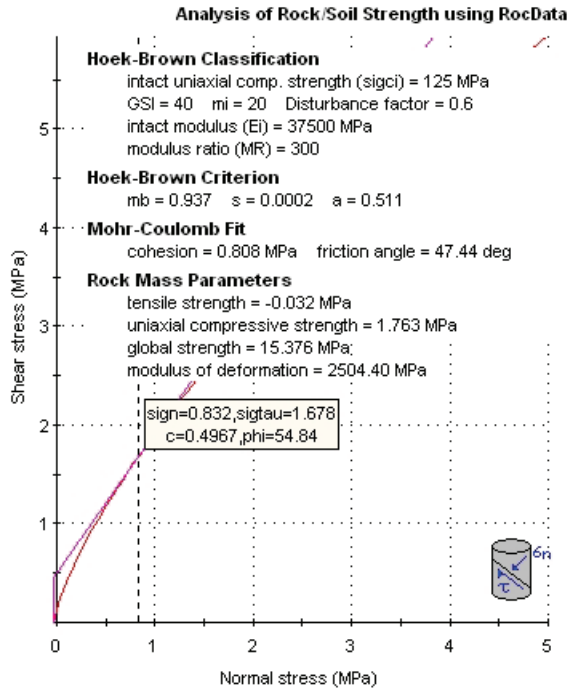


Figure A4.2: Conversion of Hoek–Brown parameters for the metarhyolite in the Svaddenipun 2 – model.

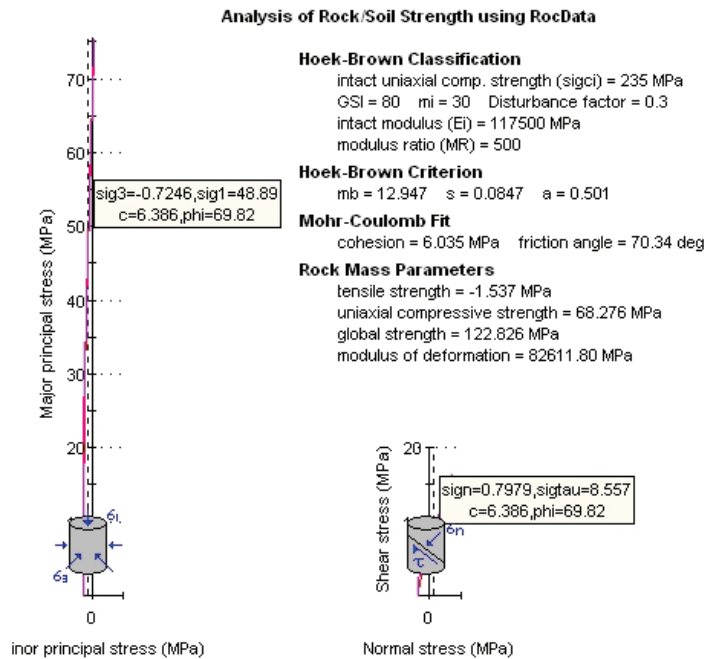


Figure A4.3: Conversion of Hoek–Brown parameters for the metarhyolite in the Svaddenipun 3 – model.

Appendix 5: Estimation of shear modulus for metarhyolite

Rock mass shear modulus G_m and intact rock shear modulus G_i where found using the following equations found in Myrvang 2001:

$$G_m = \frac{E_m}{2(1+\nu)} \quad [Equation A5.1]$$

$$G_i = \frac{E_i}{2(1+\nu)} \quad [Equation A5.2]$$

E_m value used is 15 GPa.

E_i is estimated from E_m by the relation given in Equation 5.6.

This results in:

$$G_m = 6,4 \text{ GPa}$$

$$G_i = 12,8 \text{ GPa}$$

Appendix 6: Contourplots of LiDAR Scan 6 and Scan 7

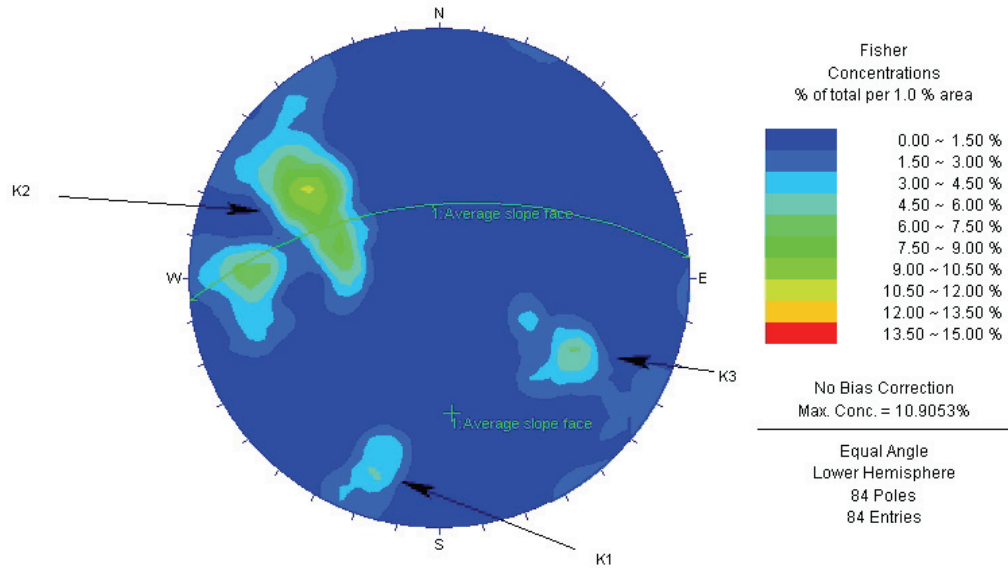


Figure A6.1: Contour plot of discontinuities detected on LiDAR Scan 6 at Svaddenipun.

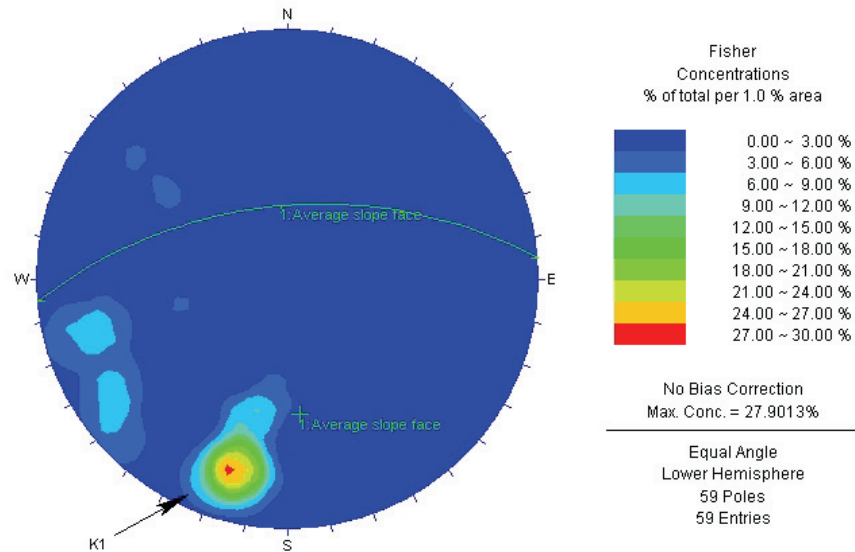


Figure A6.2: Contour plot of discontinuities detected on LiDAR Scan 7 at Svaddenipun.

Appendix 7: Relevant Phase² input parameters for shear zone strength and resulting FOS

Dry slope conditions

Table A7.1: Svaddenipun 1 – model: Initial values for metarhyolite and K1 fractures. Dry conditions.

E_m [MPa]	6000	3000	3000	1000	1000	1000	1000
ϕ_{peak} [°]	36	35	25	15	9	8	5
c_{peak} [MPa]	0,92	0,05	0,05	0,05	0,05	0,05	0,05
FOS	1,70	1,28	1,20	1,05	1,01	0,98	0,93

Table A7.2: Svaddenipun 2 – model: 30% reduced values for metarhyolite and K1 fractures. Dry conditions.

E_m [MPa]	6000	4000	4000	4000	4000	4000	6000	6000	6000
ϕ_{peak} [°]	36	30	50	50	50	50	50	50	50
c_{peak} [MPa]	0,92	0,05	0,05	0,25	0,35	0,4	0,45	0,5	0,55
FOS	1,14	0,69	0,82	0,90	0,96	0,995	1,10	1,13	1,14

Table A7.3: Svaddenipun 3 – model: 30% increased values for metarhyolite and K1 fractures. Dry conditions.

E_m [MPa]	6000	500	500	500
ϕ_{peak} [°]	36	3	4	5
c_{peak} [MPa]	0,92	0,05	0,05	0,05
FOS	3,01	0,71	0,87	1,05

Partially saturated slope conditions

Table A7.4: Svaddenipun 1 – model: Initial values for metarhyolite and K1 fractures. Partially saturated conditions.

E_m [MPa]	6000	3000	3000	1000
ϕ_{peak} [°]	36	25	20	15
c_{peak} [MPa]	0,92	0,05	0,05	0,05
FOS	1,50	1,04	1,02	1,00

Table A7.5: Svaddenipun 2 – model: 30% reduced values for metarhyolite and K1 fractures. Partially saturated conditions.

E_m [MPa]	6000	6000	6000	6000
ϕ_{peak} [°]	36	50	50	50
c_{peak} [MPa]	0,92	1,0	3,0	3,5
FOS	0,77	0,48	0,96	1,00

Table A7.6: Svaddenipun 3 – model: 30% increased values for metarhyolite and K1 fractures. Partially saturated conditions.

E_m [MPa]	6000	500	500	500
ϕ_{peak} [°]	36	9	10	20
c_{peak} [MPa]	0,92	0,05	0,05	0,05
FOS	2,84	0,95	1,01	1,63

Appendix 8: Memory stick with relevant Phase²- and PolyWorks-files

Memorystick named “Master thesis Kristian Loftesnes” include the following folders:

- *Polyworks Svaddenipun: PolyWorks project with the IMAlign and IMInspect files for the two scans. Zipped folder.*
- *Phase² Svaddenipun: All relevant Phase² files used in the numerical modelling and listed in Appendix 3. Both model files and Interpret-files. Information on geometry of profile and material boundaries and input parameters may be found in the “Info-viewer” option in each “Interpret file”.*

ISBN 00-0000-000-0

